Laser-Textured Surfaces: A Way to Control Biofilm Formation?

*Karin Schwibbert, Anja M. Richter, Jörg Krüger, and Jörn Bonse**

Bacterial biofilms pose serious problems in medical and industrial settings. One of the major societal challenges lies in the increasing resistance of bacteria against biocides used in antimicrobial treatments, e.g., via overabundant use in medicine, industry, and agriculture or cleaning and disinfection in private households. Hence, new efficient bacteria-repellent strategies avoiding the use of biocides are strongly desired. One promising route to achieve bacteria-repellent surfaces lies in the contactless and aseptic large-area laser-processing of technical surfaces. Tailored surface textures, enabled by different laser-processing strategies that result in topographic scales ranging from nanometers to micrometers may provide a solution to this challenge. This article presents a current state-of-the-art review of laser-surface subtractive texturing approaches for controlling the biofilm formation for different bacterial strains and in different environments. Based on specific properties of bacteria and laser-processed surfaces, the challenges of anti-microbial surface designs are discussed, and future directions will be outlined.

1. Introduction

Lasers represent one of the big technological revolutions of the 20th century that is increasingly conquering daily life applications in communication, entertainment, materials processing, medicine, etc. This success originates from the unique properties of the coherent optical radiation emitted by lasers that allow to locally confine optical energy and use it for surface or bulk modifications and structuring even at the micro- and nanoscales.[1]

By its principle, laser materials processing is done in a sterile and contactless manner, it is compatible with in-line demands of industry, and can be performed in a fast and efficient way, i.e., currently at areal processing rates of m^2 min^{-1}.[2] Moreover, depending on the selected processing strategy, the laser radiation allows to flexibly create very different types of surface micro- or nanostructures, or even hybrid micro-nanostructures on a large variety of different materials. These different laser-generated surface structures can result in various types of tailored surface functionalization.

Figure 1 exemplifies the possibilities of surface functionalization by laser-generated surface structures through the alteration of the physical and chemical surface properties.[3] Typical "physical properties" may include the surface topography, the intrinsic material structure (crystalline, polycrystalline, amorphous), its hardness, dielectric permittivity, superconductive properties, etc. "Chemical properties" can be altered through the laser-induced formation of an interfacial layer (e.g., due to superficial oxidation in the ambient air environment) or a laser-induced change of the near-surface stoichiometry (e.g., via the preferential ablation of certain constituents of the materials). These effects may lead to a change of surface adhesion properties, or the affinity of adsorption of specific molecules from the ambient environment or sample storage, etc.

All these physical and chemical properties may allow to establish and tailor specific surface functionalities for optical applications, liquid management and surface wetting, tribological applications, or biological applications (see the examples in the bottom row of Figure 1). The latter applications may include particularly the development of surfaces that impede formation of so-called biofilms.

Biofilms are highly organized microbial aggregates frequently encased in a self-produced matrix of extracellular polymeric substances (EPS) consisting of proteins, polysaccharides, and deoxyribonucleic acid (DNA), often visible as "slime" on surfaces or interfaces. Bacteria in biofilms enjoy advantages compared to their free-living counterparts, for example the formation of social interactions, an enhanced rate of nutrients exchange, and an increased tolerance to desiccation and antimicrobial treatment, e.g. with biocides.[4,5] The formation and dispersal of a biofilm takes place in steps which are outlined in **Figure 2**.

Bacterial biofilms often pose major problems. In the food industry, foodborne pathogens become a frequent source of outbreak of illnesses. In technical settings, biofilms are responsible for clogging and corrosion of tubes and pipelines. In a medical context, biofilms have been identified to cause a remarkable 80 % or more of all microbial infections in humans.[6–8]

K. Schwibbert, A. M. Richter[+], J. Krüger, J. Bonse
Bundesanstalt für Materialforschung und -prüfung (BAM)
Unter den Eichen 87, D-12205 Berlin, Germany
E-mail: joern.bonse@bam.de

The ORCID identification number(s) for the author(s) of this article can be found under https://doi.org/10.1002/lpor.202300753

[+]Present address: Robert Koch-Institut (RKI), Nordufer 20, D-13353 Berlin, Germany

DOI: 10.1002/lpor.202300753

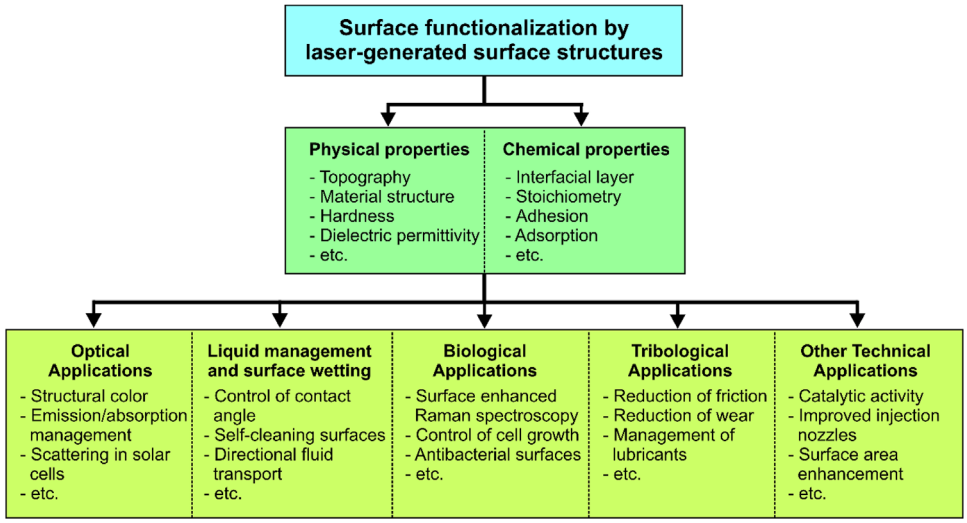

Figure 1. Overview of surface functionalization via laser-generated surface structures, enabled through physical and chemical surface properties. Adapted with permission.[3] Copyright 2020, Laser Institute of America.

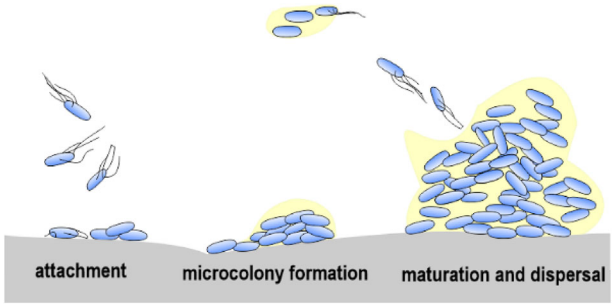

Figure 2. Major steps in biofilm formation. Initial attachment of single bacterial cells (displayed in blue) is followed by proliferation and the production and excretion of extracellular polymeric substances (EPS, displayed in yellow) that mediate attachment to the surface, fill and shape the space between bacterial cells, and promote the formation of microcolonies. Bacteria actively initiate adhesion by altering gene expression with consequent changes in, e.g., cell surface chemistry.[4,5] Microcolonies grow and finally lead to the development of a mature biofilm. The biofilm is distributed via the dispersal of single cells or even small biofilm aggregates which, in turn, will attach again to a surface.

To prevent biofilm formation, antimicrobial chemical-based approaches that depend on the release of biocides are frequently employed.[9,10] However, the gradual loss of these substances implies that their concentrations, though highly toxic at first, will decrease to a non-lethal level over time. This may result in the development of enhanced antimicrobial tolerances and even culminate in the emergence of antibiotic cross-resistances, thus, securing bacterial survival even under high antibiotic concentrations.

Despite the tremendous negative impacts, bacterial biofilms may also have beneficial effects.[8] In bioremediation and wastewater treatment, the microbes´ manifold metabolic pathways provide numerous possibilities for the degradation of man-made pollutants and the transformation of hazardous into harmless substances. In these cases, surfaces that attract and retain bacterial cells are desirable.

Overall, the need for surfaces that guide bacterial adhesion and, in addition, are long-lasting in function and "Safe by Design", without contributing to the emergence of resistances, is becoming increasingly apparent.[11] The development and engineering of passive surfaces acting through topographic rather than chemical means recently came into focus. Here, the method of laser-structuring of surfaces is a great opportunity and target.

This review article provides the reader with an overview on the main laser techniques applied for the fabrication of bacteria repellent or attractive surface topographies. Only subtractive laser-processing on the surface is considered. Additive manufacturing processes are not the subject of this work. In Section 2, we will present the current state-of-the-art of laser-texturing and discuss the most relevant laser surface processing strategies for the creation of surface micro-, nano-, and hierarchical micro-nanostructures. In Section 3 an introduction on bacterial biofilm formation and specific bacterial characteristics leading to surface adhesion is given. Exemplary surface topographies that are currently objects of intense research for their antibacterial effects are presented. Section 4 provides a critical assessment of biofilm growth conditions and bacterial adhesion characterization found in the pertinent literature. The following Section 5 orders the large amount of available literature with respect to these characteristic surface topographies created on different materials and the most relevant mechanisms. The final Section 6 deduces and identifies the challenges of anti-microbial surface designs and discusses future directions in this field.

2. Laser-Generated Surface Structures

In this article, a focus is laid on laser-generated surface structures with topographical feature sizes ranging between several tens of micrometers down to a few tens of nanometers, i.e., spanning

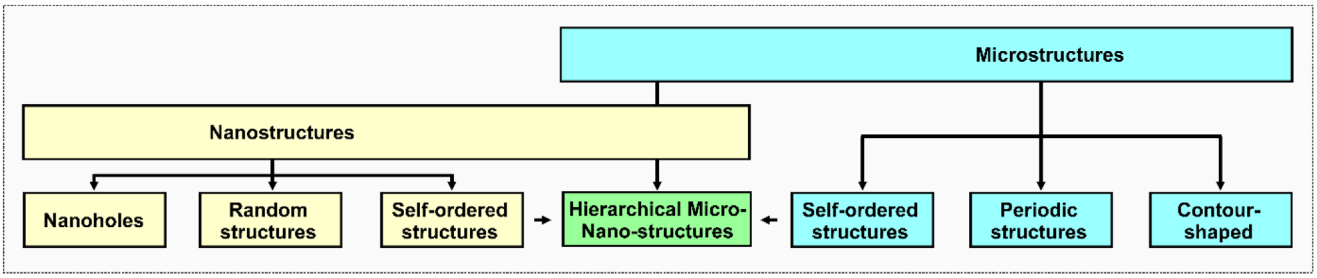

Figure 3. Scheme of laser-processed surface structures.

a range of about three orders of magnitude here. The "feature size" can be either the lateral dimension or even the depth of the surface structures. In the context of laser-processing, this regime is usually referred to micro-machining, and also includes the nanoscale surface alterations.

Figure 3 provides a scheme of the laser-processed surface structures discussed in the following. The regimes of nano- and microstructures are represented by horizontally arranged bars and can be divided in sub-categories each. In their overlap range, "hierarchical micro-nano-structures" are located as a hybrid type of two different surface topographies. Such hybrid structures then consist of a microstructure as a basis that is superimposed by some additional surface nanostructures and may be generated in a single laser-processing step either via self-organization processes or in a two- or multi-step laser-processing approach.

"Nanostructures" with feature sizes below the optical diffraction limit can be processed by laser radiation on very smooth surfaces as site-controlled individual nanoholes, taking the benefit of optical nearfield enhancement effects or via nonlinear interaction mechanisms. On already rough surfaces, laser-induced nanostructures will randomly arrange or manifest as periodic arrangements of "self-organized" surface structures.[1]

"Microstructures" can be formed also via self-organization effects. They may be tailored as 1D- or 2D- periodic surface topographies via multi-laser-beam interference structuring effects, or flexibly in 3D through direct contour-shaping with a single tightly focused laser beam along with a suitable laser-processing algorithm. More detailed insights into the different laser-processing approaches will be provided in the following section.

Numerous approaches were reported for the structuring of surfaces of solids by laser radiation.[12–15] **Figure 4** summarizes these approaches according to the number of laser beams used for the subtractive surface processing. This scheme provides the frame for Sections 2.1 to 2.3.

2.1. One-Beam Laser-Processing

In most cases, a single laser beam is used for surface structuring since this approach minimizes the costs and provides at maximum simplicity, a favorable robustness, and reliability. It can be briefly summarized as follows: the radiation emitted by the laser is guided via some optical elements such as plane mirrors to a focusing optics (e.g., lenses, curved mirrors, microscope objectives, etc.) that spatially concentrates the radiation upon beam propagation. Close to the focal region, large intensities (areal power densities in W cm^{-2}) and/or fluences (areal energy densities in J cm^{-2}) are featured that allow to permanently modify or even remove (ablate) the irradiated material. Upon tight laser beam focusing using an optics with a high numerical aperture (NA) small focus diameters ($2w_0$) in the micrometer range can be realized that allow a direct laser writing (DLW) of shallow surface structures with sub-micrometer lateral dimensions.[16,17] In contrast, loose focusing employing a lens/mirror with a low NA realizes larger focus diameters that facilitate a robust large-area surface processing upon scanning the focused laser beam across the surface.

The one-beam surface processing of individual spots (0D), lines (1D), and areas (2D) is illustrated in **Figure 5** for material removal through laser ablation.[14] For spatially Gaussian laser beams irradiating strongly absorbing materials, such as metals, typically parabolic dimples and line profiles are generated in a controlled way.

The processed surface structures can involve a plethora of different morphologies. The controlled movement of a (tightly) focused laser beam along with a set of tailored direct writing sequences allows a precise 3D contour-shaping of the surface in the micrometer range, creating even smaller surface nanostructures which typically includes the "self-ordered" formation of nanostructures along with some random roughness contributions. The

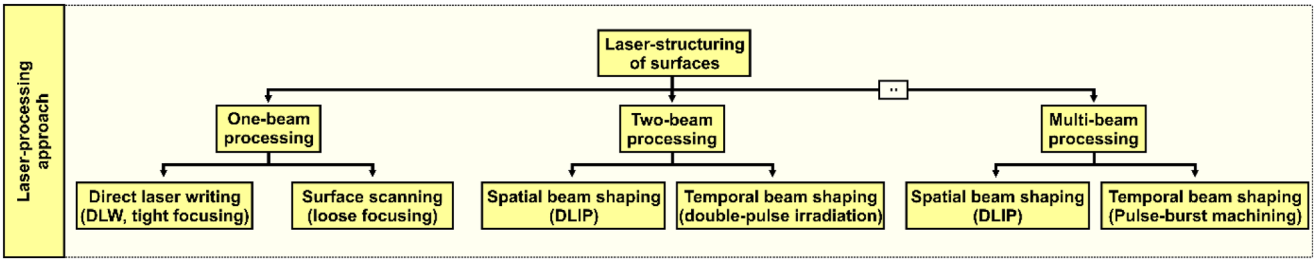

Figure 4. Scheme of laser-processing approaches.

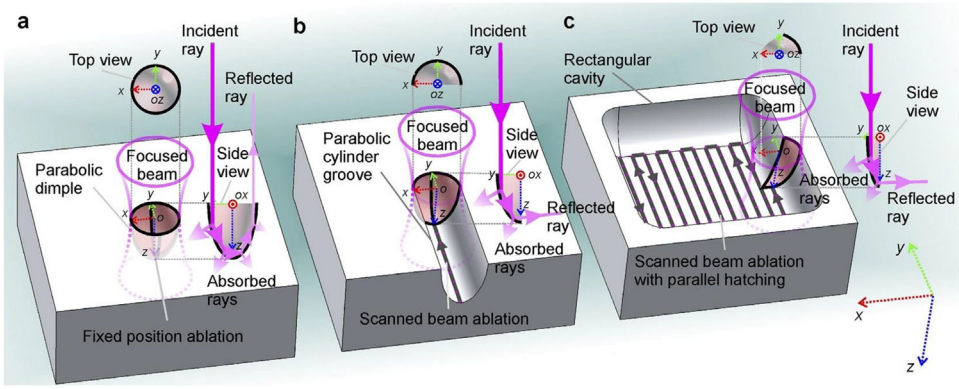

Figure 5. Scheme of one-beam laser-processing strategies employing a focused Gaussian laser beam: a) spot (dimple) processing, b) line processing, c) area processing. (Reprinted from[14] A. Zemaitis, et al., Advanced laser scanning for highly-efficient ablation and ultrafast laser structuring: experiment and model, Sci. Rep. 8:17376, Copyright 2018 under Creative Commons BY 4.0 license. Retrieved from https://doi.org/10.1038/s41598-018-35604-z).

term self-ordered aims to consider here that although the surface is irradiated using a homogeneous spatial beam profile in a spot or scanning geometry, the resulting surface topography features characteristic (quasi-)periodic surface morphologies. Apart from the kinematic strategy, the most relevant laser-processing parameters are the peak intensity and/or fluence (I_0 or ϕ_0, controlled via the average laser power P or the laser pulse energy E_p), the laser pulse repetition rate (f), the scanning velocity (v), and the line separation (hatch distance h).

2.1.1. Self-ordered Nano- and Microstructures

Figure 6 visualizes some of the most characteristic self-ordered surface structures, namely two types of sub-micrometric "laser-induced periodic surface structures" (LIPSS, often referred to as ripples), and micrometric "grooves," and "spikes" that formed at the surface of 100Cr6 alloyed steel after line scanning of a fs-laser beam, each for individually optimized laser-processing conditions (for details refer to Ref. [18]). Note that both, the ripples and the grooves orient in a characteristic manner either perpendicular or parallel with respect to the direction of the linear polarization of the laser radiation used for their processing.[19]

LIPSS can be easily processed on already-existent surface structures. **Figure 7** presents an example of LIPSS (LSFL type, meaning "low spatial frequency LIPSS") that were generated by a UV ns-laser on top of different lithographically pre-patterned ≈2 µm thick photoresist films.[20] In Figure 7a, LSFL of $\Lambda \approx$ 195 nm spatial period manifest on a photoresist line deposited on a silicon wafer. Similarly, the LSFL can be formed on top of an

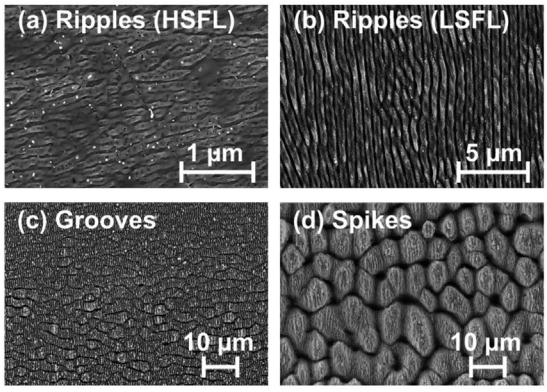

Figure 6. Scanning electron micrographs of characteristic surface morphologies (Ripples: a), b); Grooves: c); Spikes: d)) formed on alloyed steel surface after fs-laser-processing. The direction of the linear polarization is horizontal in all images. Note the different magnifications of the micrographs. (Reprinted from[18] J. Bonse, et al., Femtosecond laser texturing of surfaces for tribological applications, Materials 11:801, Copyright 2018 under Creative Commons BY 4.0 license. Retrieved from https://doi.org/10.3390/ma11050801).

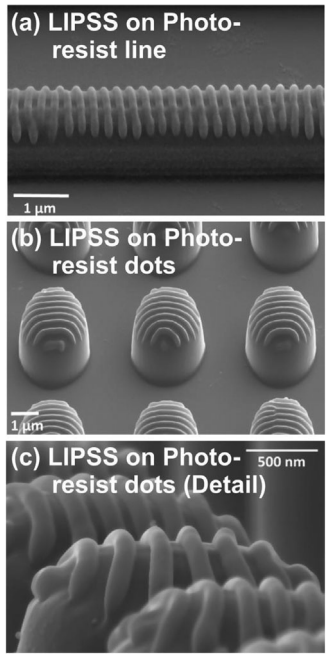

Figure 7. Tilted-view scanning electron micrographs of LIPSS processed by a UV ns-laser on a lithographically pre-structured photoresist film on a silicon wafer. a) LSFL on photoresist line structure. b) LSFL on photoresist dot array. c) Detail of LSFL depicted in (b). Note the different magnifications of the micrographs. (Reproduced with permission.[20] Copyright 2019, Elsevier).

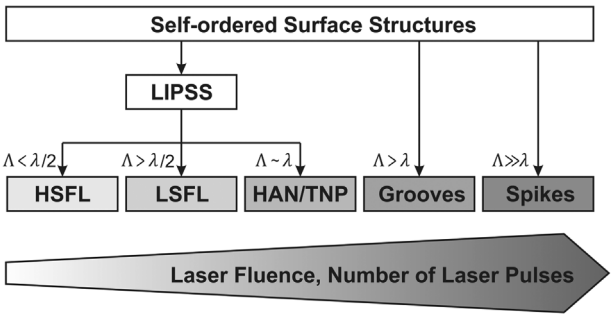

Figure 8. Classification of self-ordered surface structures. (Adapted with permission.[28] Copyright 2023, Springer).

array of photoresist micro-dots (Figure 7b). The detailed magnification provided in Figure 7c reveals a semi-circular cross-section of the LSFL ridges and an undercut at their roots.

Figure 8 provides a detailed classification of the different self-ordered surface structures, arranged according to their size (period Λ) compared to the laser irradiation wavelength (λ). For current commercial laser systems, these wavelengths are usually in the ultraviolet to near-infrared spectral range, i.e., between ≈300 and ≈1500 nm. While the most widely observed "low spatial frequency LIPSS" (LSFL, exemplified in Figure 6b) usually feature spatial periods $\lambda/2 < \Lambda \leq \lambda$, the much smaller "high spatial frequency LIPSS" (HSFL, exemplified in Figure 6a) can exhibit even sub-100 nm spatial periods[21] — by far smaller than the optical diffraction limit. For metals, their modulation depths typically are a few tens of nanometers for HSFL and a few hundreds of nanometers for LSFL.

As a general rule, for spikes and grooves gradually more laser pulses per beam spot diameter and higher peak fluences are required when compared to LIPSS, which are formed close to the ablation threshold fluence. Their depths are significantly larger than that of LIPSS, i.e., typically a few micrometers for the grooves and some tens of micrometers for the spikes. For additional information on the self-ordered surface structures, the reader is referred to comprehensive review articles.[19,21–28]

Apart from the already discussed 1D-grating-like ripple and grooves morphologies, other characteristic 2D-LIPSS surface patterns of hexagonal symmetry were reported upon laser scan processing (**Figure 9**). Romano et al.[29] observed periodic patches of hexagonally arranged triangular structures with a lattice period of ≈λ, termed "triangular nanopillars" (TNP), upon irradiation with circularly polarized radiation. An example of such TNP formed after near-infrared ps-laser-processing on a medical grade Cobalt-Chrome-Molybdenum alloy is provided in Figure 9a,b.[30]

Another characteristic morphology consisting of "hexagonally arranged nanostructures" (HAN) is exemplified in the bottom row of Figure 9. These highly regular nanostructures were formed on a Ni–W alloy upon line processing with linearly polarized ultraviolet ps-laser pulses.[31] The top-view scanning electron microscopy (SEM) micrograph (Figure 9c) reveals the hexagonal symmetry of circular nanopillars arranged at periods Λ_{HAN} ≈400 nm somewhat exceeding the laser wavelength (λ = 355 nm), while the cross-sectional transmission electron microscopy (TEM) view (Figure 9d) indicates nanopillar diameters and heights of ≈130 nm, i.e., an aspect ratio around $A \approx 1$.

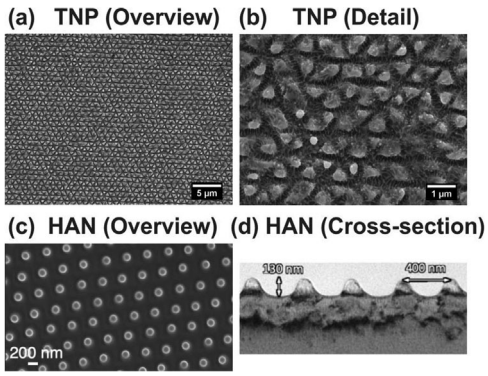

Figure 9. Characteristic surface nanostructures of hexagonal symmetry formed on metal surfaces after scanning ps-laser-processing. Top row a,b): triangular nanopillars (TNP) (Reprinted from[30] S. van der Poel, et al., Fabricating laser-induced periodic surface structures on medical grade cobalt–chrome–molybdenum: tribological, wetting and leaching properties, Lubricants 7:70, Copyright 2019 under Creative Commons BY 4.0 license. Retrieved from https://doi.org/10.3390/lubricants7080070); Bottom row c,d): hexagonally-arranged nanostructures (HAN) (Reprinted from[31] L. Porta-Velilla, et al., Highly regular hexagonally-arranged nanostructures on Ni-W alloy tapes upon irradiation with ultrashort UV laser pulses, Nanomaterials 12:2380, Copyright 2022 under Creative Commons BY 4.0 license. Retrieved from https://doi.org/10.3390/nano12142380). (a-c) represent top-view SEM micrographs, (d) displays a cross-sectional TEM image. Note the different magnifications of the micrographs.

2.1.2. Hierarchical Micro-Nano-Structures

Many surface functionalities, such as the prominent "Lotus effect" creating super-hydrophobic surfaces,[32] arise from characteristic hierarchical micro-nano-structures. Such hybrid structures are easily produced by laser scan processing, as illustrated in **Figure 10**. That figure explains the differences between the static spot processing and the dynamic line scanning with the same radially Gaussian beam profile (visualized as red lines in Figure 10).

In the "static" spot processing approach using multiple laser pulses, each surface location is hit several (N) times by the same local fluence value — according to its individual spatial position within the irradiated spot. As a consequence, different fluence regimes can be distinguished in which the distinct surface morphologies emerge (LIPSS, grooves, spikes), see the bottom part of Figure 10a. For the "dynamic" line scanning approach, however, and, as a result of the Gaussian beam profile, each surface location is initially exposed to a sequence of increasing and subsequently to a sequence of decreasing local fluences. For high laser pulse energies (peak fluences), this imposed important differences for the laser-processing. While the multiple exposure to the high fluence part of the laser beam may cause the formation of spikes or grooves, the low fluence tail of the Gaussian beam subsequently overwrites these previously generated surface morphologies with LIPSS. As an implication of the beam scanning processing, hierarchical micro-nano-structures are then formed at the laser-treated surface, see the bottom part of Figure 10b. Nevertheless, restricting the laser fluence to values close to the ablation threshold allows the generation of large surface areas that are homogeneously covered with LIPSS even for the scanning laser-processing approach (see Figure 6a,b).

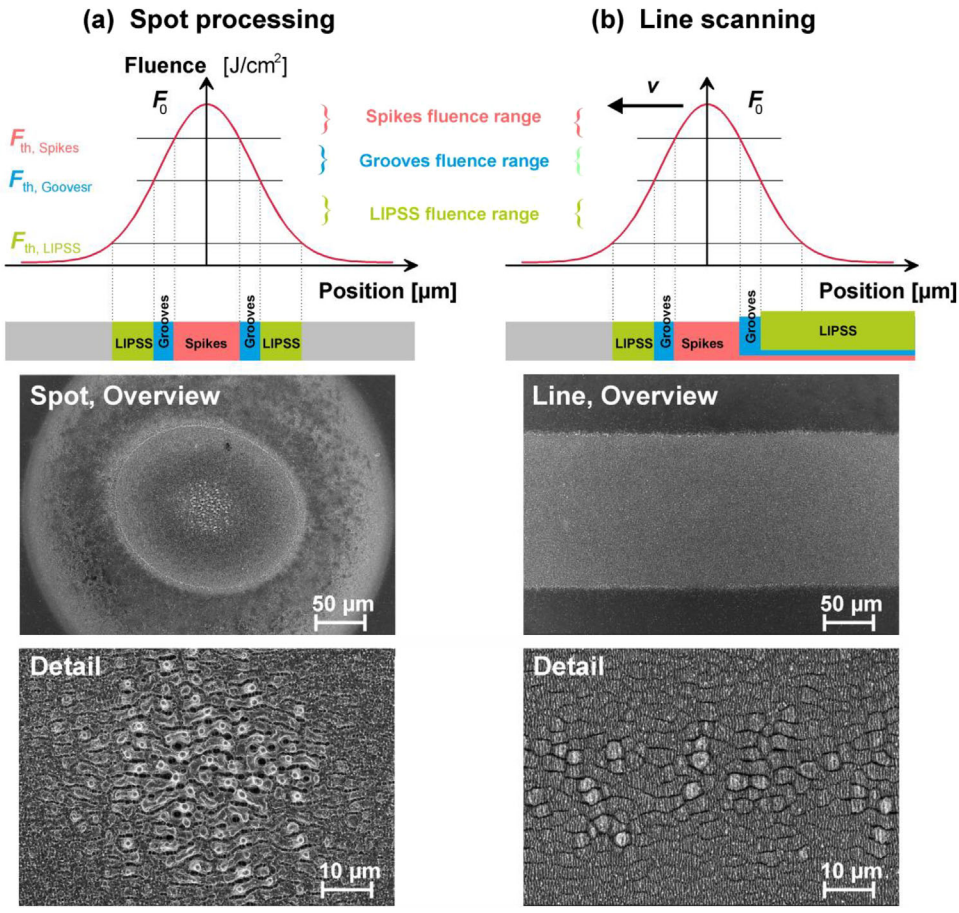

Figure 10. Scheme of laser-processing of spots (a) and lines (b) employing as spatially Gaussian beam profile at comparable laser parameters. Top: Fluence ranges of distinct surface morphologies. Bottom: Scanning electron micrographs of groove-processing on a polished alloyed steel revealing separated morphology zones (left) and hierarchical micro-nano-structures (right). (Reprinted with permission.[27] Copyright 2021, Springer).

2.1.3. Spatial and Temporal Beam Shaping

Most lasers used in materials processing deliver beams that are spatially Gaussian-like shaped (see the example in the previous section). The laser beam quality is usually quantified by the M^2-factor that provides as a measure the comparison to the fundamental Gaussian mode laser beam.[33] However, sometimes it can be beneficial to use either spatially or temporally shaped laser beams to facilitate the control of the processed surface patterns. While spatial beam shaping for obtaining nearly flat-top shaped laser intensity profiles in the surface processing plane may be classically realized, e.g., through diffractive optical elements or concepts based on Fourier optics, the availability of ultrashort pulsed lasers has offered an elegant way for temporal and spatial beam shaping. That approach relies on the fact that temporally short laser pulses — according to the theorem of Fourier — simultaneously also exhibit a broad distribution of spectral components (wavelengths). By means of liquid-crystal beam shapers,[34] these spectral components may be manipulated individually with regard to their spectral phases or spectral amplitudes. Such spectrally manipulated laser beams can then provide tailored temporal or spatial laser beam profiles.[34–36] Alternatively, for temporal beam shaping in the form of double-pulse sequences of variable delay, polarization orientation, sub-pulse energy ratio, or wavelength, classical interferometers, e.g., of Michelson- or Mach-Zehnder-type may be used for surface processing.[37–39]

2.2. Two-Beam Laser-Processing

Laser-processing approaches with increased technical complexity can rely on more than a single laser beam for the treatment of surfaces, e.g., by using two laser beams. This can be realized either by non-collinearly superimposing the two laser beams in space and in time at the sample surface[15] — or by creating and employing collinearly propagating temporal double-pulse sequences.[39] The currently most prominent two-beam approach is referred to as "direct laser interference patterning" (DLIP).[40] Its idea is illustrated in **Figure 11**.

Two non-collinearly propagating, linearly polarized laser beams are crossing at an angle θ and generate a linear grating-like interference pattern in the overlapping region (Figure 11a). The spatial period of the interference pattern is given by $\Lambda_{DLIP} = \lambda/[2\cdot\sin(\theta/2)]$ and can be varied through the angle θ. Thus, the minimum period is given by $\Lambda_{DLIP} = \lambda/2$ for counter-propagating laser beams, manifested by the optical diffraction limit. When

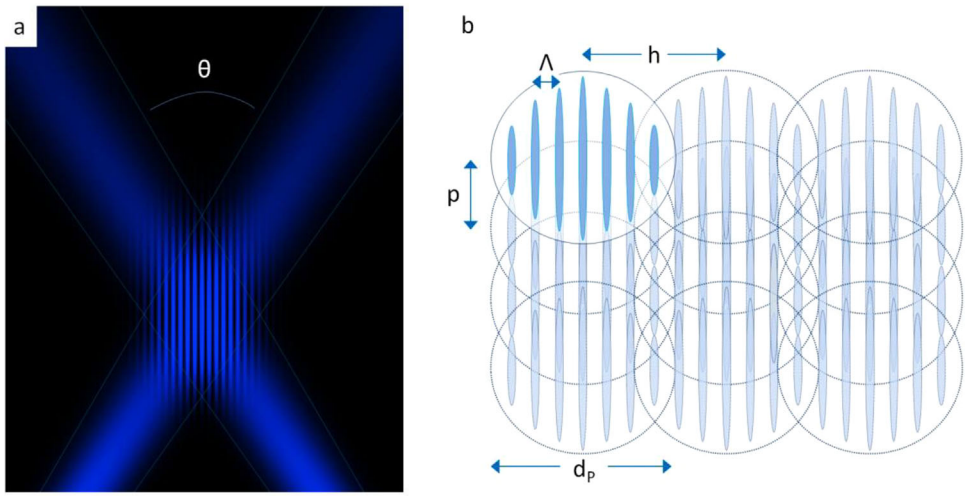

Figure 11. Periodic DLIP intensity distribution of two laser beams intersecting at an angle θ (a). Scheme of DLIP processing by areal displacement of multiple DLIP pixels (b). (Reprinted from[41] M. Mezera, et al., Hierarchical micro-/nanostructures on polycarbonate via UV pulsed laser-processing, Nanomaterials 10:1184, Copyright 2020 under Creative Commons BY 4.0 license. Retrieved from https://doi.org/10.3390/nano10061184).

choosing proper laser pulse energies for the DLIP processing, material removal (ablation) can be predominantly generated at the maxima of the interference pattern, while at its minima the surface remains widely unaffected. Since the interference pattern is confined to the micrometer-sized DLIP pixels (diameter d_p) in the overlapping focus region, they can be individually controlled and scanned across the surface for large-area processing (Figure 11b), allowing to employ all processing strategies already discussed in the context of one-beam processing in the previous section.

2.3. Multi-Beam Laser-Processing

The idea of DLIP can be straightforwardly extended to three or more interfering laser beams.[42] On the costs of the complexity of the experimental setup, more intricate laser-interference patterns can be generated and used for laser surface structuring (see the examples in **Figure 12**).[43] In analogy to the two-beam processing approach, the temporal double-pulse sequences can be extended towards generalized temporal pulse bursts that may offer advantages for specific processing conditions and materials.[44]

Additionally, the laser-processing can be performed in different individually tailored sequential steps, e.g., for obtaining hierarchical surface topographies by fabricating a surface microstructure in the first step, followed by the generation of a covering nanostructure in a subsequent second processing step — each at individually optimized laser irradiation conditions. Conceptually, all approaches DLW, DLIP, and LIPSS processing can be suitably combined, providing the possibility of generating hierarchical micro-nano-structures.

The results of joining DLW processing in a first step with multi-pulse DLIP processing as a second step (DLW+DLIP) is exemplified in **Figure 13**. At first, polished Ti samples were scan-processed by DLW generating adjacent ablation craters of ≈50 µm diameter by employing single ns-laser pulses (1064 nm, 200 ns), see the coarse pattern in Figure 13a. After that, a smaller 2D-periodic hole pattern with ≈5 µm spatial period was superimposed via 4-beam DLIP using a laser fluence of 0.93 J cm^{-2} and five ps-laser pulses (532 nm, 70 ps) per irradiated spot.[45] The average modulation depth of the laser-produced hole pattern was (1.1 ± 0.3) µm. For the structuring, the samples were translated horizontally and vertically with hatch distances of 39.5 µm and 38.5 µm in x- and y-direction, respectively. The use of five laser pulses per DLIP spot led here to the generation of LIPSS (both, LSFL and HSFL) featuring spatial periods below few hundreds of nanometers, as seen in the detailed magnification in Figure 13b.

Furthermore, the combination of DLIP microstructures with self-organized LIPSS was realized for the fabrication of hierarchical micro-nanostructures,[41,45–47] which can combine the benefits of both laser irradiation approaches on the costs of an additional laser-processing step (DLIP+LIPSS) or just by applying several DLIP irradiations to the same spot (multi-pulse DLIP). **Figure 14** presents a collage of scanning electron micrographs of a Ti-13Nb-13Zr alloy surface processed by multi-pulse DLIP (1064 nm, 12 ps) with an interference grating structure of 8.5 µm

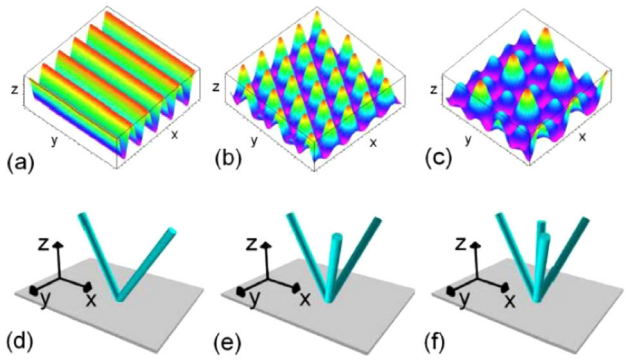

Figure 12. Calculated intensity distributions for two- (a), three- (b), and four-beam (c) interference, with (d), (e), and (f) indicating the respective beam configurations for two-, three- and four-beam interference. (Reprinted from[43] with permission of A.F. Lasagni).

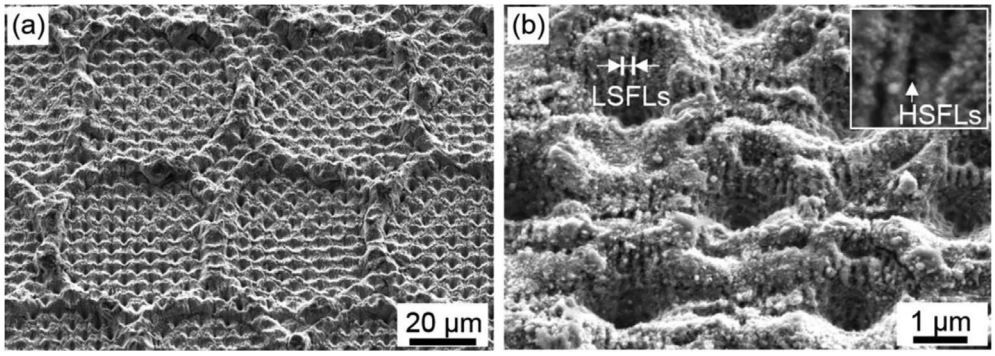

Figure 13. a) Tilted-view (30°) scanning electron micrographs of a hierarchical DLW-DLIP treated titanium surface. The 2D-DLW ablation crater pattern was produced using pulses (1064 nm) of 200 ns duration at a fluence of 5.9 J cm^{-2}. For the DLIP, five ps-laser pulses (532 nm, 70 ps, 1 kHz) were applied per irradiated spot, resulting in a cumulated fluence ($5\times F$) of 4.7 J cm^{-2}. b) High magnification micrograph resolving also the fine LIPSS features (LSFL in the image and HSFL in the inset). (Reprinted from[45] C. Zwahr, et al., Fabrication of multifunctional titanium surfaces by producing hierarchical surface patterns using laser based ablation methods, Sci. Rep. 9:6721, Copyright 2019 under Creative Commons BY 4.0 license. Retrieved from https://doi.org/10.1038/s41598-019-43055-3).

spatial period.[47] The regions of the DLIP interference maxima (grooves of the micro-topography) are additionally covered with LSFL of ≈600 nm spatial period. Moreover, the regions between the LSFL are covered by HSFL of ≈200 nm here.

Another example of multi-exposure lithography with two-beam interference is shown in **Figure 15**, where a periodic surface microstructure is generated on a photoresist material in the first DLIP-like interference lithography step using two laser beams L1 at an interference angle θ_1, before a periodic surface nanostructure is superimposed in the second subsequent interference lithography step performed with laser beams L2 at the larger angle θ_2.[48] After the laser irradiation at fluences below the damage threshold of the photoresists, it was chemically developed revealing the transfer of the "imprinted" multi-exposure intensity pattern into a regular periodic surface topography. The SEM micrographs of Figure 15b (labelled $b_1 - b_4$) demonstrate that a large variety of different hierarchical micro-nano-structures with very high regularity of the pattern can be generated by this approach termed "multi-exposure laser interference lithography" (ME-LIL) in the following.

Another remark has to be made on the processing of dielectric materials such as polymers or glasses. The exposure of polymeric material by low power continuous wave or low fluence pulsed UV laser radiation can modify locally the optical absorption coefficient without removal of material (no ablation), e.g., through structural or chemical effects featuring the formation of electronic defect states in the band gap of the laser-processed material. This phenomenon is known as "incubation".[49] If the material is irradiated in a following step with high power/fluence laser radiation, the modified material can be ablated without affecting the surrounding. With this localized "incubation plus ablation method", polymer surfaces can be patterned with precise spatial control down to the sub-µm level in a two-step process. Additionally, the ablation laser can be set to a wavelength that is only absorbed by the incubated material and not by the original (pristine) material.

Table 1 compiles a comparison of the performance of the different approaches for the laser-processing of surface nanostructures (left column), microstructures (right column), and hybrid micro-nano-structures (middle column). This includes the lower

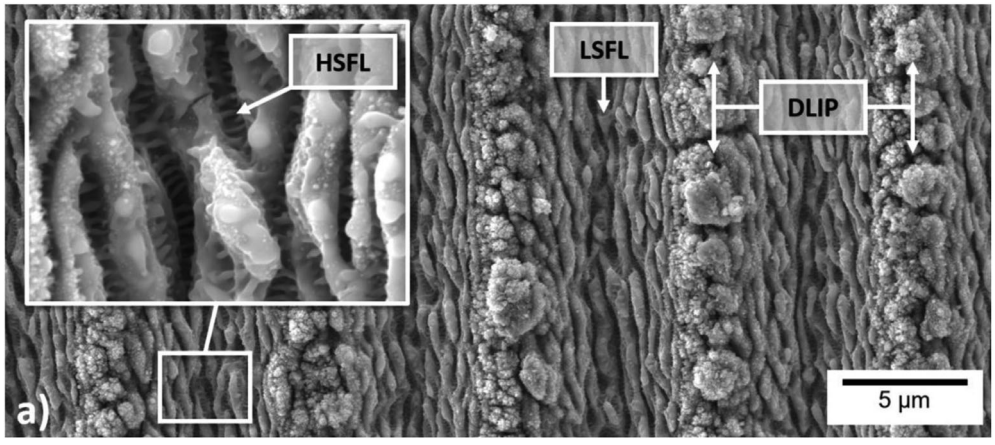

Figure 14. Top-view scanning electron micrograph of multi-level hierarchical micro-nanostructures on Ti-13Nb-13Zr alloy processed as combination of DLIP with different types of LIPSS (LSFL and HSFL). (Reprinted with permission.[47] Copyright 2022, Elsevier).

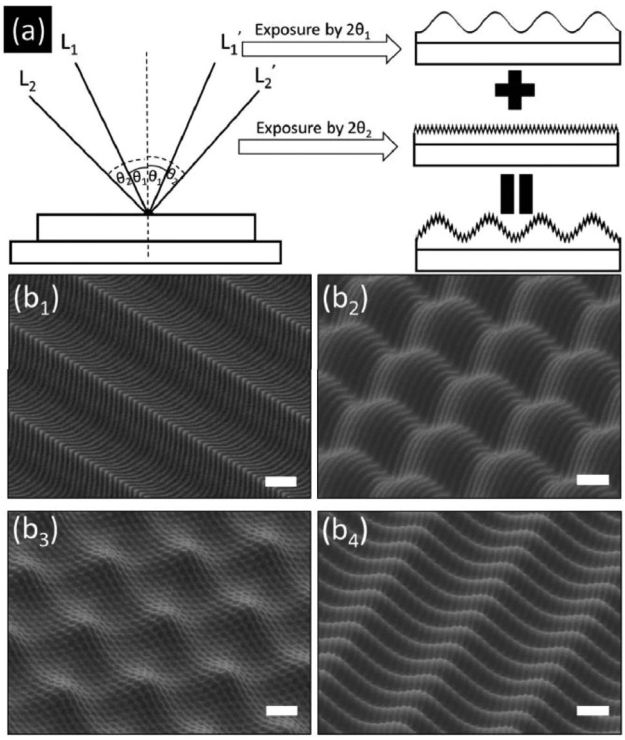

Figure 15. a) Schematic illustration of a two-step laser lithography exposure with two-beam interference, resulting in hierarchical micro-nano-structures on a photoresist material by combining the processing of a periodic microstructure (1st step: laser beams L1, interference angle θ_1) with that of a surface nanostructure (2nd step: laser beams L2, interference angle θ_2). b_1–b_4) SEM micrographs exemplifying different resulting hierarchical micro-nano-structures through the combination of different 1D- and 2D-periodic beam interference patterns (after photoresist development). All micrographs share the same scale bar of 1 µm length. (Reprinted with permission.[48] Copyright 2017, Optical Society of America).

limit of the spatial periods, an assessment of the regularity of the surface structures, the capability to independently control their heights and depths, and the technical complexity of the experimental setup for processing the structures.

3. Parameters Affecting Initial Bacterial Adhesion on Surfaces

This section introduces specific components and properties of single bacterial cells that take on key tasks in cell-surface interaction and adhesion in general. First, physical properties of bacteria and surfaces and their role in bacterial adhesion are elucidated. Secondly, filamentous cell appendages enabling cell-surface interaction are presented. Finally, different classes of nano- and micro-structured surfaces are illustrated and categorized according to their influence on bacterial adhesion. Examples that demonstrate the impact of topography on bacterial growth are given for each class. For a more detailed discussion of underlying principles affecting bacterial adhesion behavior on laser-structured surfaces, the reader is referred to Section 5.

3.1. Principles of Single Cell Adhesion to Surfaces

For single cell attachment — the step that initiates biofilm formation — three main factors must be considered: the bacterium itself, the liquid environment covering the surface, and the surface itself (**Figure 16**). At first, the bacterial cell has to reach the surface. This can be done by passive liquid transport like convection, Brownian motion, or gravity. The most efficient way to reach the surface is by actively swimming. Many bacteria are equipped with flagella, helical filamentous cell appendages responsible for swimming and swarming motility.

When approaching the surface, bacteria are exposed to different forces summarized in the so-called XDLVO (Extended Derjaguin–Landau–Verwey–Overbeek) theory.[50] Essentially, the sum of van der Waals interactions, which are generally attractive, electrostatic charge interactions, and acid-base hydrophobic interactions, which are attractive or repulsive mainly in dependence on external factors, is decisive for successful approaching. Therefore, the ionic strength and pH of the liquid environment and also the composition of the culture medium contribute to bacterial adhesion behavior.

The bacterial cell usually has a negative net charge on its surface, which is mainly due to the presence of teichonic acids embedded in the peptidoglycan layer of Gram-positive bacteria and

Table 1. Comparison of different laser-processing strategies for the fabrication of surface nanostructures, microstructures, and hierarchical micro-nano-structures. [1] λ: laser irradiation wavelength. [2] ++: very good/very high. [3] +: good/high. [4] o: medium. [5] –: low. C: continuous scanning. P: pixelwise during scanning. Abbreviations: DLIP: direct laser interference patterning; HAN: hexagonally-arranged nanopillars; HSFL: high spatial frequency LIPSS; LIPSS: laser-induced periodic surface structures; LSFL: low spatial frequency LIPSS; ME-LIL: multi-exposure laser interference lithography; TNP: triangular nanopillars.

	Nanostructures		Hierarchical Micro-Nano-Structures				Microstructures		
Processing strategy	LIPSS, HAN, TNP	DLIP	Grooves, Spikes	DLW+ LIPSS	DLIP+ LIPSS	ME-LIL	DLW	DLIP	ME-LIL
Number of steps	1	1	1	2	2	>1	1	1	> 1
Minimum spatial periods	λ/10 (HSFL) to λ (LSFL) [1]	> λ/2	> λ	> λ/2	> λ/2	> λ/2	> λ/2	> λ/2	> λ/2
Regularity of pattern	+ [3] / o [4]	++ [2]	o [4]	+	+	++	++	++	++
Flexibility of processing	C	P	C	C / P	P + C	P	C / P	P	P
Control of periods/depths	o	++	o	o / +	o / +	o / +	+/++	++	o / +
Complexity of setup	– [5]	+ / ++	–	o	++	+ / ++	– / o	+ / ++	+ / ++

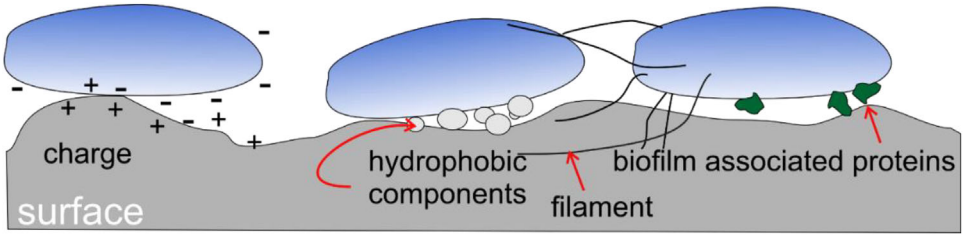

Figure 16. Major components that influence bacterial adhesion once the bacterial cell is close to the surface: Net charge and charge density of the bacterial envelope (left), the ability to produce and secrete hydrophobic components (like the release of outer membrane vesicles in Gram-negative bacteria, middle), and the occurrence of proteinaceous adhesins like members of the Bap-family (Biofilm-associated proteins), or filaments (flagella, curli, pili)[51] (right). Physico-chemical properties of the substrate surface can be altered by formation of a conditioning film.[52] (Inspired by[52]).

lipopolysaccharides present in the outer membrane of Gram-negative bacteria. As a result, negatively charged surfaces are often less susceptible to bacterial adhesion compared to surfaces with a positive net charge.

Cell surface hydrophobicity is another important parameter that contributes to attachment to or detachment from surfaces. In general, hydrophobic bacteria seem to adhere more strongly to hydrophobic surfaces, while hydrophilic bacteria to hydrophilic surfaces. Superhydrophobic or superhydrophilic surfaces are frequently reported to reduce bacterial attachment but conflicting results on the initial adhesion of bacteria on surfaces with moderate hydrophobicity and hydrophilicity become known. This might arise from the fact that the bacterial cell envelope is highly heterogeneous among individual species and can be adapted within minutes in response to changes in environmental conditions like temperature, nutrient availability, and osmotic stress. Moreover, in a bacterial population, cell surface hydrophobicity is not homogeneous. Even the surface of a single cell is highly heterogeneous, exhibiting different charges and hydrophobic patches around the cell body which locally allow the displacement of interfacial water and consequent adhesion to the surface.[52–54]

3.2. Cell Appendages for Cell-Surface Interaction

Most important bacterial characteristics leading to adhesion is the occurrence of filamentous cellular appendages like *flagella*, *pili*, or *amyloid curli* (**Figure 17**).

The *flagellum* is the most common organelle for bacterial locomotion. It consists of a filament composed of protein subunits (flagellin), which is anchored in the cell envelope via a "hook" and a "basal body" that both mediate the rotation of the flagellum relative to the cell body. Typical dimensions of flagella in *Escherichia coli* (*E. coli*) are 5–10 µm in length and ≈20 nm in diameter.[55] It is generally agreed that flagella do play a crucial role but are not mandatory for biofilm formation. Flagella support, e.g., chemotaxis and, thereby, indirectly promote biofilm formation, but non-flagellated bacterial species like *Staphylococcus aureus* (*S. aureus*) are as well able to produce a biofilm. Recent findings have shown that the occurrence of flagella clearly delay surface colonization of *E. coli*,[56] which underlines the ambiguous role of flagella in the biofilm formation process.

Pili are filamentous cell appendages, classified into different types, that may mediate specific or non-specific attachment to surfaces. Helically arranged protein sub-units of pilin-monomers form the tube-like organelle, which typically is 3–10 nm in diameter and of various lengths (1–2 µm for "type I" pili of *E. coli*).[57] Type I pili are known to adhere in a mannose-dependent manner to receptor molecules on eukaryotic cell surfaces and are also important for *E. coli* biofilm formation on abiotic surfaces,[58] "type IV" pili are "grappling hooks" that enable bacteria to move over surfaces (twitching motility).[59] The conjugative "F-pilus" in *E. coli*, primarily used to exchange genetic material between cells, plays in addition a crucial role in biofilm formation by promoting both, initial adhesion and biofilm maturation through non-specific attachment to abiotic surfaces and subsequent cell-to-cell contacts, which stabilize the structure of the biofilm.[60]

Curli are thin aggregative fibers produced by many Enterobacteriaceae including *E. coli* and *Salmonella* spp. and represent the major proteinaceous component of their extracellular matrix. These fibers are involved in adhesion to surfaces and biofilm formation.[61]

In addition to their biofilm stabilizing impact, all filamentous cell appendages are assumed to facilitate surface adhesion in general by penetrating the cloud of surface charges which otherwise would be repulsive.[50] Upon the adhesion process, bacteria

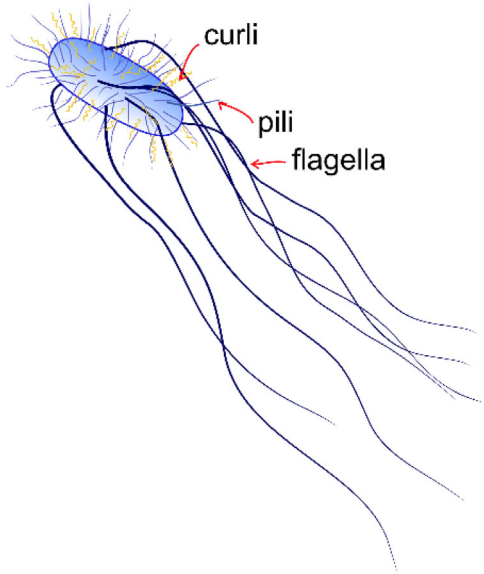

Figure 17. Scheme of a rod-like bacterial cell equipped with cell appendages (not true to scale).

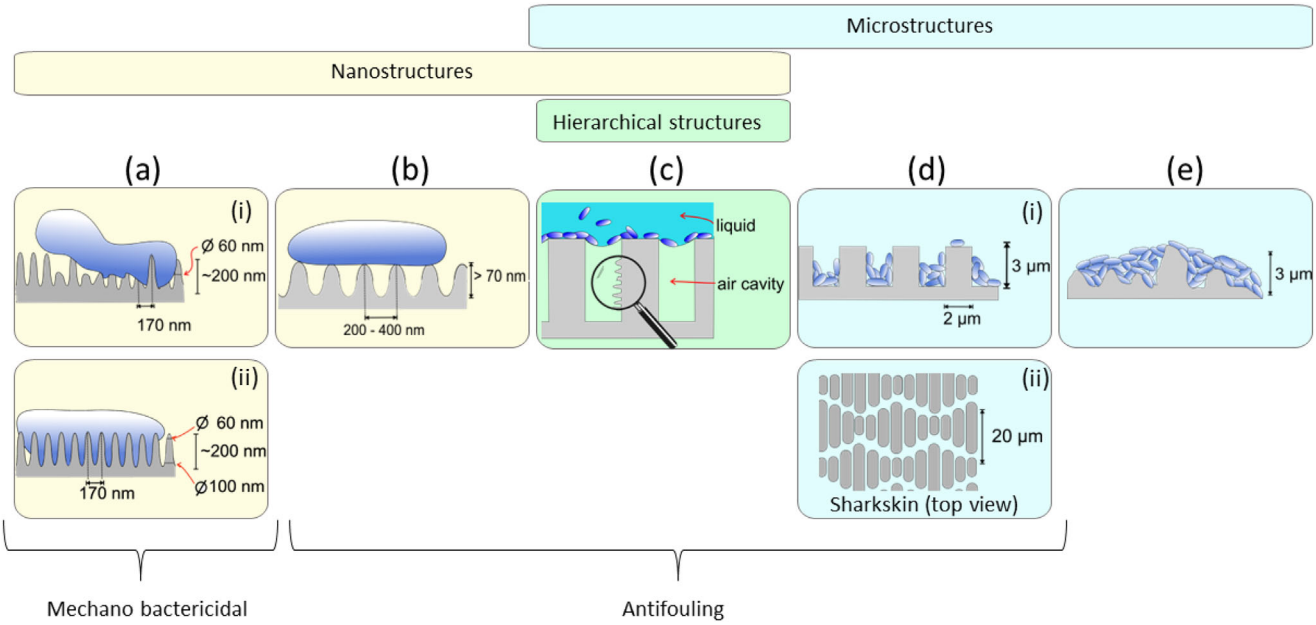

Figure 18. Schematic illustration of topographies with nano-, micro- and hierarchical structures that influence bacterial adhesion behavior and featuring mechano-bactericidal or antifouling effects. Approx. size of the bacterial cell (blue shaded): 0.5–1 µm in width and 1–2.5 µm in length, which corresponds to the typical dimensions of an *E. coli* cell. Antimicrobial modes of action: a) Mechano-bactericidal i) stretch and rupture ii) fast piercing; b–d) Antifouling; Magnification glass in (c) highlights nanorough surface structure; d) (i) cross-section of a typical sharkskin-like topography (ii); top-view on a sharkskin topography; e) surface with irregular structures at micrometer scale without bactericidal or antifouling properties. Exemplary sizes of the structures according to.[64–67]

change their physiology fundamentally, and a large variety of exopolymers, which serve as a "molecular glue" are synthesized and excreted. In the course of this, proteins that facilitate surface adhesion are produced and embedded into the cell envelope where they stay loosely associated to the cell, as the biofilm-associated protein A (BapA) in *Salmonella enterica*, or is excreted into the extracellular milieu like the large adhesion protein A (LapA) in *Pseudomonas fluorescens*.[51]

3.3. Interaction of Bacteria with Nano- and Micro-Structured Surfaces

Topographical surface properties that affect bacterial adhesion are currently the subject of lively discussion and investigation and have been extensively reviewed.[53,62–64] This aspect is particularly relevant in combination with the size and shape of the bacterial cells (spherical, rod-shaped, etc.) and crucially depends on the lateral and vertical scales of the surface topographic corrugations. As this review article focuses on bacterial adhesion on laser-structured surfaces, we present here a brief overview of topographies and associated mechanisms that are generally discussed and claimed to be antibacterial or bacteria-repellent.

Basically, engineered surface topographies as shown in **Figure 18** can be divided into bacteria-repellent ("antifouling"), and bacteria-killing ("mechano-bactericidal"), respectively, with structures roughly divided into µm-scale and nm-scale and combinations thereof.

In general, surfaces with characteristic topographic features at µm-scale of a dimension larger than a single bacterium promote bacterial adhesion (Figure 18e). Moreover, it is well documented that microbes tend to preferentially align to µm-scaled valley and pillar structures to maximize the number of attachment points.[53,68–71] Surface cavities also provide shelter and, thereby, facilitate intercellular communication which in turn fosters biofilm formation.

An exception seems to be the so-called sharkskin-topography and variations thereof (Figure 18d (i,ii)) which efficiently reduces biofilm formation although the feature size is larger than the bacterial cell body. The corresponding antifouling mechanism of sharkskin is not yet completely understood but may be based on its excellent drag-reducing surface: bony scales covering the skin alter the flow of water in overlying boundary layers. Drag reduction is significantly influenced by texture, flexibility, and hydrophobicity of these scales.[72–74] Lower drag also allows the water layer next to the skin to move faster, thus, reducing time for micro-organism settlement and helping to wash them away.[75]

In addition, it has been hypothesized that the dimensions of the sharkskin topography could be effective at physically disrupting the interactions between neighboring cells, and the physical obstacles deter small bacterial cell clusters from expansion into microcolonies and subsequent formation of biofilm.[65]

Overall, it can be concluded that µm-scaled topographies may prevent or facilitate biofilm formation, depending on their dimensions and the arrangement of the feature pattern.

Many surfaces with features at the nm-scale and, therefore, being smaller than a single microorganism exhibit reduced bacterial adhesion.[71,76–78] Here, the spatial density of features is of special importance and can be considered as a simple indicator of the number of available contact points for bacterial cells

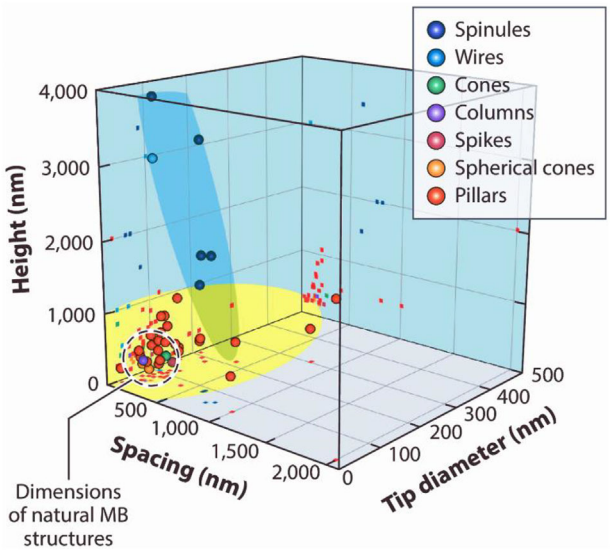

Figure 19. 3D mapping of various synthetic mechano-bactericidal nanoprotrusions; the dashed circle in the lower left corner marks the dimensions of naturally occurring mechano-bactericidal surfaces (data published in[86] and[85]). (Reprinted from[86] Y. Cheng, et al., Mechano-Bactericidal Surfaces: Mechanisms, Nanofabrication, and Prospects for Food Applications, Annu. Rev. Food. Sci. Technol. 14:449, Copyright 2023 under Creative Commons BY 4.0 license. Retrieved from https://doi.org/10.1146/annurev-food-060721-022330).

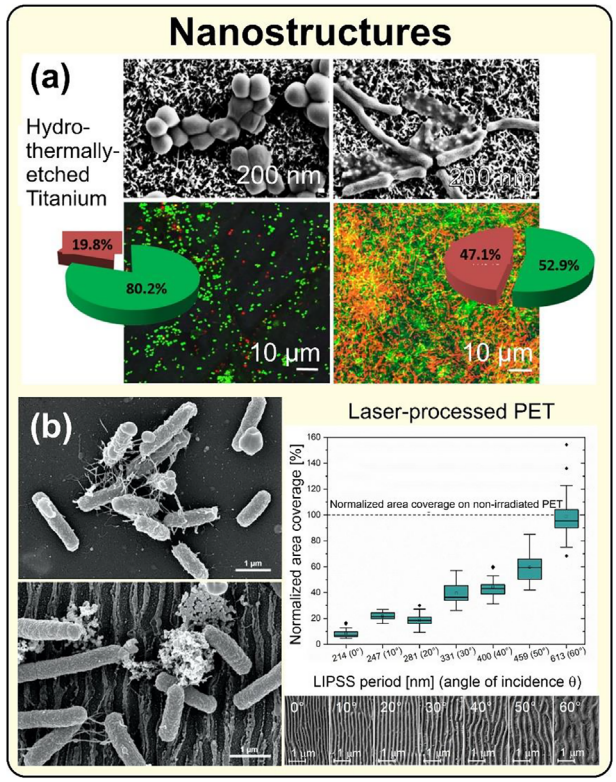

Figure 20. Collage of results of the impact of surface nanostructures on the bacterial colonization. For details refer to the main text. a) reprinted from[91] C.M. Bhadra, et al., Antibacterial titanium nano-patterned arrays inspired by dragonfly wings, Sci. Rep. 5:16817, Copyright 2015 under Creative Commons BY 4.0 license. Retrieved from https://doi.org/10.1038/srep16817; b) reprinted from[67] A.M. Richter, et al., Spatial Period of Laser-Induced Surface Nanoripples on PET Determines *Escherichia coli* Repellence, Nanomaterials 11:3000, Copyright 2021 Creative Commons BY 4.0 license. Retrieved from https://doi.org/10.3390/nano11113000).

based on their dimensions (Figure 18b). A strong dependence of bacterial adhesion on structure dimensions and densities could be demonstrated for topographies like cones and holes or laser-induced periodic surface structures (LIPSS)[67,79,80] (Figure 18c).

Moreover, nanostructured surfaces may also act mechano-bactericidal (Figure 18a (i,ii)). The lethal mechanisms of nanostructured surfaces are associated with a surface composed of nanopillars and -edges that induce the mechanical stretching and rupture of the bacterial membrane.[81,82] Surfaces composed of sharp nanopillars may also induce pore formation in the bacterial cell membrane followed by cell death (fast piercing).[83] Pillar density, radius, height, and aspect ratio play significant roles in deciding bactericidal activity. The majority of nanopattern dimensions of pillars, cones, spikes, or nanowires with bactericidal efficacy lie in the range of 100 nm < Height < 500 nm, 10 nm < Diameter < 300 nm, and 10 nm < Spacing < 330 nm, but also structures with a height of up to 5 µm are occasionally reported to act bactericidal, see **Figure 19**.[84,85]

Another class of surface features at µm-scale or hierarchical features at combinations of µm-nm-scales result in superhydrophobic surfaces with structures that allow the formation of air-pockets (like Lotus- or Salvinia-leaf inspired structures) that prevent the contact between bacterial cells and surface as shown in Figure 18c. However, air pockets are reported to be short-lived as they are replaced by the surrounding liquid.[87–90]

Figures 20–22 compile selected results from the literature, ordered according to the topographical surface characteristics, i.e., demonstrating the impact of nanostructures (Figure 20), microstructures (Figure 22), and hierarchical micro-nano-structures (Figure 21) on bacterial growth.

Figure 20a presents *S. aureus* (left part) and *P. aeruginosa* (right part) on nanostructured titanium samples after being subjected to hydrothermal etching. The top part displays SEM micrographs (scale bar 200 nm), while the bottom part assembles confocal laser scanning microscopy (CLSM) fluorescence images after Live/Dead staining. Green and red colors of bacterial cells correspond to viable and non-viable bacteria, respectively (scale bar 10 µm). The antibacterial activity of the samples is shown in pie charts. For comparison (not visualized here): on "as-received" titanium without nanostructures, the proportion of viable cells was >90 %.[91]

Figure 20b (left column) assembles results on the influence of the spatial period of laser-induced surface nanogratings (LIPSS, type LSFL) on poly(ethyleneterephthalate) (PET) surfaces on adhesion behavior of *E. coli*. The left part shows top-view SEM micrographs of *E. coli* TG1 on non-irradiated (top) and laser-nanostructured (bottom) PET with 214 nm LIPSS spatial period. Nanofiber-like cell appendages and extracellular matrix are visible. The right column (top part) shows Box–whisker plots of the relative surface areas covered by *E. coli* TG1 after 24 h incubation on flat and LIPSS-covered PET, normalized to surface coverage on flat PET. Bacterial attachment clearly depended on the

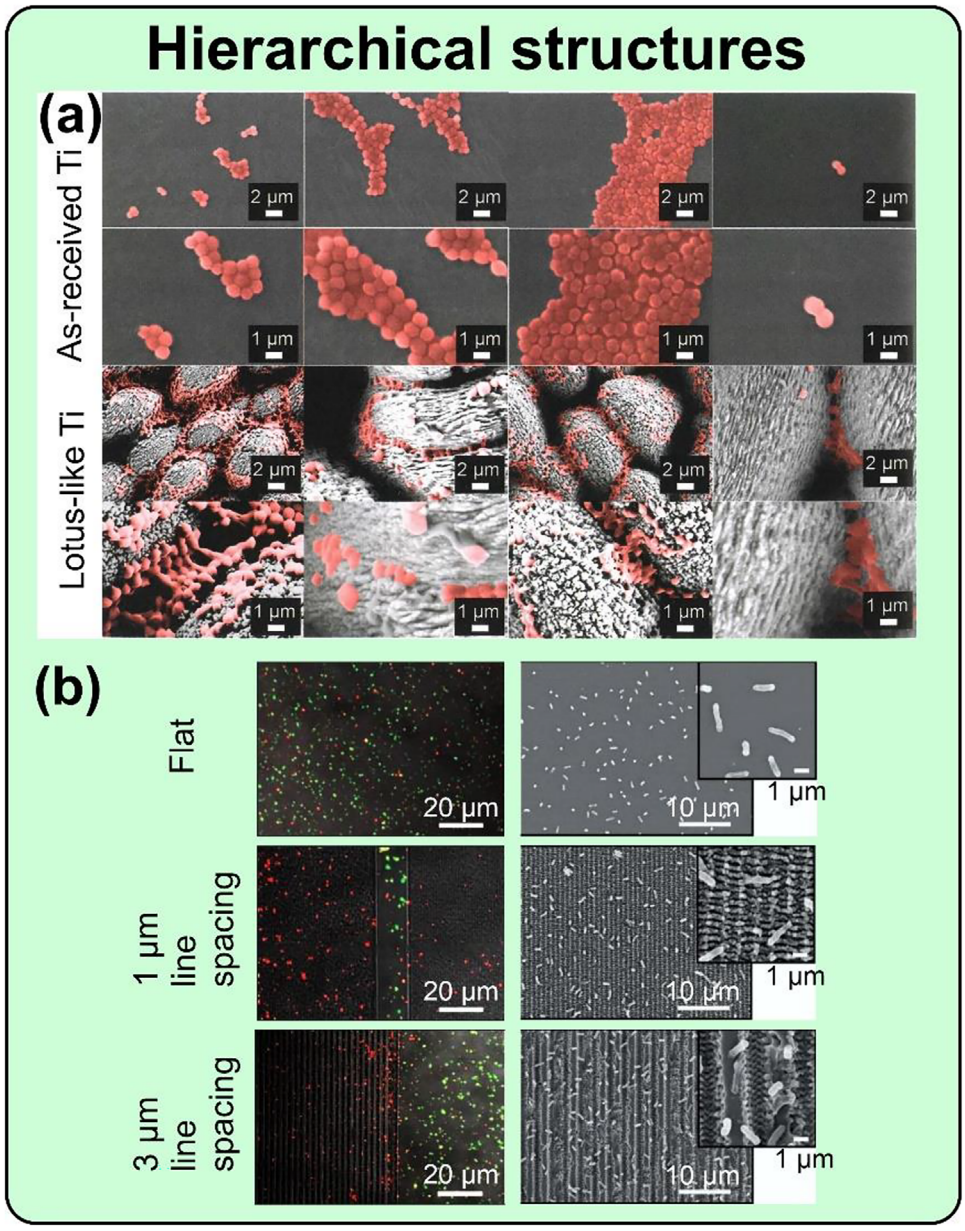

Figure 21. Collage of results of the impact of hierarchical micro-nano-structures on the bacterial colonization. For details refer to the main text. (a) Reprinted with permission.[88] Copyright 2012, Taylor & Francis Ltd; b) Reprinted with permission.[92] Copyright 2020, Elsevier).

LIPSS spatial period with minimal surface coverage at a spatial period of 214 nm. The bottom part of the right column shows top-view SEM micrographs of laser-structured PET featuring LIPSS of different spatial periods. The variation of the spatial period was achieved by applying the selected angle of incidence $\theta = 0° - 60°$ upon UV ns-laser irradiation.[67]

Figure 21a exemplifies the adhesion behavior of coccoid bacterial species (*Staphylococcus, Planococcus*) on hierarchical micro-nano-structures. Post-colorized SEM images visualize bacterial coverage on as-received (top) and hierarchical Lotus-like (bottom) titanium surfaces after 18 h cultivation. The bacterial cells were localized almost exclusively in the crevices between the microscale topographical features and not on top. The presence of air bubbles within the nanofeatures possibly impaired a tight cell-surface contact, leading to bacteria accumulation in the crevices, where rapid disappearance of trapped air occurs.[88]

Results for rod-like bacteria on another morphology of hierarchical micro-nano-structures are given in Figure 21b. The left part displays CLSM fluorescence images of stained *E. coli* after 18 h incubation on flat or micro- and nanoscale-structured borosilicate glass (scale bar 20 µm). All surfaces were modified by layer-by-layer polyelectrolyte to generate a positive surface charge. The bactericidal effect was followed using a Live/Dead assay where green and red colors of bacterial cells correspond to viable and non-viable bacteria, respectively. The right part of Figure 21b shows SEM images of bacteria on flat and structured surfaces

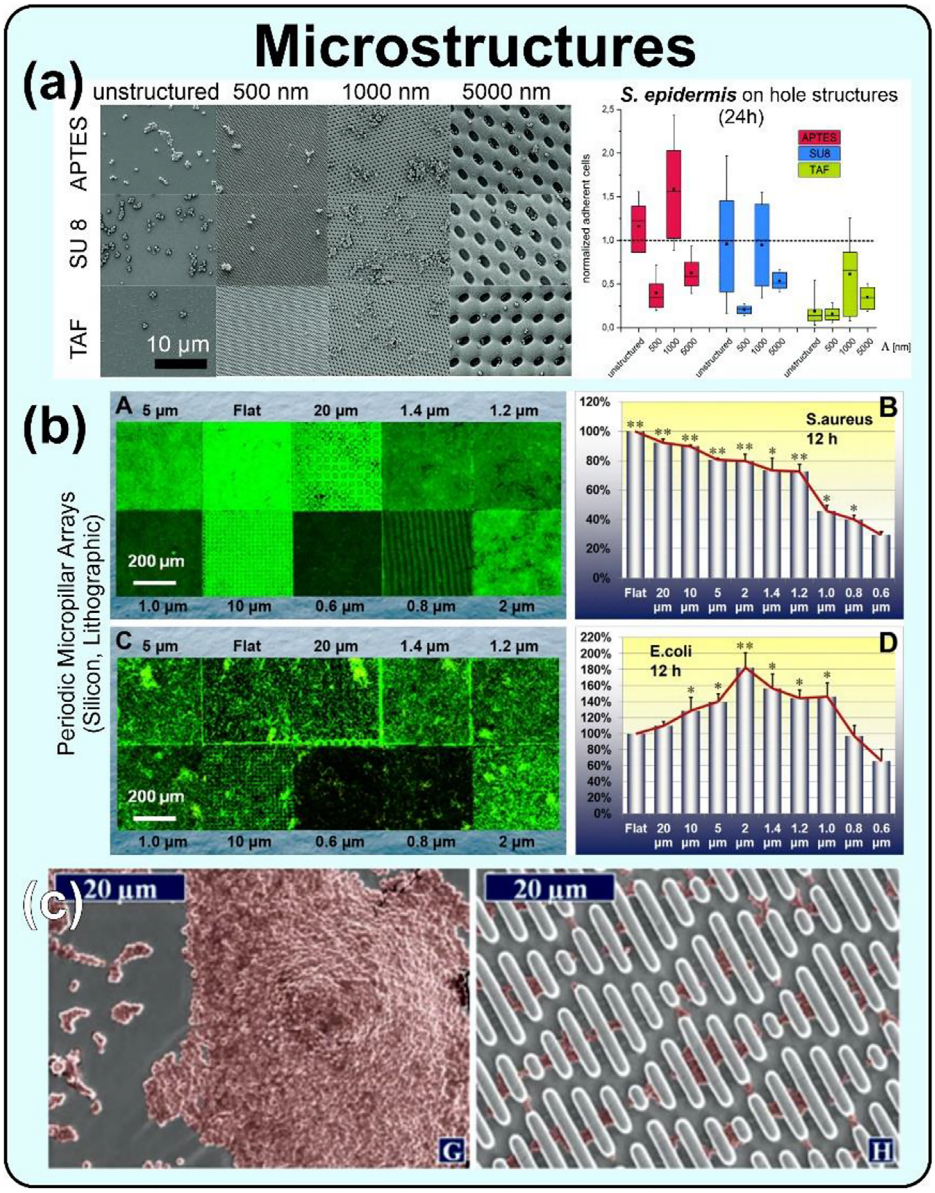

Figure 22. Collage of results of the impact of surface microstructures on the bacterial colonization. For details refer to the main text. (a) used with permission of The Royal Society of Chemistry, from[71] Copyright 2016; permission conveyed through Copyright Clearance Center, Inc.; b) Reprinted with permission.[93] Copyright 2014, John Wiley and Sons; c) Reprinted from[65] K.K. Chung, et al., Impact of engineered surface microtopography on biofilm formation of *Staphylococcus aureus*, Biointerphases 2:89-94, Copyright 2007, American Vacuum Society under Creative Commons BY 4.0 license. Retrieved from https://doi.org/10.1116/1.2751405).

(scale bar 10 µm, 1 µm for the insets). The combination of surface structure and surface charge resulted in an enhanced bactericidal effect against *E. coli*.[92]

Figure 22a addresses the role of micrometric holes on bacterial adhesion behavior. The left part compiles SEM images of *S. epidermidis* on functionalized APTES- ((3-aminopropyl) triethoxysilane), SU8-photoresist, and TAF- (amorphous fluoropolymer) hole structures (scale bar 10 µm). The materials differed in their water contact angle, with TAF displaying the most hydrophobic and APTES the most hydrophilic character. Box-whisker plots in the right part display the number of adherent *S. epidermidis* cells after 24 h, normalized to the median of unstructured SU8. Hole-pattern periodicities in the range of the cell size increased, whereas smaller periodicities decreased cell retention, independent of contact time (minutes to hours) and surface hydrophobicity.[71]

Figure 22b resumes bacterial adhesion patterns on photolithographically structured silicon surfaces, featuring periodic (2D) gratings of square-shaped pillars of 3 µm heights with periods in the micrometer to sub-micrometer range (pillar width = length = spacing). The left part displays typical CLSM fluorescence images of stained *S. aureus* (top) and *E. coli* (bottom) after 30 min of culture. The right provides two bar graphs illustrating the retention of *S. aureus* and *E. coli* on structured surfaces, normalized

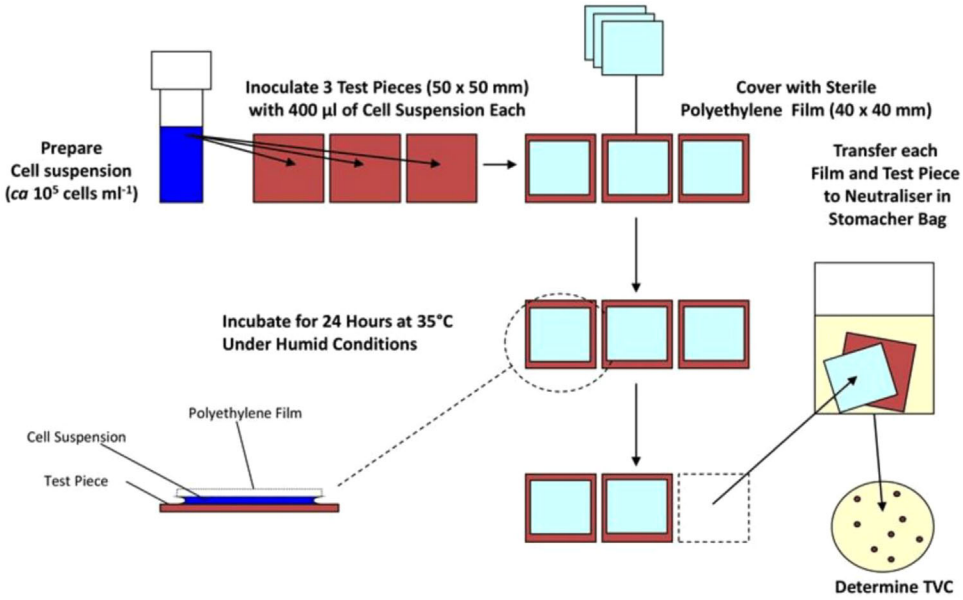

Figure 23. Diagram describing essential steps of the ISO 22196 procedure. TVC: total viable count. (Reprinted from[96] A.J. Cunliffe, et al., How Do We Determine the Efficacy of an Antibacterial Surface? A Review of Standardised Antibacterial Material Testing Methods, Antibiotics 10:1069, Copyright 2021 under Creative Commons BY 4.0 license. Retrieved from https://doi.org/10.3390/antibiotics10091069).

to that of a flat surface. The *S. aureus* population decreased with decreasing pillar size. In contrast, pillar patterns favored adhesion of *E. coli* compared to the flat surface unless the pillar size is reduced to a sub-µm level.[93]

In Figure 22c, an artificial sharkskin-inspired surface micropattern was tested for bacterial response. The post-colorized SEM images of *S. aureus* were taken after 14 days of cultivation on flat and structured (Sharklet AF) PDMSe surfaces. The sharkskin-like topography reduced bacterial coverage and delayed biofilm formation compared to unstructured surface.[65]

4. Selection of Bacterial Test Conditions and Assessment Procedures

This section provides an assessment of experimental setups and approaches for characterizing biofilm growth, bacterial adhesion, and contact killing on textured surfaces.

4.1. Selection of an Appropriate Experimental Setup

To evaluate the antibacterial efficacy of laser-textured surfaces, reproducible, and inter-comparable test conditions have to be applied that ideally mimic the conditions of the intended use and meet adequately the antimicrobial action exerted by the surface topography. The antibacterial action of a surface topography without the release of chemical agents could be either killing bacteria directly upon adhesion (mechano-bactericidal, contact killing) or prevention of adhesion (antifouling). Adequate evaluation methods for mechano-bactericidal activity can be classified in methods comprising high area-to-volume ratio (ratio of sample surface to volume of bacterial suspension), adhesion methods, and biofilm methods.[94]

"Industrial standard evaluation tests" do exist, but they often do not consider the different environmental conditions that are set by the intended application. For example, the industrial standard ISO 22196:2011[95] is a method comprising a high area-to-volume ratio and specifies a process of evaluating the antibacterial activity of plastics and other non-porous surfaces. Originally designed to test surfaces equipped with antibacterial chemical agents, this test method could also be employed to assess the mechano-bactericidal efficacy of surfaces. As this procedure is simple, cheap, straight-forward, and has been widely adopted, important steps of this standard method are outlined in **Figure 23**.

In brief, a surface is inoculated with a bacterial suspension of defined volume and cell number. The surface is then covered with a polyethylene foil and incubated at 35 °C in minimal 90 % humidity for 24 h. Subsequently, bacteria are removed from the surface by mechanical detachment and re-suspended in a neutralizing diluent, before the number of colony-forming units (cfu) is determined as a measure for the number of bacteria that are still viable. However, none of the experimental conditions relate to end-use environments.[96] As a consequence, modifications of ISO 22196:2011 have been introduced. For example, the deposition of the bacterial load onto the surface has been done via spraying to simulate accumulation of airborne bacteria more adequately. Also, bacteria are inoculated onto a filter and then deposited on the test surface to address more realistic humidity conditions which are typically less than the 90 % required in ISO 22196.

"Adhesion-based methods" assess the number of bacteria that adhere from a static or flowing fluid to a surface. Samples are submerged in a suspension with a defined number of viable bacteria and incubated several hours or overnight at a defined temperature. Typically, this method is applied in a batch approach under static conditions, mild shaking (typically 50–100 rpm) or

random flow achieved by stirring, where an intimate contact between bacterial cells and surface is inevitable. In a flow chamber approach, a continuous oriented flow with fresh nutrient medium is switched on directly after inoculation or after an initial static incubation period. Depending on flow velocity and consequent shear forces, only bacterial cells that are tightly attached to the surface are able to stay, proliferate, and grow into a biofilm. The duration of the experiment decides whether primary adhesion or biofilm formation is assessed. Thus, an experimental setup in a flow chamber is particularly suited to test for biofilm formation as used nutrition medium and metabolic products are continuously replaced by fresh medium which allows continuous bacterial cultivation over days and weeks.

Once an appropriate experimental setup has been selected, suitable test organisms have to be defined. When industrial standard procedures are employed, mandatory bacterial test strains are defined like *E. coli* and *S. aureus* when the procedure of ISO 22196 is followed. These strains are representatives of bacteria that are typically found in a clinical context. *E. coli* is a major causative of catheter infections, *S. aureus* is frequently encountered with inflammation of joint prostheses and pacemakers. For materials intended to use in drinking water systems, *Legionella* species would be appropriate test organisms, as these are known to cause Legionnaires' Disease and Pontiac Fever, for food processing facilities *Listeria* are human pathogens. In pipeline distribution systems, microbial corrosion is of major concern typically caused by a diverse group of sulfate-reducing bacteria, which should be employed as test organisms when such an issue becomes important.[97,98] It is obvious that the selection of an appropriate test organism is fundamental to obtain significant results and should be done with respect to the intended application area – if known. Additionally, it must be considered that individual test strains of a single bacterial species differ in their ability to form biofilms at all. Therefore, it goes without saying that biofilm formation of the selected test strain on a non-textured control surface should result in an adequate baseline for further studies. Results obtained by a standardized procedure, like ISO 22196, with the test strains proposed in there will nonetheless provide the information needed to compare different materials for their antimicrobial efficacy and give an indication of how materials could perform under application conditions.

Apart from the selected bacterial test strain, it is essential to bear in mind that for any experimental setup in particular 1) incubation time, 2) starting concentration of the bacteria, 3) physiological state of the bacteria (stationary or exponential phase of growth, see **Figure 24**), and 4) concentration of the nutrients are identified as critical factors that influence test results significantly[99,100] and should, therefore, be documented in detail to obtain reproducible results. For reasons of better reproducibility, it is recommended to use exponentially growing cells. In this growth phase, most bacterial cells in culture are roughly in the same physiological condition and grow at maximum rate. The concentration of living cells introduced into the test setup should be carefully determined for each experiment and should be in line with the intended application area, if possible.

To separate the effect of surface topography from unwanted (mainly chemical) effects introduced by the manufacturing procedure or the environment, a sample preparation procedure is usually established and carried out prior to testing. It typically

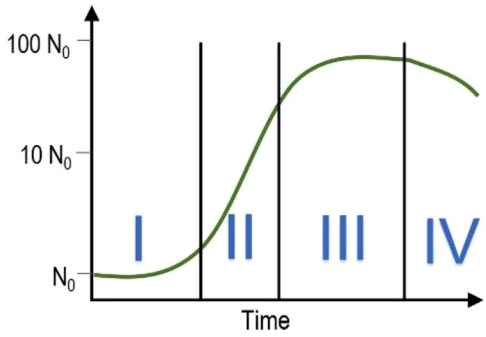

Figure 24. Typical bacterial growth curve (green) of a batch culture in a semilogarithmic plot of logN_0, versus time (N_0 = viable cell number). Growth is divided into four phases. After inoculation of a culture into fresh medium, cells have to adapt to the new environmental conditions (temperature or nutrient changes) and growth will start at a lower speed, also depending on the age of the inoculum (I: Lag phase). During exponential growth phase (II), the time for the doubling of the cell number is constant and maximum. Ongoing depletion of nutrients and accumulation of waste products over time forces the culture into transition, stationary, and finally death phase (stages III and IV, respectively).

comprises steps like washing the samples with detergents, rinsing them with water or buffer, sterilization, drying, storage until use, and should be always carried out in exactly the same manner for each bacterial test. If materials are used that tend to oxidation, the samples might require a conditioning period in an environment with defined temperature and moisture. When samples are ready to use, they should be sterile, dust-free, free of chemical residues from the production or sterilization process, and without drying rims.

4.2. Methods to Assess Bacterial Adhesion or Contact Killing

There are numerous techniques to assess adhesion extent or killing efficiency described in the literature. Nearly all techniques have in common, that a surface washing procedure is required directly after biofilm cultivation to remove loosely attached cells. However, often only a little attention is paid to this step, although it is known to influence results significantly.

Washing could be done either by repeatedly removing all the supernatant and replacing it with fresh buffer or water, by removing and replacing only a part of the supernatant, or by dipping the sample multiple times into fresh buffer. Washing by dipping should be avoided, as by passing the air–liquid interface high detachment forces are exerted that may result in the unwanted removal of previously attached cells.[94] Also, complete removal of the supernatant should be avoided wherever possible to minimize shear forces and to ensure that the biofilm does not dry during the whole testing. Overall, to obtain reproducible and comparable results, a standardized washing protocol should be established and then used for all the samples under investigation in a given laboratory.

To quantify adhesion extent, direct measurements using microscopy are still the "gold-standard" and probably most widespread (**Figure 25**). Especially fluorescence microscopy is becoming increasingly popular. Manifold fluorescent dyes are available today, and the main targets for fluorescence staining comprise nucleic acids, different proteins, and glycoconjugates.[102]

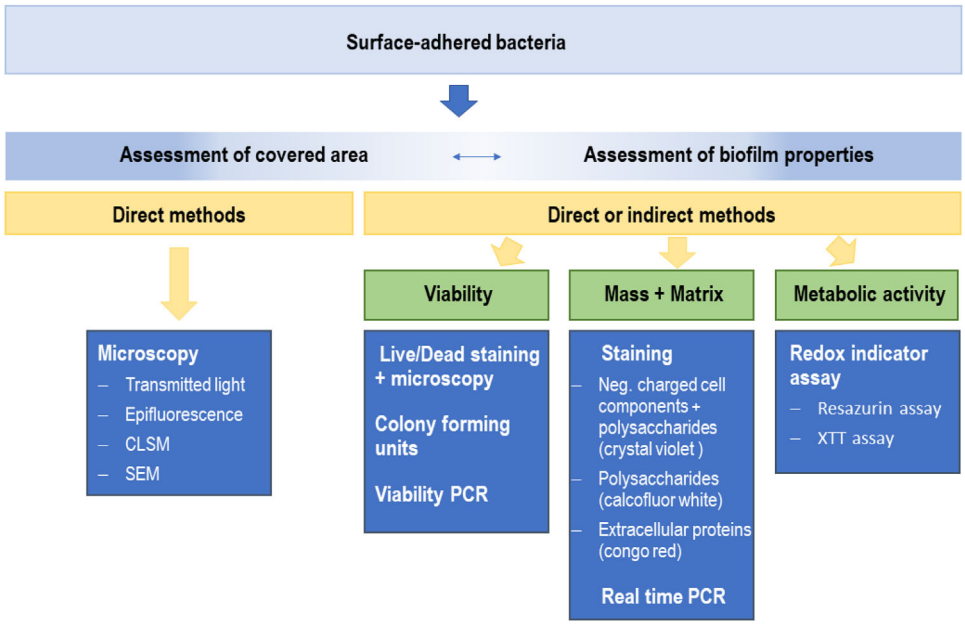

Figure 25. Summary of widely used methods to assess adhesion extent and biofilm properties like mass, viability and metabolic activity. See the text for abbreviations and more details. (Inspired by Azeredo et al.[101]).

For example, the widely used fluorescent dye DAPI (4′,6-Diamino-2-phenylindol) enters viable and dead bacterial cells, but fluorescent dyes are also used to differentiate between viable and dead bacteria (Live/Dead staining). The most common dyes for this are Syto9 (green fluorescent) and propidium iodide (PI, red fluorescent) which are used in combination. The membrane-permeable dye Syto9 enters and stains all cells whereas PI only enters cells with membrane defects, considered to be dead. For evaluation of the results several factors such as bleaching effect of Syto9, background fluorescence, and different binding affinity of Syto9 to live and dead cells must be considered.[103,104]

Epifluorescence imaging is a good choice if the area covered with bacteria is the target value. If the thickness of the bacterial layer or the amount of EPS is in focus, confocal laser scanning microscopy (CLSM) should be preferred. If a fluorescence intensity-related comparison among different surface topographies/textures is aimed at, care must be taken that the depth-of-focus (imaging) is always larger than the laser-induced topographic height modulation (and also the bacterial film thickness). Otherwise, results may not be meaningful since not all fluorescence is properly detected. This constraint may limit the selected microscope objective's magnification factor and could be particularly relevant for the assessment of surface microstructures such as the self-ordered spikes (see Section 2.1).

In case the substrate material exhibits autofluorescence (occurring, e.g., for many polymeric samples) which interferes with the spectra of fluorescent dyes, reflected light microscopy with safranine of crystal violet bacterial staining could be used alternatively to assess adhesion extent. Electron microscopy, in particular scanning electron microscopy (SEM) or Environmental SEM (ESEM), is widely used to visualize the surface morphology of microcolonies and biofilms and the exact location of bacterial cells relative to the surface topography as well as their interaction with the laser-generated structures.

To characterize the biofilm itself, also indirect techniques are employed (Figure 25). A widely used technique to assess biofilm cell viability is the determination of colony-forming units (cfu). The biofilm mass must be removed from the surface, resuspended, diluted, and plated onto nutrient agar. The number of grown colonies indicates the number of viable cells in the biofilm. The polymerase chain reaction (PCR) is a powerful molecular biological technique that also allows discrimination between live and dead bacteria (viability PCR) and is commonly used for bacteria detection and quantification (real-time PCR).

Specific stains are employed to estimate the amount of certain biofilm components. For example, for quantification of the biofilm mass in total, staining with crystal violet (CV), which binds to negatively charged bacteria and polysaccharides of the EPS, is widespread. The absorbed CV is eluted with ethanol or acetic acid and measured photospectrometrically. Cellulose and polysaccharides with monomers linked via ß-1,4 or ß-1,3 linkage can be stained separately from the cell body with, e.g., Calcofluor white and analyzed via microscopy. Carbohydrate-binding proteins (lectins) are specific to oligosaccharides and are commercially available as conjugates with fluorophores. They allow sensitive detection and localization of specific oligosaccharides on the surface or in between the bacterial cells.

Metabolic activity of a biofilm can be assessed via colorimetric assays using redox-sensitive dyes that experience a change in color upon reduction by cellular metabolic activity, like the yellow tetrazolium salt XTT (sodium 3′-[1-(phenyl aminocarbonyl)−3,4-tetrazolium]-bis (4-methoxy6-nitro) benzene sulfonic acid hydrate) or the non-fluorescent resazurin, which are reduced by cellular metabolic activity and converted to a colored formazan or the pink-fluorescent resorufin, respectively. Color changes are measured photospectrometrically. For more detailed information on currently applied techniques for assessment and characterization of biofilms and a discussion of

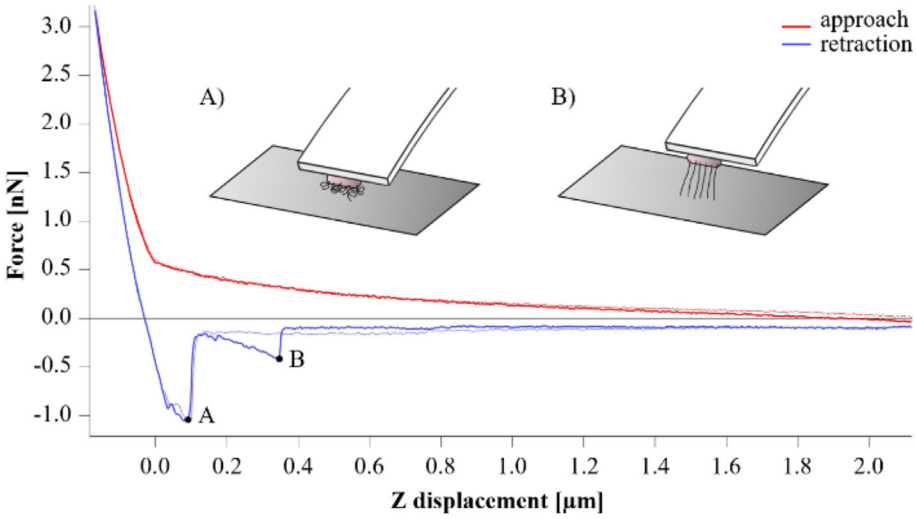

Figure 26. Two force-displacement curves of single *E. coli* cells with (red/blue) or without pili (light grey) when approaching or detaching a polished titanium surface (immersed in buffer). The insets illustrate the contact scenario at the characteristic detachment positions A and B. (Reprinted from[113] J. Zubia Aranburu, et al., Quantification of the adhesion force of *E. coli* on Ti via single-cell force spectroscopy, Libro del Actas, XL Congreso Anual de la Sociedad Española de Ingeniería Biomédica CASEIB 2022:217-220, ISBN: 978-84-09-45972-8, Copyright 2022 under Creative Commons CC BY-NC-ND 4.0 license. Retrieved from https://gib.tel.uva.es/CASEIB2022_LibroActas.pdf).

advantages and disadvantages, the reader is referred to the reviews of Azeredo et al. and Pantanella et al.[101,105]

Some of the techniques considered in Figure 25 require the removal of the biomass from the surface, which is also a critical step and a source of error. Widely used methods are sonication, vortexing (or a combination thereof), or, according to the international standard ISO 18593:2004(E),[106] scraping with a spatula or a cotton swab, and the usage of contact plates. Sampling techniques determined in the ISO 18593:2004(E) are, as defined by this ISO standard, "not quantitatively" reliable or reproducible, and results should only be used in a "trend analysis". One reason for this might be that biofilm removal via spatula or swab from surfaces with complex topographies providing narrow and deep grooves (for example micrometric spikes, as a typical result of laser-processing) is almost impossible. In such a test, bacteria are "mechanically" confined at the tested surface and, thus, will be systematically underestimated.

Beside surface area coverage and metabolic activity of a biofilm, the assessment of the adhesion force between a single cell or cell agglomerate to a surface is a valuable tool to characterize the influence of a surface topography on bacterial adhesion. Atomic force microscopy (AFM) is the state-of-the-art method for the quantification of bacterial adhesion forces on surfaces. To this, a single bacterial cell or bacterial consortium is immobilized on a tipless cantilever, and force–distance curves are experimentally recorded. From these curves, the maximum adhesion force needed to detach a single cell (or consortium) from the surface can be calculated. This method allows the investigation of many different surface binding mechanisms of a bacterial consortium, single-cells, or even at the molecular level. It has been employed to understand the dynamics of lipopolysaccharides, peptides, and extracellular pili and their contribution in modulating bacterial attachment to surfaces.[107–112]

Figure 26 shows exemplary two force-displacement curves for single *E. coli* cells attached to a tipless AFM cantilever when approaching to or detaching from a polished titanium surface (immersed in water). The approach curve is shown in red or light grey, the trigger (maximum approaching) force was set to 3 nN. For a piliated cell, the retraction curve (blue) reveals two force peaks (labeled A and B) with the maximum adhesion force (negative) at position A. The second force peak at position B can be attributed to the binding of pili to the surface while the cell body is already detached. The underlying retraction curve (light grey), with a single force peak at position A corresponds to a non-piliated bacterial cell. Under the test conditions applied, maximum adhesion force of *E. coli* was in the order of 1 nN per cell.

All bacterium-surface interactions are influenced by a large variety of physical and/or chemical parameters like surface charge, wettability, roughness, and topography, in combination with environmental factors like composition of the surrounding medium. In addition, the development of a conditioning film (a thin layer of complex substances like adhering proteins, polysaccharides or humic substances deposited on a surface immersed in liquid) can modify the physico-chemical properties of the solid surface by altering its chemistry, charge, or surface energy and, thus, affect local adhesion.[52]

Note that not only the choice of assessment method but also the experimental environment has a strong influence on the results as demonstrated impressively by the study of Michalska et al.[114] Significant variations in bactericidal efficiencies of chemically etched silicon towards two different bacterial species (*E. coli* versus *Rhodobacter capsulatus*) were observed in dependence of the type of liquid medium (with or without nutrients) used for suspension of bacteria during contact with the surface (see **Figure 27**a). Also, absence or implementation of a recovery phase prior to assessment did result in significantly different bactericidal efficiencies (Figure 27b). Further variations of results could be introduced simply by using nutrient-rich or nutrient-free liquids during the recovery phase. In addition, the comparison of two viability assays (plate count method versus

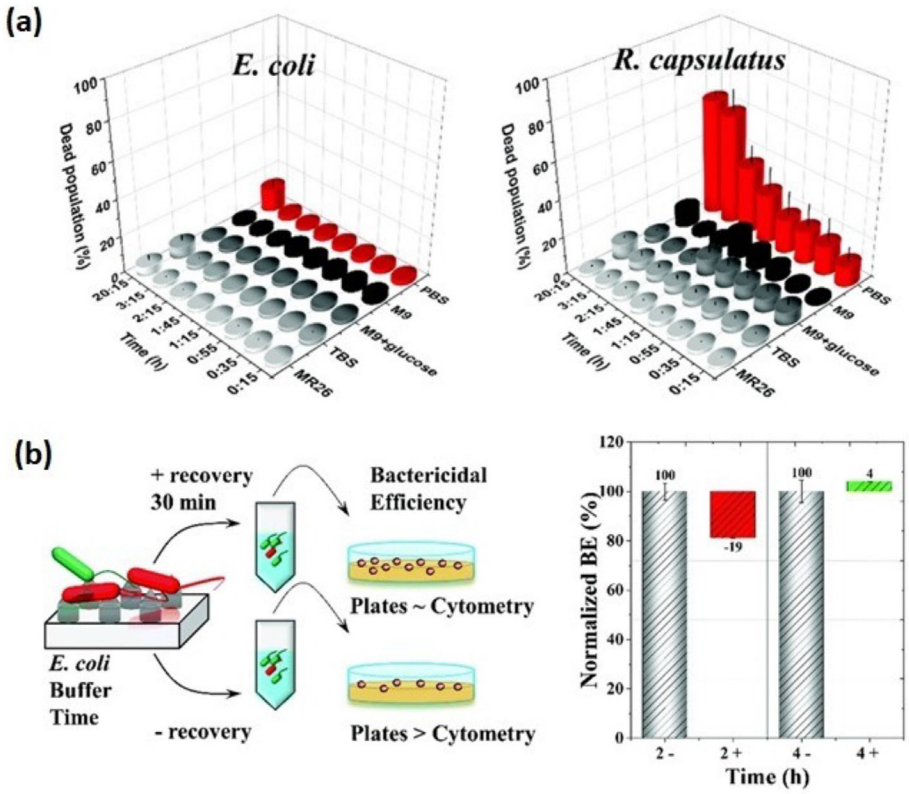

Figure 27. a) Susceptibility of *E. coli* and *R. capsulatus* cells towards the bactericidal impact of structured silicon in dependence of contact time and the type of liquid medium (PBS, M9, M9 with glucose, TBS, or M26) used for bacterial suspension during contact time with the structured surface. Increase in dead population was highest with nutrient-free buffer (PBS) as suspension medium for both strains (expressed as percentage of the total cell population). b) Effect of a 30 min recovery phase in complex medium on bactericidal efficacy of a structured silicon surface with *E. coli* as test strain. Left: outline of the experimental setup. The authors noted that results obtained with plate counting method are not per se the same as obtained by cytometry. Right: Normalized bactericidal efficacy of structured silicon surface after 2 and 4 h contact time with (+) or without (-) a recovery phase prior to plating. After 2 h contact time, a recovery phase decreased bactericidal efficacy by 19 %, after 4 h, a slight increase in bactericidal efficacy could be observed. (Used with permission of The Royal Society of Chemistry, from[114] Copyright 2016; permission conveyed through Copyright Clearance Center, Inc.).

Live/Dead staining plus cytometry) did show that both methods do not necessarily produce consistent results, again depending on the specific experimental environments.

The discussion given above reveals that a direct comparison of scientific results on bacterial adhesion to laser-textured surfaces is often difficult since different experimental setups (static versus dynamic) and biofilm growth conditions (bacterial strains, nutrition, inoculation times, temperatures) and adhesion assessment methods (imaging, fluorescence, staining, etc.) are used in the pertinent literature. A better inter-comparability of the scientific results would be highly desired, underlining a demand for further standardization here.

5. Bacterial Adhesion on Laser-Generated Surface Structures

This section aims to order the overabundant available literature on the impact of laser-processed surface micro- and nanostructures on bacterial adhesion. **Table A1** in the Appendix Section compiles the relevant literature on bacterial adhesion on laser-textured surfaces. For practical use, the literature is ordered there according to the processed material classes (metals, semiconductors, polymers, glasses, and ceramics) being relevant to the laser processing. For each listed publication, the laser-processing strategy is identified (according to Section 2), the geometry of the surface topography (according to Table 1) is listed along with the type of bacteria, the corresponding test methods and conditions, and the key observations. In view of potentially deviating results, special attention should be attributed to particular differences in the sample preparation and biological assessment methods that we listed intentionally in detail in the table.

From the bare number of material-specific table entries, it becomes immediately clear that the focus of scientific interest lies on metals (mainly steel, titanium alloy, and copper) as well as on polymers. Both can be explained by the immense technological relevance of these metals as medical implant materials and by the ubiquity of metals and polymers in the food industry and in our daily life. Most publications report on a reduction of the bacterial adhesion/growth on the laser-textured surfaces of investigation when compared with a non-textured reference surface.

The most relevant findings are briefly summarized and discussed in the following. Note that in some cases listed in Table A1, contradictory effects were reported by different authors/groups. Here, particular care must be taken to identify relevant differences in the laser-processing or the specific bacterial adhesion test procedures and the involved materials.

5.1. Size and Geometry of Laser-Generated Structures

Numerous studies address the role of (laser-generated) topographical features in bacterial adhesion behavior and it is generally agreed that ratios of feature height, width, or pitch to bacterial cell dimensions are significant influence factors. In particular for *E. coli* as test strain it is well documented that a bacteria-repellent effect can only be achieved by surface structuring if the resulting mean size of topographic cones, holes, valleys, and crevices is smaller than the dimensions of the bacterial cell body (for *E. coli*: 0.5 µm × 2 µm).[67,77,79,80,115–121] In general, the importance of reducing the area of contact between a single cell and the surface is pointed out. In this context, Lutey et al. concluded that the Surface-Peak-Density can be considered as a simple indicator of available contact points for bacterial cells based on their dimensions, hence as indicator for bacterial retention.[79] However, it was also noted that surface properties like wettability and average surface roughness might dominate bacterial retention behavior if test strains other than *E. coli* are used.

Not only feature height in ratio to bacterial cell dimension is crucial for bacterial attachment, but also the absolute height and aspect ratio of structures which was investigated in detail by Meinshausen et al. for laser-structured PE and Ti surfaces.[122] Results showed a significantly decreased bacterial coverage on structures with an aspect ratio range of 0.02 to 0.05 with a minimal coverage for an aspect ratio of about 0.02 for PET surfaces. In that work, the aspect ratio was defined as *Rz*/*RSm*, with *Rz* being average profile heights and *RSm* the mean line spacing of profile peaks. For titanium, a reduced adherence for all structured samples compared to a control group could be found and absolute profile height, and not aspect ratio, was crucial here.

A recent study by Lai et al. investigated the far-reaching consequences of grated surfaces at cellular and sub-cellular sizes on bacterial attachment, growth, and generated biofilm volume.[123] With *P. aeruginosa* as test strain, the peak biovolume density was reduced and bacterial cells were more dispersed and isolated on nanogratings with depths greater than or equal to 350 nm. The growth and decline of bacterial cells were also accelerated on nanogratings when compared to flat control surfaces.

The complexity of signaling and sensing pathways that are activated upon bacterial attachment to surfaces highlighted in this study reveals the difficulties one has in making predictions about the influence of topography on bacterial adhesion behavior.

5.2. Laser-Induced Chemistry

Laser-induced surface structuring changes a material's surface in several aspects. It can lead to an increase in surface area and/or might change its wettability and also chemical composition of the surface. Changes in the chemical composition that occur upon laser-processing and oxidation reactions are frequently documented (via X-ray photoelectron spectroscopy (XPS), energy-dispersive X-ray analysis (EDX), TEM, or Raman spectroscopy), and are often, but not necessarily, associated with bacterial adhesion behavior.

Materials that act per se antimicrobial (like Cu or Ni) will very likely show a more pronounced antimicrobial effect when laser-processing results in the generation of holes and cavities that increase the contact area between bacterial cells and surface.[124–127] Additionally, papers describe combinations of surface structure and killing agents like polyaniline,[128] acetylsalicylic acid,[129] and surface charge.[92]

Ahmed et al. revealed the role of the chemical modification of fs-laser DLIP-structured copper-alloy (brass with 37% of Zn, CuZn37) concerning the antimicrobial efficiency through the presence of a near-surface layer of a few hundred nanometers thickness.[130] Multi-method high-resolution chemical and structural characterization confirmed the abundant presence of zinc oxide, along with cuprous oxide and with cupric oxide in a comparatively low concentration. Additionally, transition regions containing Cu-Zn-O were detected. For *E. coli*, the samples exhibited a significantly decreased killing rate on the fs-laser-treated surfaces when compared to the polished surface. The effect was attributed to a reduced release of Cu ions from the laser-modified surface and to an increased corrosion resistance of the zinc-rich oxide phases in wet environments.

Romoli et al.[131] proposed that nanosecond pulsed laser irradiation plays a crucial role in promoting a thin layer of iron oxide that reduces *E. coli* adhesion through local repulsive electrostatic interactions.

The studies of Nastulyavichus et al. indicated that the antibacterial properties of laser-structured steel surfaces can only be attributed to the oxidation products generated by laser processing.[132] The authors claimed that the bacterial inactivation was apparently caused by the photodynamic activity of the nickel nanoparticles due to the generation of singlet oxygen on the surface.

The surface modification of titanium with a fs-laser favors the formation of Ti(IV) oxide which, in turn, contributes to a more hydrophobic surface character, leading to a reduced bacterial adhesion compared to non-irradiated Ti.[133]

Oxidation is not always an unwanted by-reaction, but also employed to generate coatings. Chang et al. developed various composite structures of titanium and vanadium oxide (Ti-V-O) coatings on pure titanium through laser-induced oxidation.[134] In dependence of the laser parameters, the processing leads to the generation of Ti and V oxides and also to a Lotus leaf-like structure with superhydrophobic properties (140° water contact angle) which both contributed to a superior antibacterial effect.

Overall, the chemical composition of the substrate might change during laser-processing, leading to a bacteria-attracting or -repellent character, independent of the substrate's topography and, therefore, experiments aimed to compare topographies should be designed with care.

5.3. Cell Appendages Used for Surface Interaction and Adhesion

The role of cell appendages (e.g., pili, flagella) in adhesion to (laser-structured) surfaces has been discussed in a few studies only, although their impact was demonstrated as pivotal. Most studies cited in Table A1 were conducted with *E. coli*, *P. aeruginosa* and *Staphylococcus* ssp., the latter representing coccoid cells without extracellular filamentous structures such as flagella or pili. In contrast, *E. coli* and *P. aeruginosa* both possess flagella and different types of pili, enabling bacterial motility, surface sensing, and initial attachment (see also Section 3). Thus, the choice of

bacterial test species (and, therefore, the presence and type of flagella or pili) might already exclude several hypotheses on cell-surface interaction, which are based on filamentous cell appendages.

By using piliated as well as pili-deficient *E. coli*, Richter et al. clearly showed that F pili mediate attachment to non-structured PET and also ensure better attachment to laser-structured surfaces.[67] In parallel, Lai combined the results on *P. aeruginosa* biofilm formation to laser-textured surfaces with current knowledge of cell-surface interaction to simulate the effect of motility on surface adhesion and hypothesized that surface nanogratings might reduce pili-mediated surface locomotion and, therefore, microcolony formation.[123] Consequently, especially for those fields of application, where the presence of flagella or pili-harboring bacteria could be a realistic scenario, appropriate test species should be considered with care, as they might overcome bacterial-repellent effects of laser-structuring better than non-flagellated or non-piliated cells.

5.4. (Super)Hydrophobicity Induced by Laser-Structuring

Laser-processing changes topography and chemistry and, in parallel, might also change hydrophobicity of the substrate which, in addition, might change over time.[135,136] Without a doubt, a material's hydrophobicity influences its susceptibility to bacterial adhesion, but consensual results are mainly reported for superhydrophobic surface structures. The low bacterial adhesion to such surfaces is usually attributed to trapped air in between the surface textures which ensures a minimal interaction area between bacteria and substrate.[134,137–140]

Truong et al. proposed a mechanism by which bacterial cells slide across nanoscale bubbles on a Lotus-like structured Ti surface. Bacteria finally accumulate on microbubbles located in the crevices of the structure where they find shelter from liquid turbulences.[88] However, presence and dimension of air pockets on submerged surfaces may change over time, resulting in complete wettability of a surface, thus, limiting the effect of superhydrophobicity.

Beside the surface structure itself, external factors like temperature and turbulences determine lifetime of the air-substrate interface. Experiments performed by Pan et al. revealed that also a contamination of the structured surface with organic matter significantly reduces the durability of the antibacterial effect.[141] So, for comparison of structured materials, the experimental setup and duration of experiment should be considered.

The studies of Lutey et al. and Mateescu et al. clearly show that water repellency plays a very limited role in influencing initial bacterial adhesion and air-trapping does not necessarily avoid bacterial adhesion on surfaces.[79,90] In conclusion, it seems to be the topography, and not the wettability, that dominates a surface's bacterial-repellent properties, and the presence of air/substrate interface is of minor importance only. However, Lutey et al. pointed out that dominance of an individual surface characteristic — e.g., wettability or surface morphology in relation to cell size — in the end depends on bacterial species and the absolute cell size.[79]

In general, laser-structuring is a promising method of choice for surface modification and manufacturing of cell repellent (or cell attracting) surfaces, also with regard to eukaryotic cells (e.g., bone cell integration on implants), which have not been discussed here.

6. Design of Anti-Microbial Surfaces: Challenges and Future Directions

This section discusses challenges of the processing of anti-microbial surfaces with a focus on the laser-texturing step, certain materials aspects, and a critical assessment of the optimum selection of suitable bacterial adhesion tests. Moreover, design aspects and potential concepts for anti-bacterial surfaces are provided and future directions in this field will be outlined.

6.1. Challenges of Laser-Processing: Keep It Uniform and Clean

Certain aspects of laser-processing should be considered for enabling an anti-microbial surface functionality. One aspect is the optimum choice of the laser-processing strategy for a desired surface texture. The different processing strategies discussed in detail in Section 2 may have certain strengths or even disadvantages. Comparing for example the processing of self-ordered LIPSS with that of interference-based DLIP – both well suitable for creating periodic 1D-grating-like surface textures with spatial periods ranging from the micrometer to the nanometer range – certain differences can be identified.[26] As an example, the control of the height (modulation depth) of the laser-induced surface topographies is rather limited for the LIPSS (LSFL and HSFL) and not decoupled from their spatial periods. In contrast, the optical interference pattern realized for DLIP rules its periodicity, while its depth can be independently controlled by the number of laser pulses applied per DLIP-spot. On the other hand, DLIP periods are usually limited to values larger than half the laser irradiation wavelength ($\lambda/2$), while for LIPSS processing with ultrashort laser pulses periods of less than $\lambda/10$ may be created through HSFL. In all cases, the simplicity and robustness of the laser-processing approach must be additionally considered.

Similarly, the optimum choice of the laser-processing strategy for a selected material has to be made. While metals can be easily textured on large surface areas with laser radiation due to the linear absorption mechanisms, the direct processing of transparent (dielectric) materials such as polymers or glasses may be challenging due to the required nonlinear laser-matter interaction and the temperature sensitivity of the processed materials. Here, additional surface absorbing layers may be used for enabling large area-processing.[142] Another appealing strategy may be the laser-texturing of a "master" in a suitable (hard) metal surface, which is subsequently replicated on a (soft) polymer surface via molding. This procedure is feasible even for large surface areas and comes with the additional advantage to exclude any influences of potential laser-induced oxidation or other chemical alterations.

Another important aspect is related to the uniformity of the laser-textured surface topographies. In all cases, where laser beam scanning is involved in the surface texturing process care should be taken to avoid the creation of surface irregularities, such as i) regions that remained non-textured (e.g., due to a too large hatch distance h), ii) severe laser ablation at surface

contaminations (e.g., via increased optical absorption), iii) irregular ablation due to laser-induced heat-accumulation (e.g., through locally varying thermal sample properties), etc. Such unwanted surface spots may act as initial seeds of biofilm growth at "bacterio-philic" surface defects. The latter can counteract a targeted bacteria-repellent effect of the local surrounding. Thus, a very homogeneous laser texturing is required.

A fourth aspect may be relevant if the laser-texturing is performed in the ablative regime, i.e., when material is removed via laser ablation from the treated surface. This usually involves the formation of atomic species, clusters, or nano- and microparticles that are departing from the surface into the surrounding. Most of these are removed via a suction and exhaust system of the laser-processing machine/system but a part of these particles can redeposit around the laser-irradiated spot as so-called "debris". A large part of the debris may be removed by a sample cleaning following the laser-processing. However, the particulates remaining at the surface may also have an influence on the bacterial growth, e.g., if nanoparticles or chemically altered ablation products are created. In such cases, the effects of the laser-generated surface texture must be distinguished from that of the covering residual debris.

Finally, a comment should be made on the surface wettability of laser-textured surfaces that may not be stable and could change over time, potentially affecting the growth of bacteria. For example, the laser-texturing of metals in air environment usually results in hydrophilic or super-hydrophilic surfaces due to laser-induced oxidation. Within a few weeks, however, such samples can turn hydrophobic or super-hydrophobic[143] — even without any measurable change of the laser-induced topography. This phenomenon is caused by the adsorption of hydrocarbon molecules from the ambient atmosphere. These molecules may be partly removed again via surface cleaning activities or thermal treatment, however, it is very difficult to obtain a long-term stable surface-wetting state of the laser-textured surfaces.[144]

6.2. Challenges of Specific Materials: Providing the Ground

Regardless of the surface topography (laser-induced textures or initial roughness) the bacterial adhesion at surfaces may be affected in different other ways by the pristine material itself. Here, chemical aspects must be named, since compound materials can release specific constituents acting toxic to bacteria. A well-known example is brass that was historically used for centuries as material for handles of doors, windows, and other everyday objects being touched frequently by many different persons. Brass is an alloy composed of copper and zinc and has an inherent ability to kill rapidly a wide range of harmful microbes — often within 2 h or less — and with a high degree of efficiency. It acts bactericidal when high concentrations of copper ions are released from the surfaces that are able to generate detrimental perturbations for the bacterial cell induced by the ionic imbalance or excessive production of reactive oxygen species (ROS) that in turn can lead to membrane, protein and DNA damages and eventually to cell death.[145]

Other aspects may arise from surface contaminations that may reside from the manufacturing, e.g., transferred by a rolling process. Also, material imperfections such as microscopic or macroscopic pores or sinkholes may provide a protected habitat for bacteria. Regarding all of these aspects, it is essential to establish a "standard protocol" of efficient surface cleaning and subsequent disinfection that finally brings the surfaces always into a defined state. All samples (laser-processed or not) should be always treated in the same manner to allow a direct comparison of their bio-assessment results. For sensitive materials such as polymers, rubber, etc., care must be taken to not exceed critical temperatures (e.g., for disinfection) or to not use chemical agents/solvents that could affect the material structure, or could induce chemical surface reactions or the subsequent release of material constituents. Similarly, sample storage conditions should be controlled and unified.

6.3. Outlook into the Future: Design Aspects and Potential Concepts for Anti-Microbial Surfaces

The emergence of bacterial multidrug resistance in turn imposes an increasing demand for antimicrobial surfaces that are "safe by design" and act without the use of chemicals. Abundant literature dealing with this topic is available by now and significant progress has been made in understanding how and why some surfaces act bactericidal or bacteria-repellent (antifouling). The upcoming question is here: Do general mechano-bactericidal and antifouling concepts exist?

Looking into nature, general concepts seem to exist. For example, rigid nanopillar arrays with a strong "bactericidal effect" are found on cicada wings. Ivanova et al.[146] demonstrated that the effect is based on the physical structure of the wing, not on its chemistry. Inspired by this, the most common type of bactericidal design of surface nanopatterns under investigation are nanopillars. Generally, effective dimensions for bactericidal nanopatterns are known by now (see Figure 19 above) and are comprehensively described in the review article of Modaresifar et al.[85]

For "antifouling surface structures", various general mechanisms are under discussion, partly also inspired by nature. For example, the leaves of the well-known Lotus plant or of the water fern Salvinia are both strongly superhydrophobic and, for Salvinia, exert a long-lasting air-retaining capacity. For both examples, the superhydrophobicity confers a self-cleaning potential by removing dirt together with rolling-off water droplets, thereby minimizing adherence of organic matter including bacteria, while keeping the leaf dry. Here, hydrophobicity is mainly achieved via hierarchical micro-nanostructures on the leaf surfaces. Note that the Lotus leaf shows an outstanding water repellence particularly on its upper side. The reasons for these properties can be ascribed to the combination of surface micro- and nanostructures with optimized geometry and the unique chemical composition of the epicuticular waxes.[147]

However, even for the most potent surface topography, it is obvious that the spectrum of activity and applicability is limited since the bactericidal or antifouling effects manifest only under certain environmental conditions in combination with the specific bacterial test strains. Generally, for bacteria, clear importance can be attributed to their cell size and shape, the occurrence of cell appendages (pili/flagella), or the ability to EPS production. Once the bacterial test species and strain are defined, a combination with environmental factors that are set

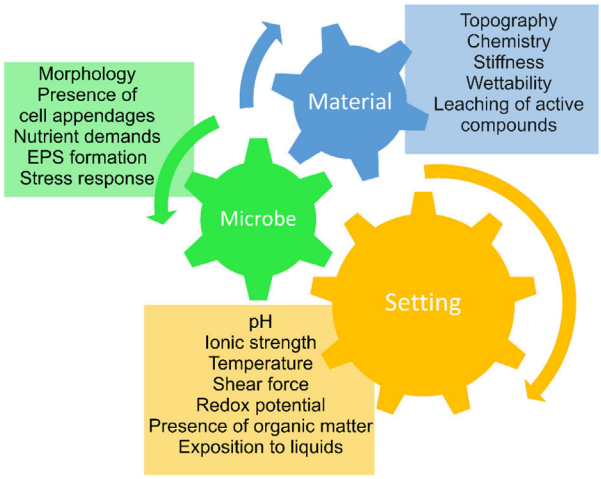

Figure 28. Interacting factors that contribute to microbial adhesion to a surface.

by the specific intended field of application has to be considered. Salt concentration influences adhesiveness with impaired adhesion under low ionic strength compared to high ionic strength conditions[148] but also affects the expression of several cell surface appendages.[149] The availability of organic matter may lead to the formation of a conditioning film that will cover nanorough structures and change the chemistry of the surface, thus, potentially counteracting its topographically desired antiadhesive effect. Temperature influences the physiology and metabolism of bacteria and regulates the expression of certain cell appendages and adhesive proteins, just to mention a few (**Figure 28**).

Additionally, questions regarding the intended application (e.g., medical or technical) should be discussed at the earliest possible stage of surface design. It is important if the functionalized surface will be submerged in a liquid, and if so, whether permanently or occasionally. Nutrient-rich liquids can result in superficial residues from drying, which may interfere with surface structures and encourage microbial attachment. The choice of culture medium and, therefore, nutrient availability, affects cell growth rates and EPS synthesis and can also lead to the formation of a conditioning film. Generally, Lotus-like and easy-to-clean structures might be more suitable for applications, where surfaces were usually kept dry.

If a biological contamination of the surface cannot be avoided, it is necessary to know if the surface is accessible for cleaning. If so, periodically removal of organic material (e.g., cell debris) can ensure accessibility of surface structures. This can avoid the formation of a so-called "secondary biofilm", which may form atop killed bacteria. However, aggressive cleaning may attack sensitive nanostructures in a chemical or mechanical way, particularly for soft organic samples. Here, care must be taken to preserve the functionality of the surface topography. On the other hand, it was proven already that laser-texturing can produce very stable nano-, micro- and hybrid nano-micro-textures at the surface on inorganic materials (e.g., metals) with beneficial tribological properties featuring reduced friction and wear (see the review articles[18,150]).

Such a synergetic surface design combining a bactericidal effect with bacteria-releasing properties was explored by Salatto et al. for nanopillar-covered surfaces – inspired by the anti-bacterial wings of cicada.[151] The authors also presented Molecular Dynamics (MD) simulations revealing that when the bacterium–substrate interaction is strong, the lipid heads of the bacterial cell membrane strongly adsorb at the hydrophilic nanopillar surfaces. This can eventually conform the lipid bi-layer membrane to the curved structure of nanopillars, while locally generating high mechanical stress within the cell membrane as the driving force for its rupture. Membrane rupture then starts with the formation of pores between the nanopillars (i.e., the bactericidal effect) and ultimately leads to the membrane withdrawal from the nanopillar surface (i.e., the bacteria-releasing effect).

It is scientifically and economically significant that the antimicrobial surface effect is durable and stable. The current state of technology may not ensure the development of ever-lasting bacterial-repellent structures. Biofilm and cell adhesion tests performed by studies given in Table A1 were limited with respect to incubation time, thus, statements regarding long-term effects might be inconclusive or impossible to make at all.

Overall, due to its flexibility and wide range of applications, laser-processing is one of the most promising tools for the production of customized surface topographies. Laser-treatment allows the production of different types of surface structures with dimensions from the nanometer to the micrometer scale. Even hybrid micro-nano-structures can be created (see Section 2). These structures can serve for tailored surface functionalization by modifying physical or chemical properties like the surface topography or the chemistry of the top layer, respectively.

On the laser source side, a selection of the laser wavelength can be made to match the material-specific optical absorption. In addition, ultrashort laser pulses can also enable nonlinear absorption of the laser pulse energy, and, therefore, materials that are actually transparent to the laser wavelength can also be processed. The energy density (fluence) / intensity on the target material and the number of laser pulses per spot, as well as the processing strategy, are of particular importance for the final processing result. Depending on the specific requirements for the surface structures, single and multiple beam geometries can be used on 2D- and 3D surfaces, as systematically explored in Section 2.

At present, ultrashort laser-processing rates of the order of $m^2\ min^{-1}$ can be achieved with a clear tendency towards higher processing speeds in the future due to the rapid progress in the field of high-repetition-rate laser sources and novel beam delivery concepts. Since about 20 years the average output power of ultrafast lasers doubles every two to three years and follows a type of Moore's law with the multi-kW level already demonstrated.[152] Ultrafast polygon-mirror-based scan systems currently allow laser beam moving speeds of the order of $km\ s^{-1}$. So, this technique is suitable for application on an industrial scale.

Overall, it can be said that tailoring the surface topography by laser treatment, in combination with a suitable selection of materials, appears to be a powerful strategy to achieve bacteria repellent (or even attractive) surfaces for various applications. Furthermore, a product whose antibacterial effect is based on topography shall be safe by design.

Appendix A

Table A1. Detailed literature survey on bacterial adhesion on laser-textured surfaces.

Material	Processing strategy	Geometry	Bacteria	Test methods	Effect	Ref.
Metals						
Brass / Copper alloy (CuZn37)	DLIP	1D line gratings, Period 3 µm, Depth ≈1.3 µm	*Escherichia coli* (K12 BW25113)	40 µl of 3–5×10^9 cfu/ml (see[125] for cfu/ml), stationary phase culture, nutrient-free solution, Inc(22 °C, 30–120 min, SI), cfu quantification	Decreased bactericidal activity of laser-structured surfaces due to reduced release of Cu ions as consequence of laser-induced chemical alterations	[130]
CoCrMo alloy	DLW: Meandering area processing	Rosette-like markings with secondary micro- /nano-sized features such as ripples, radial lamellae, nanospikes	*Staphylococcus aureus* (ATCC 6538)	1–2.4×10^6 cfu/ml, diluted stationary phase culture, complex medium, Inc(37 °C, 24 h, 100 rpm), S(LIVE/DEAD), FM, SEM	No antibacterial effect was observed in the laser-treated CoCrMo	[153]
Copper (99.95 %)	DLIP	1D line gratings, Period 4.7 µm or 18 µm, Height ≈1 µm	*Escherichia coli*, *Variovorax spec*.	13 µl of 2.15×10^9 cfu/ml, diluted stationary phase cultures, complex medium (*E. coli*), minimal medium (*Variovorax*), Inc(°C n.s., 0–120 min, SI), S(LIVE/DEAD), FM	*E. coli*: up to 100 % killing within 5 min, *Variovorax*: up to 87 % killing within 2 h	[124]
Copper (> 99.95 %), with and without chemical etching (3% citric acid) after laser-processing	DLIP	1D line gratings, Period 2.2 µm, Height ≈1 µm	*Escherichia coli* K12 (BW25113)	120 µl of 3–5×10^9 cfu/ml, stationary phase culture, nutrient-free solution, Inc(°C n.s., 30–120 min, SI), cfu quantification, SEM	Laser-structuring increased quality and quantity of contact of bacterial cells on the surface, hereby enhancing antimicrobial effects of copper; Reduction of bacterial cell viability of up to 15-fold on laser-processed surfaces in comparison to smooth surfaces	[125]
Copper (99.1 %)	Spikes	Irregular hierarchical micro-nano-structures; microscale protuberances and wrinkles with an average Width of 100 µm on the surfaces and mesoporous nanostructures ≈3 – 22 nm	*Escherichia coli* (ATCC 25922), *Pseudomonas aeruginosa* (ATCC 1827), *Staphylococcus aureus* (ATCC 25923), *Staphylococcus aureus* (MARS USA 300)	10^5 to 10^8 cfu/ml, diluted stationary phase culture, nutrient-free solution, Protocol 1: 25 µl *E. coli* on Cu, Inc(22 °C, 2 h, SI); Protocol 2: 25 µl on Cu, Inc(37 °C, 0–150 min, SI); for both protocols: cfu quantification, Protocol 3: 25 µl of 10^8 cfu/ml, stationary phase culture culture of *E. coli* or *S. aureus*, nutrient-free solution, Inc(22 °C, 0 and 2 h, SI), S(LIVE/DEAD), FM	Depending on the strain and initial cfu, LT(laser-textured)-Cu needs 40–120 min to completely eradicate bacteria and causes membrane damage to the bacterial cells immediately after exposure, most likely due to superhydrophilic property and higher surface Cu_2O content of the LT-Cu	[126]
Copper alloy (M1M)	Spikes	Irregular hierarchical micro-nano-structures; Surface covered by aggregated copper oxide nanoparticles with diameters of tens of nanometers, aggregated to several hundred nanometers in size	*Escherichia coli* (K12 C600), *Klebsiella pneumoniae* (811)	10^7 cfu/ml, stationary phase culture, complex medium, Protocol 1: 10 µl inoculum (≈10^5 cfu), Inc(°C n.s., 30 min to 6 days, SI), cfu quantification; Protocol 2: 15 ml inoculum (≈1.5×10^8 cfu), Inc(22 °C, 6 days, SI), cfu quantification, SEM	Death of bacterial cells adsorbed on textured surfaces occurred due to disintegration and perforation of the outer membrane & also cells in suspension will be killed, if suspension comes in contact with the copper	[127]

(*Continued*)

Table A1. (Continued)

Material	Processing strategy	Geometry	Bacteria	Test methods	Effect	Ref.
Gold	LIPSS	1D line gratings (LSFL-I), Period 0.58 µm, Height n.s., Irregular hierarchical micro-nano-structures, 1D rods, cones, spherical nanoparticles (Diameters > 10 nm)	*Escherichia coli* (K12 DH5α)	1.6×10^7 cfu/ml, stationary phase culture, complex medium, growth phase n.s., Inc(37 °C, 24 h, 80–100 rpm), SEM	Except for surfaces with only random nano-roughness, all structures significantly reduced the formation of bacterial colonies, LSFL-I with strongest antibacterial adhesion properties of 99 %	[154]
Magnesium alloy (MA8)	Spikes	Irregular hierarchical micro-nano-structures; Surfaces decorated with micro- and nanoparticles of magnesium oxide	*Escherichia coli* (K12, C600)	5×10^7 cfu/ml, stationary phase culture, complex medium, Inc(37 °C, 15 min – 24 h, SI), cfu quantification, SEM	Bactericidal effect developed earlier and stronger on laser-structured samples (after 24 h up to 100 % killing)	[155]
NiTi alloy, with and without fluorination	LIPSS & Micro-holes	Hierarchical micro-nano-structures, Self-ordered honeycomb-like micro-holes of 28 µm diameter, 47 µm depth, 40 µm period	*Staphylococcus aureus* (ATCC 25923), *Pseudomonas aeruginosa* (ATCC 27853)	10^8 cfu/ml, diluted stationary phase cultures, complex medium, Inc(37 °C, 24 h, SI), S(LIVE/DEAD), FM, SEM	Coverage was reduced by factor ≈6 for both strains (mainly due to stable air-liquid interface)	[140]
Steel (V4A), Steel (S235JRC)	LIPSS	1D line gratings (LSFL-I), Period 0.7 µm, Height n.s.	*Escherichia coli* (BAM 237), *Staphylococcus aureus* (BAM 480)	OD 0.0375, diluted exponential phase culture, complex medium, Inc(37 °C, 3/20 h, FC), S(DAPI), FM	Reduced (*E. coli*) or increased (*S. aureus*) adherence	[77]
Steel (surgical stainless steel, n.s.), Steel (austenitic stainless steel, n.s.)	LIPSS	1D line gratings (LSFL-I) of different roughness (n.s.)	*Staphylococcus aureus*	cfu/ml n.s., stationary phase culture, medium and Inc n.s., S(LIVE/DEAD), FM, SEM	Antibacterial effect for laser-structured surgical stainless steel; bacterial inactivation related to the photodynamic activity of the nickel nanoparticles due to the generation of singlet oxygen on the surface	[132]
Steel (AISI 304L)	LIPSS, Spikes	1D line gratings (LSFL-I), Period n.s., Height n.s., surface/roughness parameters *Sa* 11 – 75 nm, *Sq* 18 – 42 nm, *Spv* 226 – 5633 nm; Irregular hierarchical Spikes, Period n.s., Height n.s., surface/roughness parameters *Sa* 9 – 32 µm, *Sq* 10 – 39 µm, *Spv* 60 – 180 µm	*Staphylococcus aureus* (NCIMB 11832 / NCTC 4163)	10^6 cfu/ml, stationary phase culture, suspension in water or milk sprayed onto samples, up to 20 cycles of SI and drying (1 h) followed by cleaning, S(acridine orange), FM	Assays conducted with bacteria-water suspensions revealed lower adhesion compared to bacteria-milk suspensions. Bacterial adhesion on Spikes was less pronounced compared to LIPSS and influenced by the Spike size	[156]
Steel (AISI 304L)	Spikes	Irregular hierarchical micro-nano-structures, Average roughness R_a 0.2 – 15 µm	*Escherichia coli* (K12 pVIB, *lux* genes expression from plasmid), *Acinetobacter baumannii* (MAR002)	*E. coli*: 1 µl of OD600 ≈0.3, exponential phase culture, complex medium, Inc(22 °C, 0.5/1/2.5 h, SI), cfu quantification, bioluminescence measurement; *A. baumannii*: cfu n.s., diluted stationary phase culture, complex medium, Inc(37 °C, 48 h, SI), cfu quantification, SEM	Structure F2-10 revealed 2 log phases reduction of *E. coli* adherence already after 0.5 h contact time and reduced *A. baumannii* biofilm formation better compared to other structures in this study	[157]

(*Continued*)

Table A1. (Continued)

Material	Processing strategy	Geometry	Bacteria	Test methods	Effect	Ref.
Stainless steel (AISI 316L)	LIPSS	1D line gratings, Periods 0.8 – 1.0 µm, Heights < 0.4 µm	*Escherichia coli*, *Staphylococcus aureus*	3 ml of a 10^5 cfu/ml, stationary phase culture, nutrient-free solution, Inc(37 °C, 24 h), S(DAPI), FM, AFM	Reduced coverage rates on LIPSS surfaces for all materials for both organisms by factor 10 to 16; decreased adhesion force on LIPSS surfaces for both organisms	[158]
Steel (AISI 316L)	LIPSS, Spikes	1D line gratings (LSFL-I), Period 0.5 – 0.9 µm, Areal surface roughness 0.09 µm; 2D arrays of TNP, Periods 0.8 – 1.3 µm, Areal surface roughness 0.06 µm, Irregular hierarchical Spikes, Separation 20 – 40 µm, Areal surface roughness 8.6 µm	*Escherichia coli* (ATCC 8739), *Staphylococcus aureus* (ATCC 6538P)	*E. coli* 10^7 cfu/ml, *S. aureus* 10^6 cfu/ml, stationary phase cultures, diluted complex medium, Inc(24 °C, 2 h, shaking conditions), cfu quantification (detachment by horizontal sampling using swabs)	Reduced adherence for *E. coli* and *S. aureus*	[79]
Stainless steel (AISI 316L); Laser-processed surfaces with and without 2 h immersion to 1 % heptadecafluoro-1,1,2,2-tetrahydro-decyl-1-trimethoxysilane methanol solution and 80° drying in oven	LIPSS	1D line gratings (LSFL-I), Period 0.59 µm, Depth ≈0.18 µm	*Escherichia coli* (NCTC 9001)	2.83×10^9 cfu/ml, diluted stationary phase culture, nutrient-free solution, Attachment assay: inoculum sprayed on substrate followed by washing step; Adhesion assay: inoculum sprayed on substrate, no washing step; Retention assay: 25 ml of suspension with OD 1.0, Inc(°C n.s., 1 h, SI), all protocols: SEM	Following attachment, adhesion and retention assays, lower numbers of bacteria retained on laser-structured surfaces.	[120]
Steel (AISI 316L)	LIPSS, Spikes	1D line gratings (LSFL-I), Period 0.8 µm; Roughness *Ra* = 0.72 µm; Irregular hierarchical Spikes, Separation 10 – 15 µm, Surface roughness 3.1 µm	*Staphylococcus aureus* (ATCC 6538)	10^{10} cfu/ml, growth phase n.s., complex medium, Inc(37 °C, 12 h, SI), Bacterial adhesion force measuring using AFM, S(DAPI), FM, SEM	Reduced adhesion force and bacterial coverage on laser structured surfaces (especially on LIPSS) compared to polished surfaces. Improved detachment (e.g., using ultrasonic vibration) of LIPSS surfaces	[159]
Steel (AISI 316L), with and without fluoro-alkylsilane (FAS) treatment	LIPSS	1D line gratings (LSFL-I), Period 0.59 µm, Height ≈100 nm	*Escherichia coli* (JM109 Promega UK)	OD540 = 1 (≈10^7 cfu/ml), stationary phase culture, complex medium, Inc(37 °C, 30 min & 24 h, SI), S(DAPI), FM	Best bacterial adherence on surface with high roughness, low WCA, high surface free energy; after chemical modification and increase in hydrophobicity of the surface: lowest bacterial retention on high roughness, high WCA and low surface free energy surfaces	[137]
Steel (AISI 316L), S phase pre-treated through active screen plasma nitriding	LIPSS	2D arrays of TNP, Periods 0.88 – 0.94 µm, Channel spacings 0.23 – 0.73 µm, Depth < 300 nm	*Escherichia coli*, *Staphylococcus aureus*	20 µl of 10^4 (*S. aureus*) or 10^5 (*E. coli*) cfu/ml, diluted stationary phase culture, complex medium, Inc(37 °C, 6 h, SI), cfu quantification	TNP reduced adherence by >90 % for *S. aureus* and >75 % for *E. coli*	[160]

(*Continued*)

Table A1. (Continued)

Material	Processing strategy	Geometry	Bacteria	Test methods	Effect	Ref.
Steel (AISI 316L)	DLW	2D arrays of dimples (Diameter ≈50 µm, Separation ≈100 µm); 1D line gratings (h = 100 µm), max. Depth 7 µm	*Escherichia coli* (ATCC 8739)	OD 0.5, diluted stationary phase culture, complex medium, Inc(24 °C, 2 h, SI), cfu quantification (detachment using swap)	Reduction of bacterial adherence by max. 98 % in dependence of energy dose applied during structuring process (mainly due to generation of oxide layers upon laser treatment)	[131]
Steel (AISI 316L)	DLIP, two-step approach	2D square gratings, Period 0.85 µm, Height 0.5 µm, Peak density 1 – 2 μm^{-2}	*Escherichia coli* (ATCC 8739), *Staphylococcus aureus* (ATCC 6538P)	2.6×10^7 (*E. coli*) or 8.2×10^6 (*S. aureus*) cfu/ml, diluted stationary phase culture, complex medium, Inc(24 °C, 2 h, shaking conditions), cfu quantification (detachment by horizontal sampling using swabs)	Reduced adherence by 99.8 % and 70.6 % for *E. coli* and *S. aureus*, respectively	[80]
Steel (AISI 420)	DLW, 3 overscans	2D micro-crossed groove patterns, Period 30 µm, Depth ≈27 µm, additional nanoparticles (debris) present	*Staphylococcus aureus* (CIP 65.8) *Escherichia coli* (ATCC 25922)	OD 0.3 each, exponential phase culture, both strains were mixed in complex medium, Inc(10 min dipping & drying), S(safranin, CV), FM	Reduced adherence of *E. coli* and *S. aureus* by 99 % and 93 %, respectively after 50 min submerged in bacterial solution due to the formation of air cushions on the superhydrophobic surface	[141]
Titanium (99.7 %)	LIPSS,Grooves	1D line gratings (LSFL-I): Periods 0.4 – 0.5 µm, "Grooves" of 1 µm Width and < 1.6 µm Depth	*Escherichia coli* (ATCC 25922)	10^4 cfu/ml, growth phase and medium n.s., Inc(37 °C, 24 h, SI), cfu quantification, SEM	40 – 56 % reduction of bacterial adherence on all types of LIPSS tested	[118]
Titanium (99.6 %, grade 1)	LIPSS	1D line gratings, Period 0.52 – 0.74 µm, Height 0.15 – 0.25 µm	*Escherichia coli* (ATCC 25922) *Staphylococcus aureus* (ATCC 25923)	According to ISO 22196:2001	Morphological and surface chemical composition changes upon laser-structuring resulted in a reduction of cfu by 99 % for *S. aureus* and >80 % for *E. coli*	[133]
Titanium (99.99 %) with silver or selenium nanoparticles	LIPSS	1D line gratings (LSFL-I), Period ≈1 µm, Height n.s.; different nanoscale roughness named "nanoripples" and "nanospikes"	*Staphylococcus aureus*	Cfu n.s., diluted stationary phase culture, medium n.s., Inc(37 °C, 18 h, SI), S(LIVE/DEAD), FM	The most efficient bactericidal type of nanostructures were found to be Ti nanospikes, increasing the dead/alive ratio by ≈8 compared to flat surfaces	[161]
Titanium (grade 2)	n.s.	Irregular dendritic lines after laser-induced surface melting and recrystallization; Average roughness increased to $R_a \approx 1$ µm	*Streptococcus sanguis* (clinical isolate), *Streptococcus mutans* (DSM 10664)	1.5×10^7 cfu/ml, growth phase n.s., nutrient-free solution, Inc(37 °C, 1 h, gentle rotation), S(AO), FM	Differences for laser-processed and polished Ti surfaces were not significant	[162]
Titanium (grade 2)	Spikes	Irregular hierarchical micro-nano-structures (Self-ordered Spike structures), 10 -20 µm size, Nanoscale structures < 0.2 µm	*Staphylococcus aureus* (CIP 65.8), *Pseudomonas aeruginosa* (ATCC 9027)	OD 600 ≈0.3, exponential phase culture, complex medium, Inc(22 °C, 18 h, SI), S(Syto17/concanavalin A), FM, SEM	Increased adherence for *S. aureus*, reduced adherence for *P. aeruginosa* (only EPS, without bacteria was detectable)	[89]

(*Continued*)

Table A1. (Continued)

Material	Processing strategy	Geometry	Bacteria	Test methods	Effect	Ref.
Titanium (grade 2)	Spikes	Irregular hierarchical micro-nano-structures (Self-ordered Spike structures), 5 - 10 µm size, 5 - 10 µm separation, nanoscale structures < 0.8 µm period	*Staphylococcus aureus* (CIP 65.8 & ATCC25 923),*Staphylococcus epidermidis* (ATCC 14990), *Planococcus maritimus* (KMM 3738)	5 ml of OD 0.3 suspensions, exponential phase culture, complex medium, Inc(22 °C, 18 h), S(Syto9/concanavalin A), FM, SEM	Each strain preferentially attached to the crevices located between the microscale surface features, while upper regions of the microscale features remained essentially cell-free. *P. maritimus* showed lowest attachment levels	[88]
Titanium (grade 2)	LIPSS, one-step and two-step (cross-polarized) processing	1D line gratings (LSFL-I), Period 0.71 µm, Height 0.25 µm; 2D crossed grating, Period 0.75 µm, Height 0.175 µm	*Staphylococcus aureus* (ATCC 25923)	7.3×10^8 cfu/ml, stationary phase culture, complex medium, Inc(37 °C, 48 h, SI), S(CFSE), FM, SEM	Laser-treatment reduced significantly the bacterial surface adhesion as well as biofilm formation compared to a polished reference surface	[117]
Titanium (99.2 %, grade 2)	DLW: Meandering area processing	Rosette-like markings with secondary micro-/nano-sized features such as ripples, radial lamellae, nanospikes	*Staphylococcus aureus* (ATCC 6538)	1-2.4×10^6 cfu/ml, diluted stationary phase culture, complex medium, Inc(37 °C, 24 h, 100 rpm), S(LIVE/DEAD), FM, SEM	Laser-treated pure Ti surfaces revealed a noticeable reduction in bacterial adhesion and had a bactericidal effect, most likely due to reduced hydrophobicity, thicker and stable oxide films and laser-induced nano-features	[153]
Titanium (grade 4)	DLIP	1D line gratings, Periods 0.7 – 5 µm, Heights 0.1 – 0.8 µm	*Staphylococcus aureus* (SH1000 pSB2035, GFP expression from plasmid)	OD600 ≈1.0, diluted stationary phase culture, complex medium, Inc(37 °C, 24 h, SI), FM, SEM	Reduced adherence for all structured samples compared to control. Decreasing profile height from 1.5 µm to 0.18 µm reduced adherence. Correlation of *S. aureus* adhesion with aspect ratio of features with minimal adhesion for an aspect ratio of 0.02 – 0.05	[122]
Titanium (grade 4)	DLW, DLIP, DLW +DLIP, DLIP +LIPSS	DLW: 2D arrays of micro-dimples: 50 µm Separation and Diameter; Depths 1.7 – 6.4 µm; DLIP: 2D arrays of 5 µm spatial Period hole-like patterns with Depths < 1.5 µm; LIPSS: LSFL-I of 0.4 µm Period and HSFL-II with 0.15 µm Period	*Escherichia coli* (K12 W3110)	OD 0.001, diluted stationary phase culture, complex medium, Inc(37 °C, 24 h, 80 rpm), SEM	Average bacterial adhesion on the DLW+DLIP combined pattern was reduced by about 30 %	[45]
Titanium (grade 4)	n.s. (Commercial surface finish "Laser-Lok®")	1D line gratings of microchannels, Width ≈8 µm Depths 8.7 – 9.1 µm	In-vivo testing in healthy patients: microbial flora of the mouth	Incorporation of test surfaces into splints, which were worn by probands for 24 h and 48 h, S(Erythrosine), OM, SEM	Laser-Lok® surfaces showed less initial biofilm formation after 24 and 48 h compared to other surfaces (≈50 % and ≈20 % reduction, respectively)	[163]

(*Continued*)

Table A1. (Continued)

Material	Processing strategy	Geometry	Bacteria	Test methods	Effect	Ref.
Titanium (grade 4), infused (coated) with different perfluoropolyethers after laser-processing	DLW, LIPSS, Spikes	1D line gratings: DLW-Grooves of 5 µm Width, 10 µm Period, and 2 µm Depth; LSFL-I of 0.7 µm Period and < 0.7 µm Depth; Irregular hierarchical Spikes of 10 – 20 µm Width and > 11 µm Depth	*Streptococcus oralis* (ATCC 9811)	Biofilm assay: 4×10^{10} cfu/ml, diluted stationary phase culture, complex medium, Inc(37 °C, 18 h, SI), Initial adhesion assay: 3×10^{11} cfu/ml, stationary phase culture, nutrient-free solution, Inc(37 °C, 5 h, 150 rpm); both protocols: S(LIVE/DEAD), FM	Full biofilm coverage on all uncoated surfaces; up to 100-fold reduction of *S. oralis* biofilms on spike structures combined with coating	[164]
Titanium alloy (Ti6Al4V, grade 5)	DLW: Meandering area processing	Rosette-like markings with secondary micro-/nano-sized features such as ripples, radial lamellae, nanospikes	*Staphylococcus aureus* (ATCC 6538)	1-2.4×10^6 cfu/ml, diluted stationary phase culture, complex medium, Inc(37 °C, 24 h, 100 rpm), S(LIVE/DEAD), FM, SEM	Laser-treated Ti6Al4V surfaces revealed a noticeable reduction in bacterial adhesion and had a bactericidal effect, most likely due to reduced hydrophobicity, thicker and stable oxide films and laser-induced nano-features	[153]
Titanium alloy (Ti6Al4V-ELI)	DLW	2D arrays of dimples, Diameters 100 – 400 µm, Periods 200 – 750 µm, Height n.s.	*Escherichia coli* (ATCC 8739)	10^8 cfu/ml, stationary phase culture, complex medium, Inc(37 °C, 24 h, SI), S(LIVE/DEAD), FM, cfu quantification	Increase or reduction of adherence; max. reduction: 2 orders of magnitude (on a 0.3 mm circular microrosette-like structure)	[165]
Titanium alloy (Ti6Al4V-ELI)	n.s. (Commercial surface finish "Laser-Lok®")	1D line gratings of microchannels, Width ≈8 µm Depths 8.7 – 9.1 µm	In-vivo testing in healthy patients: microbial flora of the mouth	Incorporation of test surfaces into splints, which were worn by probands for 24 h and 48 h, S(Erythrosine), OM, SEM	Laser-Lok surfaces showed less initial biofilm formation after 24 and 48 h compared to other surfaces (≈50 % and ≈20 % reduction, respectively)	[163]
Titanium alloy (Ti6Al4V)	LIPSS	1D line gratings, Periods 0.39 – 0.76 µm, Depths 0.08 – 0.15 µm	*Streptococcus mutans* (ATCC 25175), *Porphyromonas gingivalis* (ATCC 33277)	10^8 cfu/ml (*S. mutans*), cfu n.s. (*P. ging.*), diluted stationary phase culture, complex medium, Inc(37 °C, 48 h, 160–180 rpm/SI), S(calcein), FM, SEM	Reduction of adherence for *P. ging.* (0.76 µm LIPSS by 21 %, 0.39 µm - LIPSS by 30 %) but less for *S. mutans* (0.76 µm - LIPSS no reduction, 0.39 µm - LIPSS 4 %)	[119]
Titanium alloy (Ti6Al4V, TC4)	LIPSS	1D line gratings, Periods 0.8 – 1.0 µm, Heights < 0.4 µm	*Escherichia coli*, *Staphylococcus aureus*	3 ml of a 10^5 cfu/ml, stationary phase culture, nutrient-free solution, Inc(37 °C, 24 h), S(DAPI), FM, AFM	Reduced coverage rates on LIPSS surfaces for all materials for both organisms by factor 10 to 16; decreased adhesion force on LIPSS surfaces for both organisms	[158]
Titanium alloy (Ti6Al4V)	DLW	2D arrays of micro-dimples: Distance 40 µm, Diameters 24 – 35 µm, Depths 4.6 – 78 µm	*Staphylococcus aureus* (ATCC 25175)	Static biofilm assay: 50 µl of a 10^5 cfu/ml suspension, colonies (= stat. growth phase) suspended in complex medium, Inc(22 °C, 2 h plus 37 °C, 0/24/72 h, SI), cfu quantification; Biofilm under flow: 10^6 cfu/ml, colonies (= stat. growth phase) suspended in complex medium, Inc(37 °C,12 h, FC), cfu quantification	For static biofilms, micro-texturing resulted in reduced *S. aureus* adhesion (−75 %). On all surfaces, structured and pristine, a significant reduction in *S. aureus* was observed as the duration of incubation increased. Under dynamic flow conditions, laser texturing inhibits bacterial adhesion (−50 %)	[166]

(*Continued*)

Table A1. (Continued)

Material	Processing strategy	Geometry	Bacteria	Test methods	Effect	Ref.
Titanium alloy (Ti6Al4V)	DLW	2D arrays of dimples, squares, triangles, brick-shapes, hexagons, Diameters 54- 297 µm, Heights 38 – 127 µm	*Staphylococcus aureus* (ATCC 6538)	OD 0.1 (cfu/ml n.s.), diluted stationary phase culture, medium n.s., Inc(37 °C, 4 h), SEM	Laser-texturing increased *S. aureus* adhesion from 35 % to 60 % coverage	[139]
Titanium alloy (Ti6Al4V)	Spikes	Irregular hierarchical micro-nano-structures (Self-ordered Spike structures), Distances 5 – 12 µm, Depths > 20 µm, Nanoscale roughness < 200 nm	*Staphylococcus aureus* (36/07)	10 µl of a 10^5 cfu/ml (10^3 cfu) suspension, colonies (= stat. growth phase) suspended in nutrient-free solution, surgical introduction of inoculated test surfaces into tibia of rats, 21 days post-surgery incubation, cfu quantification (detachment by swabbing), FM, SEM	Laser-structured implants showed a higher bacterial load on the implant surface but better bone integrity	[167]
Titanium alloy (Ti6Al4V)	n.s.	2D quasi-periodic arrangements of pits with Spacing between pits of 40, 60, and 80 µm	*Escherichia coli* (DH5α), *Staphylococcus aureus*	cfu/ml n.s (OD 0.6), exponential phase culture, complex medium, Inc(°C n.s., 48 h, SI), CV assay, SEM	Significantly less biofilm formation on laser-textured (superhydrophobic) surfaces (especially for 40 µm spacing), most likely due to air pockets or antibacterial nanotitania	[138]
Titanium alloy (Ti6Al4V)	LIPSS	1D line gratings, Periods 0.65 – 0.85 µm, Average roughness *Ra* 0.1 – 0.25 µm	*Staphylococcus aureus* (ATCC 25 923), *Escherichia coli* (ATCC 25922)	1×10^4 cfu/ml, exponential phase culture, complex medium, Inc(37 °C, 24 h, SI), Resazurin assay, cfu quantification, SEM	*S. aureus*: inhibitory effect of laser-structured compared to unstructured surfaces, but more pronounced when initially unpolished (compared to polished) surfaces were laser-structured; *E. coli*: inhibitory effect only on unpolished laser-structured surfaces (compared to unpolished, unstructured) and signs of cell damage on structured surfaces	[168]
Titanium alloy (Ti6Al4V) with and without fluoro-alkylsilane (FAS) treatment	LIPSS, Spikes	1D line gratings (LSFL-I), Period 0.6 µm, Height ≈0.2 µm; Irregular Spikes, Depth ≈3 µm, Width ≈ 10 µm	*Escherichia coli* (NCTC 9001)	2.83×10^9 cfu/ml, diluted stationary phase culture, nutrient-free solution, Attachment assay: inoculum sprayed on substrate followed by washing step; Adhesion assays: inoculum sprayed on substrate, no washing step; Retention assay: 25 ml of inoculum, Inc(°C n.s., 1 h, SI); all protocols: SEM	No significant differences between textured surfaces for attachment assays (with washing step); regarding adhesion (no washing step) and retention assays, Spikes-covered surface showed lowest cell numbers	[169]

(*Continued*)

Table A1. (Continued)

Material	Processing strategy	Geometry	Bacteria	Test methods	Effect	Ref.
Titanium alloy (Ti6Al4V), with and without silver nanoparticles	DLW	1D line gratings of micro-grooves covered by nano-roughness, 2D arrays of micro-dimples	*Streptococcus oralis* (ATCC 9811)	OD 0.05, diluted stationary phase culture, initial adhesion tests: nutrient-free solution, Inc(37 °C, 5 h, SI); biofilm tests: complex medium, Inc(37 °C, 24 h, SI), both protocols: S(LIVE/DEAD), FM	Up to 50 % reduced biofilm formation	[170]
Titanium alloy (Ti6Al4V), with silver nanoparticles	LIPSS, Spikes	1D line gratings (LSFL-I), Period ≈0.85 µm, Height ≈0.2 µm; Irregular Spikes, Period 2.5 – 10 µm, Depths 2.5 – 6 µm	*Escherichia coli* (ATCC 25922),*Staphylococcus aureus* (ATCC 25923)	10^5 cfu/ml, growth phase and medium n.s., Inc(37 °C, 6/24 h, SI), S(LIVE/DEAD), FM, SEM, cfu quantification	Poorest adhesion on surfaces structured with Spikes (*E. coli*) and LIPSS (*S. aureus*), respectively. Results indicate that bacteria adhesion not only depends on the surface characteristics but also on the bacteria type. The bacteria behavior is inhibited by hierarchical micro/nano-structures and the bacteria are killed by AgNPs	[121]
Titanium alloy (n.s.)	DLW	Microstructure patterns author-named "grooves", "micro-holes", "directional grain pattern", "stripe pattern"	*Staphylococcus aureus* (ATCC 6538), *Staphylococcus epidermidis* (CMCC(B)26069)	10^6 cfu/ml, growth phase n.s., complex medium, Inc(37 °C, 6 h, SI), S(LIVE/DEAD), FM, SEM, cfu quantification	All structures reduced adhesion of both strains significantly	[171]
Titanium alloy (Ti6Al7Nb)	DLW	2D arrays of dimples, Diameter ≈200 µm, Heights 5 – 78 µm, Areal densities 10% – 50%	*Staphylococcus epidermidis* (ATCC 12228)	1.5×10^7 cfu/ml, colonies (= stat. growth phase) suspended in complex medium, Inc(35 °C, 48 h, SI), cfu quantification, CV assay	A correlation was found: for surface free energy (SFE) and depth & density of single texture, for number of adhering bacteria and SFE, for CV absorption and density. No correlation was found between CV absorption and SFE. Facilitated bacterial adhesion on surfaces with a high SFE	[172]
Titanium-vanadium alloy layers ($Ti_{40}V_{60}$) with different subsequent heat treatments	DLW	1D line gratings of microchannels, Period ≈50 µm, Depths < 10 µm	*Staphylococcus aureus*	500 µl of 2×10^7 cfu/ml, growth phase and medium n.s., Inc(37 °C, 6 h, SI), S(Syto9), fluorescence quantification via enzyme-linked assay	Antibacterial effect most likely due to vanadium oxide and titanium oxide and because of superhydrophobic structure (at least for 100 kHz-structure)	[134]
Zr bulk metallic glasses (4 types): V105s ($Zr_{43.3}Cu_{27.8}Ni_{15.2}Al_{9.1}Ti_{4.6}$), V105 ($Zr_{57.5}Cu_{21.1}Ni_{14.2}Al_{3.7}Ti_{3.5}$), 106c ($Zr_{63.2}Cu_{21.4}Ni_{11.3}Al_{4.1}$), Zum ($Zr_{58.9}Cu_{33.2}Ni_{4.2}Al_{3.7}$)	LIPSS	1D line gratings, Period 0.8 µm, Height 50 nm, with nanoscale roughness	*Escherichia coli* (AS1.0.2385), *Staphylococcus aureus* (ATCC 6538)	5 ml of a 10^7 cfu/ml (≈5×10^7 cfu), exponential phase culture, complex medium, Inc(37 °C, 24 h, 100 rpm), S(DAPI), FM	The nanoparticle surfaces and LIPSS exhibited obvious antibacterial adhesion properties (compared to non-treated surfaces, cell adhesion reduced by half)	[173]

(*Continued*)

Table A1. (Continued)

Material	Processing strategy	Geometry	Bacteria	Test methods	Effect	Ref.
Zr bulk metallic glass ($Zr_{43.3}Cu_{27.8}Ni_{15.2}Al_{9.1}Ti_{4.6}$), with and without silver nanoparticles	LIPSS	1D line gratings, Period 0.8 µm, Roughness *Ra* ≈0.46 µm	*Staphylococcus aureus* (ATCC 6538)	10^7 cfu/ml, growth phase and medium n.s., Inc(°C n.s., 1/7/14 days), S(Alexa Fluor 488), re-incubation of planktonic phase, FM, AFM	LIPSS had a better antibacterial adhesion capability compared to NP or polished surfaces	[174]
Zr bulk metallic glass ($Zr_{43.3}Cu_{27.8}Ni_{15.2}Al_{9.1}Ti_{4.6}$)	LIPSS	1D line gratings, Periods 0.8 – 1.0 µm, Heights < 0.4 µm	*Escherichia coli*, *Staphylococcus aureus*	3 ml of a 10^5 cfu/ml, stationary phase culture, nutrient-free solution, Inc(37 °C, 24 h), S(DAPI), FM, AFM	Reduced coverage rates on LIPSS surfaces for all materials for both organisms by factor 10 to 16; decreased adhesion force on LIPSS surfaces for both organisms	[158]
Semiconductors						
Silicon (111)	LIPSS	1D line gratings (LSFL-I processed in air and various liquids), Periods 0.1 – 0.2 µm or 0.9 µm, Heights < 1 µm	*Staphylococcus aureus*	cfu n.s., diluted stationary phase culture, complex medium, Inc(37 °C, 2/24 h), S(LIVE/DEAD), FM	Bactericidal effect on all structures after 2 and 24 h, (control without laser-treatment is missing in biofilm assays)	[175]
Silicon (100)	LIL in combination with Al-layers, lift-off, and subsequent etching	1D line gratings (25 different) of constant groove Width 0.3 µm and different trench Widths (0.1 – 0.5 µm) and Depths (0.05 – 0.65 µm)	*Pseudomonas aeruginosa* (PAO1 fluorescently labelled through genetic insertion of eGFP gene)	15 µl of OD 0.4 culture, exponential phase culture, diluted complex medium, Inc(20 °C, 48/72/96 h, medium changed every 24 h), FM, SEM	Compared to flat surfaces, approx. 1/3 of the nanograting geometries exhibited lower biofilm volume and smaller microcolonies, especially if trenches are deep (>70 % of cell diameter)	[123]
Polymers						
Chitosan	DLW	1D line gratings of micro-channels, Periods 8 – 12 µm, Widths 0.5 – 1.3 µm	*Staphylococcus aureus* (ATCC 25923)	600 µl of 10^8 cfu/ml, growth phase n.s., complex medium, Inc(35 °C, 5 days, SI), SEM	On chitosan surfaces an increase in biofilm formation in the structured regions (most likely due to increased hydrophilicity) was observed	[176]
PCL (3D printed microscaffold)	DLW	1D arrays of micro-channels (depth ≈ 33 µm, width ≈29 µm), 2D arrays of micro-protrusions (height ≈12 µm)	*Staphylococcus aureus* (ATCC25923), *Escherichia coli* (ATCC 25922)	10^4 cfu/ml, growth phase n.s., complex medium, Inc(°C n.s., 6/24/48 h, SI), cfu quantification, SEM	Reduced adherence for *S. aureus* but not for *E. coli*, especially on micro-channels. Loose biofilm, no continuous sticky matrix could be produced by *E. coli*	[177]
PE	LIPSS	Roughness, 1D line gratings, Period 0.6 – 2.0 µm, Height n.s.	*Escherichia coli* TG1 DSM 6056, *Staphylococcus aureus* BAM 480)	10^7 cfu/ml, exponential phase culture, *E. coli*: minimal medium, Inc(37 °C, 3 h, FC); *S. aureus*: complex medium, Inc(30 °C, 21 h, FC); SEM	Reduced (*E. coli*) or non-affected (*S. aureus*) adherence	[116]
PEEK, combined with silver nanoparticles	LIPSS	1D line gratings, Period ≈0.2 µm, Height ≈80 nm	*Escherichia coli* (DBM 3138)	1.1×10^4 cfu, diluted stationary phase culture, nutrient-free solution, Inc(24 °C, 3/24 h, SI), cfu quantification	Strong antibacterial effect after 24 h of treatment, more pronounced in the case of a structured surface (LIPSS without silver nanoparticles were not evaluated for their antibacterial effect)	[178]

(*Continued*)

Table A1. (Continued)

Material	Processing strategy	Geometry	Bacteria	Test methods	Effect	Ref.
PET	DLW (projection method)	2D arrays of dimples, Diameter 15 µm, Distance 20 µm, Roughness *Ra* ≈ 30 µm	*Escherichia coli* (ATCC 25922)	OD600 ≈0.01, diluted stationary phase culture, complex medium, Inc(37 °C, 2 days, FC), S(Syto9), cfu quantification, FM, SEM	Reduction in adherence on structured samples was not significant, bacteria preferably attached to the surface surrounding the engineered dimples	[179]
PET, with and without PANI films	DLIP	1D line gratings, Period ≈1 µm, Height ≈220 nm	*Pseudomonas aeruginosa* (ATCC 15692/PAO1)	100 µl of 10^6 cfu/ml, stationary phase culture, complex medium, Inc(37 °C, 24 h, SI), S(LIVE/DEAD), CV assay, cfu quantification, FM, SEM	When comparing PET modified by PANI (and unstructured) and the same film topographically modified by DLIP, the latter shows fewer biofilm formation, suggesting that PANI is the major biofilm inhibition agent and a synergistic effect is generated by the micro structuring of PANI surface.	[128]
PET	DLIP	1D line gratings, Periods 1.5 – 4.3 µm, Heights 0.1 – 0.6 µm	*Staphylococcus aureus* (SH1000 pSB2035, GFP expression from plasmid)	OD600 ≈1.0, diluted stationary phase culture, complex medium, Inc(37 °C, 24 h, SI), FM, SEM	Correlation of *S. aureus* adhesion with aspect ratio of features with minimal adhesion for an aspect ratio of 0.02 – 0.05	[122]
PET	LIPSS	1D line gratings, Period 0.21 –0.61 µm, Height 64 nm – 117 nm	*Escherichia coli* (TG1)	5 ml of 10^5 cfu/ml, exponential phase culture, minimal medium, Inc(28 °C, 22 h) S(Safranine), OM, SEM	Up to 90 % reduced adherence depending on LIPSS period	[67]
PLLA	DLW	2D arrays of round-shaped micro-protrusions (Diameter 20 µm, Height 3 µm Distance 30 µm)	*Staphylococcus aureus* (ATCC 6538)	1×10^5 cfu/ml, stationary phase culture, complex medium, Inc(37 °C, 24 h, SI), cfu quantification	Bacteria covered modified and unmodified structures in an even, non-preferential manner	[180]
PLLA	DLW	2D scanned areas and 1D line gratings of grooves (Spacing 50 µm)	*Staphylococcus aureus* (ATCC 6538)	1×10^5 cfu/ml, stationary phase culture, complex medium, Inc(37 °C, 24 h, SI), cfu quantification	No significant differences in the number of biofilm-forming cells were observed between the structured samples and the controls	[181]
PI (Kapton®)	DLIP	1D line gratings, Periods 1, 2, 10 µm, Height 150 – 350 nm	*Pseudomonas aeruginosa* (ATCC 15692/PAOl)	100 µl of 10^6 cfu/ml, exponential phase culture, complex medium, Inc(37 °C, 24/48 h, SI), S(LIVE/DEAD), CV assay, cfu quantification, FM, SEM	Adhesion was impaired on structures with periods of 2 µm or below, but not on structures with periods of 10 µm	[182]

(*Continued*)

Table A1. (Continued)

Material	Processing strategy	Geometry	Bacteria	Test methods	Effect	Ref.
PDMS (Sylgard 184), with additional UV/ozone treatment to induce hydrophilicity	LIPSS, DLW	Roughness and porosity, *Ra* n.s. (R1), 1D line grating or 1D arrays with micro-spots, Line separation 11 µm (R2)	*Staphylococcus aureus* (ATCC 25923)	450 µl of a 2×10^5 cfu/ml suspension, mid-log phase, complex medium, Inc(37 °C, 6 h, SI), S(Syto24), FM, SEM	No cell adhesion on R1 surface structures (regardless of hydrophobicity); cell adhesion on R2 structures was more decreased on hydrophobic surfaces compared to hydrophilic ones	[90]
PDMS, surface textures replicated from laser-processed steel master (AISI 430)	LIPSS, DLW	1D line gratings, Period 0.8 – 0.9 µm, Depth 100 – 200 nm; 2D arrayed multiscale micro-nanostructures, Period 40 µm, Height < 6 µm	*Escherichia coli* (BL21 (DE3) pBSK, GFP expression from plasmid)	500 µl of 10^8 cfu/ml, stationary phase culture, nutrient-free solution, Inc(37 °C, 2 h, SI), FM	LIPSS and multiscale structures reduced adherence significantly (by > 89 %)	[115]
PFPE, replicated from laser-processed stainless steel (X6Cr17) master; laser-processing with and without silica microspheres layer	LIPSS, Optical nearfield structuring	1D line gratings (LSFL-I), Period ≈1 µm; 2D arrays of TNP, Period ≈0.9 µm; 2D arrays of hexagonally arranged nanoholes, Spacing ≈ 1 µm, Diameters 0.1 – 1 µm, Depths 0.04 – 0.06 µm	*Escherichia coli* (K12 W3110)	OD 0.4, diluted stationary phase culture, complex medium, Inc(37 °C, 4 h, SI), SEM	Slightly decreased bacterial adhesion on structures showing transitions from hexagonally ordered nanoholes to LIPSS, but strongly increased adhesion on LIPSS structures	[183]
PMMA	DLW	1D line gratings of micro-channels, Periods 8 – 12 µm, Widths 0.5 – 1.3 µm	*Staphylococcus aureus* (ATCC 25923)	600 µl of 10^8 cfu/ml, growth phase n.s., complex medium, Inc(35 °C, 5 days, SI), SEM	For PMMA, no difference was observed on *S. aureus* growth between patterned and non-patterned surface. Hydrophilicity was observed	[176]
PMMA	DLW	2D arrays of dimples, squares, triangles, brick-shapes, hexagons, Diameters 54- 297 µm, Heights 38 – 127 µm	*Staphylococcus aureus* (ATCC 6538), *Escherichia coli* (DH5α)	OD 0.1 (cfu/ml n.s.), diluted stationary phase culture, medium n.s., Inc(37 °C, 4 h), SEM	Laser-texturing reduced *E. coli* adhesion up to ≈54 % (PMMA height 124 µm, diameter 76 µm) explanation: increase in WCA on laser textured compared to non-textured surfaces. Laser-texturing reduced *S. aureus* areal coverage from 20 % to 10 % coverage	[139]
PS	DLIP	1D line gratings, Periods 1,3, 5 µm, Depths 1.6 – 1.8 µm; 2D arrays of "pillars", Periods 1, 3, 5 µm, Depths 1.6 – 1.8 µm; 2D array of hierarchical crossed lines (Periods 6, 8 µm, Depth ≈4.3 µm) and "lamella" (Periods 2 µm, Depths ≈0.47 µm)	*Staphylococcus aureus* (ATCC 15981)	Attachment assay: 2 ml of an 1:100 diluted stationary phase culture, complex medium, Inc(37 °C, 2 h, shaking conditions), Biofilm assay: 10^8 cfu, stationary phase culture, complex medium, Inc(37 °C, 6 h, FC), cfu quantification, SEM	Line- and pillar-like patterns enhanced *S. aureus* adhesion, whereas complex lamella microtopography reduced *S. aureus* adhesion in static and continuous flow culture conditions	[184]

(*Continued*)

Table A1. (Continued)

Material	Processing strategy	Geometry	Bacteria	Test methods	Effect	Ref.
PS, overcoated with gold layer (≈100 nm thick) or silver layer after laser-processing	LIPSS	1D line gratings, Periods 0.2 –0.55 µm, Heights 50 nm – 250 nm	*Staphylococcus epidermis* (DBM 3179)	4×10^4 cfu/ml, stationary phase culture, nutrient-free solution, Inc(24 °C, 2/ 24 h, SI), cfu quantification	The lowest numbers of cfu were observed on PS sample overcoated with silver and LIPSS structures of ≈100 nm height and 0.5 µm period	[185]
PS, doped with acetylsalicylic acid by solvent casting method	LIPSS	1D line gratings, Period ≈0.24 µm, Height ≈0.1 nm; 2D array of self-ordered honeycomb-like micropatterns, Period ≈2.5 µm, Height ≈0.6 µm	*Staphylococcus aureus* (CCM 3953)	4×10^4 cfu/ml, stationary phase culture, nutrient-free solution, Inc(24 °C, 3 h), cfu quantification	Only laser-treatment itself without an antibacterial effect, but combination of LIPSS and acetylsalicylic acid doping strongly decreased bacterial adhesion	[129]
PU, surface textures replicated from laser-processed steel master (AISI 430)	LIPSS, DLW	1D line gratings, Period 0.8 – 0.9 µm, Depth 100 – 200 nm; 2D arrayed multiscale micro-nanostructures, Period 40 µm, Height < 6 µm	*Escherichia coli* (BL21 (DE3) pBSK, GFP expression from plasmid)	500 µl of 10^8 cfu/ml, stationary phase culture, nutrient-free solution, Inc(37 °C, 2 h, SI), FM	LIPSS and multiscale structures reduced adherence significantly (by > 89 %)	[115]
Silicone, surface textures replicated from laser-processed silicon master (wafer)	DLW	2D arrays of micro-protrusions (inverted dimples: Diameters 20 – 40 µm, Separations ≈4 – 13 µm, Depths/Heights 1 – 9 µm	*Escherichia coli* (K12 MG1655), *Staphylococcus epidermis* (RP62a)	10^7 cfu/ml, diluted stationary phase culture, nutrient-free solution, Inc(37 °C, 5 h, SI), S(LIVE/DEAD), FM	Distance between features did not have a significant effect on cell adherence. Non-patterned samples showed a random distribution of biofilm on the surface. On non-patterned surfaces multi-layered biofilm	[186]
Glasses						
Borosilicate glass (D 263TM M, VWR, Stockholm, Sweden), with layer-by-layer (3L) polyelectrolyte overcoatings	DLW	1D line gratings: DLW-Grooves of 1 µm Width, 1 – 4 µm Period, and 1 – 2 µm Depth	*Staphylococcus aureus* (208), *Escherichia coli* (K12)	10^7 cfu/ml, growth phase n.s., nutrient-free solution, Inc(37 °C, 30 min /4 h/18 h, shaking conditions), S(LIVE/DEAD), FM, SEM	Negative charge density of unmodified (non-coated) surfaces led to poor bacterial adhesion on both flat and laser-patterned surfaces, while a combination of surface structure and surface charge resulted in an enhanced adhesion and bactericidal effect	[92]
Ceramics						
Hydroxyapatite (HAp)	DLW	2D arrays of dimples, squares, triangles, brick-shapes, hexagons, Diameters 54- 297 µm, Heights 38 – 127 µm	*Staphylococcus aureus* (ATCC 6538), *Escherichia coli* (DH5α)	OD 0.1 (cfu/ml n.s.), diluted stationary phase culture, medium n.s., Inc(37 °C, 4 h), SEM	Laser-texturing reduced *E. coli* adhesion up to 30 % (HAp, triangles, height 55 µm, diameter 88 µm). Laser-texturing reduced *S. aureus* areal coverage from ≈83 % to ≈72 % coverage	[139]

Acknowledgements

The authors acknowledge the project BioCombs4Nanofibers (http://biocombs4nanofibers.eu). This project has received funding from the European Union's Horizon 2020 research and innovation programme under grant agreement No 862016. The authors would like to thank J. Zubia Aranburu (BAM 4.1) and B. Cappella (BAM 9.5) for the single-cell force spectroscopy measurements presented in Figure 26; I. Feldmann (BAM 4.2), S. Benemann, and T. Lange (both BAM 6.1) for SEM characterization; and D. Thiele (BAM 4.1) for technical assistance.

Open access funding enabled and organized by Projekt DEAL.

Conflict of Interest

The authors declare no conflict of interest.

Keywords

Antibacterial surfaces, biofilms, biomimetic, laser processing, laser-induced periodic surface structures (LIPSS), microbial adhesion

Received: August 7, 2023
Revised: September 22, 2023
Published online:

[1] R. Stoian, J. Bonse, *Ultrafast Laser Nanostructuring — The Pursuit of Extreme Scales*, Springer Nature, Cham **2023**.
[2] J. Schille, L. Schneider, S. Mauersberger, S. Szokup, S. Höhn, J. Pötschke, F. Reiß, E. Leidich, U. Löschner, *Lubricants* **2020**, *8*, 33.
[3] C. Florian, S. V. Kirner, J. Krüger, J. Bonse, *J. Laser Appl.* **2020**, *32*, 022063.
[4] R. M. Donlan, *Emerg Infect. Dis.* **2002**, *8*, 881.
[5] J. W. Costerton, *Int. J. Antimicrob. Agents* **1999**, *11*, 217.
[6] R. M. Klevens, J. R. Edwards, C. L. Richards, T. C. Horan, R. P. Gaynes, D. A. Pollock, D. M. Cardo, *Public Health Rep.* **2007**, *122*, 160.
[7] X. J. Bai, C. H. Nakatsu, A. K. Bhunia, *Foods* **2021**, *10*, 2117.
[8] J. Wingender, H. C. Flemming, *Int. J. Hyg. Environ. Health* **2011**, *214*, 417.
[9] D. Pinna, *Int. Biodeterior. Biodegradation* **2022**, *172*, 105437.
[10] M. Cloutier, D. Mantovani, F. Rosei, *Trends Biotechnol.* **2015**, *33*, 637.
[11] C. Adlhart, J. Verran, N. F. Azevedo, H. Olmez, M. M. Keinänen-Toivola, I. Gouveia, L. F. Melo, F. Crijns, *J. Hosp. Infect.* **2018**, *99*, 239.
[12] D. Bäuerle, *Laser Processing and Chemistry*, Springer-Verlag, Berlin, Heidelberg **2011**.
[13] K. M. T. Ahmmed, C. Grambow, A.-M. Kietzig, *Micromachines* **2014**, *5*, 1219.
[14] A. Žemaitis, M. Gaidys, M. Brikas, P. Gečys, G. Račiukaitis, M. Gedvilas, *Sci. Rep.* **2018**, *8*, 17376.
[15] J.-H. Klein-Wiele, A. Blumenstein, P. Simon, J. Ihlemann, *Adv. Opt. Technol.* **2020**, *9*, 41.
[16] P. P. Pronko, S. K. Dutta, J. Squier, J. V. Rudd, D. Du, G. Mourou, *Opt. Commun.* **1995**, *114*, 106.
[17] A. P. Joglekar, H.-h. Liu, E. Meyhöfer, G. Mourou, A. J. Hunt, *Proc. Natl. Acad. Sci. U S A* **2004**, *101*, 5856.
[18] J. Bonse, S. V. Kirner, M. Griepentrog, D. Spaltmann, J. Krüger, *Materials* **2018**, *11*, 801.
[19] J. Bonse, S. Gräf, *Laser Photonics Rev.* **2020**, *14*, 2000215.
[20] M. Ehrhardt, S. Lai, P. Lorenz, K. Zimmer, *Appl. Surf. Sci.* **2020**, *506*, 144785.
[21] J. Bonse, S. Höhm, S. V. Kirner, A. Rosenfeld, J. Krüger, *IEEE J. Sel. Top. Quantum Electron.* **2017**, *23*, 9000615.
[22] J. Reif, F. Costache, O. Varlamova, G. Jia, M. Ratzke, *Phys. Status Solidi C* **2009**, *6*, 681.
[23] R. Buividas, M. Mikutis, S. Juodkazis, *Prog. Quantum Electron.* **2014**, *38*, 119.
[24] M. J. Abere, M. Zhong, J. Krüger, J. Bonse, *MRS Bull.* **2016**, *41*, 969.
[25] E. Stratakis, J. Bonse, J. Heitz, J. Siegel, G. D. Tsibidis, E. Skoulas, A. Papadopoulos, A. Mimidis, A. C. Joel, P. Comanns, J. Krüger, C. Florian, Y. Fuentes-Edfuf, J. Solis, W. Baumgartner, *Mater. Sci. Eng.: R* **2020**, *141*, 100562.
[26] J. Bonse, *Nanomaterials* **2020**, *10*, 1950.
[27] J. Bonse, S. V. Kirner, J. Krüger, in *Handbook of Laser Micro- and Nano-Engineering*, Springer, Cham **2021**, pp. 879-936.
[28] M. Mezera, C. Florian, G. R. B. E. Römer, J. Krüger, J. Bonse, in *Ultrafast Laser Nanostructuring*, Springer Nature Switzerland AG, Cham **2023**, pp. 827-886.
[29] J.-M. Romano, A. Garcia-Giron, P. Penchev, S. Dimov, *Appl. Surf. Sci.* **2018**, *440*, 162.
[30] S. van der Poel, M. Mezera, G. R. B. E. Römer, E. de Vries, D. Matthews, *Lubricants* **2019**, *7*, 70.
[31] L. Porta-Velilla, N. Turan, A. Cubero, W. Shao, H. Li, G. F. de la Fuente, E. Martínez, A. Larrea, M. Castro, H. Koralay, S. Çavdar, J. Bonse, L. A. Angurel, *Nanomaterials* **2022**, *12*, 2380.
[32] W. Barthlott, M. Mail, B. Bhushan, K. Koch, *Nano-Micro Lett.* **2017**, *9*, 23.
[33] H. J. Eichler, J. Eichler, O. Lux, *Lasers — Basics, Advances and Applications*, Springer Nature Switzerland AG, Cham **2018**.
[34] A. M. Weiner, *Rev. Sci. Instrum.* **2000**, *71*, 1929.
[35] N. Sanner, N. Huot, E. Audouard, C. Larat, J. P. Huignard, B. Loiseaux, *Opt. Lett.* **2005**, *30*, 1479.
[36] K. Sugioka, Y. Cheng, *Adv. Opt. Technol.* **2012**, *1*, 353.
[37] M. Rohloff, S. K. Das, S. Höhm, R. Grunwald, A. Rosenfeld, J. Krüger, J. Bonse, *J. Appl. Phys.* **2011**, *110*, 014910.
[38] S. Höhm, M. Herzlieb, A. Rosenfeld, J. Krüger, J. Bonse, *Appl. Surf. Sci.* **2015**, *336*, 39.
[39] A. Rosenfeld, S. Höhm, J. Krüger, J. Bonse, in *Reference Module in Chemistry, Molecular Sciences and Chemical Engineering*, Elsevier, North Andover, MA, USA **2018**, pp. 338–347.
[40] A. F. Lasagni, *Adv. Opt. Technol.* **2017**, *6*, 265.
[41] M. Mezera, S. Alamri, W. A. P. M. Hendriks, A. Hertwig, A. M. Elert, J. Bonse, T. Kunze, A. F. Lasagni, G. R. B. E. Römer, *Nanomaterials* **2020**, *10*, 1184.
[42] Y. Nakata, *Adv. Opt. Technol.* **2016**, *5*, 29.
[43] A. F. Lasagni, Ph.D. Thesis, Saarland University, Germany **2006**.
[44] D. J. Förster, B. Jäggi, A. Michalowski, B. Neuenschwander, *Materials* **2021**, *14*, 3331.
[45] C. Zwahr, R. Helbig, C. Werner, A. F. Lasagni, *Sci. Rep.* **2019**, *9*, 6721.
[46] S. Alamri, F. Fraggelakis, T. Kunze, B. Krupop, G. Mincuzzi, R. Kling, A. F. Lasagni, *Materials* **2019**, *12*, 1018.
[47] F. Schell, S. Alamri, A. Hariharan, A. Gebert, A. F. Lasagni, T. Kunze, *Mater. Lett.* **2022**, *306*, 130920.
[48] M.-N. Liu, L. Wang, Y.-H. Yu, A.-W. Li, *Opt. Mater. Express* **2017**, *7*, 2208.
[49] S. Küper, M. Stuke, *Appl. Phys. A* **1989**, *49*, 211.
[50] A. T. Poortinga, R. Bos, W. Norde, H. J. Busscher, *Surf. Sci. Rep.* **2002**, *47*, 1.
[51] C. Chagnot, M. A. Zorgani, T. Astruc, M. Desvaux, *Front. Microbiol.* **2013**, *4*.
[52] C. Berne, C. K. Ellison, A. Ducret, Y. V. Brun, *Nat. Rev. Microbiol.* **2018**, *16*, 616.
[53] S. Zheng, M. Bawazir, A. Dhall, H. E. Kim, L. He, J. Heo, G. Hwang, *Front. Bioeng. Biotech.* **2021**, *9*, 643722.
[54] A. Krasowska, K. Sigler, *Front. Cell. Infect. Microbiol.* **2014**, *4*, 00112.

[55] K. Namba, I. Yamashita, F. Vonderviszt, *Nature* **1989**, *342*, 648.
[56] W. Benyoussef, M. Deforet, A. Monmeyran, N. Henry, *Front. Cell. Infect. Microbiol.* **2022**, *12*, 896898.
[57] P. W. Russell, P. E. Orndorff, *J. Bacteriol.* **1992**, *174*, 5923.
[58] C. Beloin, A. Roux, J. M. Ghigo, in *Bacterial Biofilms*, Springer, Berlin, Heidelberg **2008**, pp. 249–289.
[59] B. Maier, *Soft Matter* **2013**, *9*, 5667.
[60] J. M. Ghigo, *Nature* **2001**, *412*, 442.
[61] M. M. Barnhart, M. R. Chapman, *Annu. Rev. Microbiol.* **2006**, *60*, 131.
[62] Y. F. Cheng, G. P. Feng, C. I. Moraru, *Front. Microbiol.* **2019**, *10*, 191.
[63] S. Z. Wu, B. T. Zhang, Y. Liu, X. K. Suo, H. Li, *Biointerphases* **2018**, *13*, 060801.
[64] A. Tripathy, P. Sen, B. Su, W. H. Briscoe, *Adv. Colloid Interface Sci.* **2017**, *248*, 85.
[65] K. K. Chung, J. F. Schumacher, E. M. Sampson, R. A. Burne, P. J. Antonelli, A. B. Brennan, *Biointerphases* **2007**, *2*, 89.
[66] S. M. Wu, F. Zuber, K. Maniura-Weber, J. Brugger, Q. Ren, *J. Nanobiotechnol.* **2018**, *16*, 20.
[67] A. M. Richter, G. Buchberger, D. Stifter, J. Duchoslav, A. Hertwig, J. Bonse, J. Heitz, K. Schwibbert, *Nanomaterials* **2021**, *11*, 3000.
[68] L. Rizzello, R. Cingolani, P. P. Pompa, *Nanomedicine-Uk* **2013**, *8*, 807.
[69] S. Y. Hou, H. A. Gu, C. Smith, D. C. Ren, *Langmuir* **2011**, *27*, 2686.
[70] A. J. Scardino, J. Guenther, R. de Nys, *Biofouling* **2008**, *24*, 45.
[71] R. Helbig, D. Günther, J. Friedrichs, F. Rössler, A. Lasagni, C. Werner, *Biomater. Sci.* **2016**, *4*, 1074.
[72] K. M. T. Ahmmed, J. Montagut, A. M. Kietzig, *Can. J. Chem. Eng.* **2017**, *95*, 1934.
[73] J. Oeffner, G. V. Lauder, *J. Exp. Biol.* **2012**, *215*, 785.
[74] B. Dean, B. Bhushan, *Philos. Trans. A Math. Phys. Eng. Sci.* **2010**, *368*, 5737.
[75] G. D. Bixler, B. Bhushan, *Philos. Trans. A Math. Phys. Eng. Sci.* **2012**, *370*, 2381.
[76] L. C. Xu, C. A. Siedlecki, *Biomed. Mater.* **2014**, *9*, 035003.
[77] N. Epperlein, F. Menzel, K. Schwibbert, R. Koter, J. Bonse, J. Sameith, J. Krüger, J. Toepel, *Appl. Surf. Sci.* **2017**, *418*, 420.
[78] M. X. Tang, C. Chen, J. R. Zhu, H. R. Allcock, C. A. Siedlecki, L. C. Xu, *Bioact. Mater.* **2021**, *6*, 447.
[79] A. H. A. Lutey, L. Gemini, L. Romoli, G. Lazzini, F. Fuso, M. Faucon, R. Kling, *Sci. Rep.* **2018**, *8*, 10112.
[80] A. Peter, A. H. A. Lutey, S. Faas, L. Romoli, V. Onuseit, T. Graf, *Opt. Laser Technol.* **2020**, *123*, 105954.
[81] D. P. Linklater, V. A. Baulin, X. Le Guével, J. B. Fleury, E. Hanssen, T. H. P. Nguyen, S. Juodkazis, G. Bryant, R. J. Crawford, P. Stoodley, E. P. Ivanova, *Adv. Mater.* **2020**, *32*, 2005679.
[82] E. P. Ivanova, D. P. Linklater, M. Werner, V. A. Baulin, X. M. Xu, N. Vrancken, S. Rubanov, E. Hanssen, J. Wandiyanto, V. K. Truong, A. Elbourne, S. Maclaughlin, S. Juodkazis, R. J. Crawford, *P. Natl. Acad. Sci. USA* **2020**, *117*, 12598.
[83] D. P. Linklater, V. A. Baulin, S. Juodkazis, R. J. Crawford, P. Stoodley, E. P. Ivanova, *Nat. Rev. Microbiol.* **2020**, *19*, 8.
[84] K. Modaresifar, L. B. Kunkels, M. Ganjian, N. Tümer, C. W. Hagen, L. G. Otten, P. L. Hagedoorn, L. Angeloni, M. K. Ghatkesar, L. E. Fratila-Apachitei, A. A. Zadpoor, *Nanomaterials* **2020**, *10*, 347.
[85] K. Modaresifar, S. Azizian, M. Ganjian, L. E. Fratila-Apachitei, A. A. Zadpoor, *Acta Biomater.* **2019**, *83*, 29.
[86] Y. Cheng, X. Ma, T. Franklin, R. Yang, C. I. Moraru, *Annu. Rev. Food Sci. Technol.* **2023**, *14*, 449.
[87] G. B. Hwang, K. Page, A. Patir, S. P. Nair, E. Allan, I. P. Parkin, *ACS Nano* **2018**, *12*, 6050.
[88] V. K. Truong, H. K. Webb, E. Fadeeva, B. N. Chichkov, A. H. F. Wu, R. Lamb, J. Y. Wang, R. J. Crawford, E. P. Ivanova, *Biofouling* **2012**, *28*, 539.
[89] E. Fadeeva, V. K. Truong, M. Stiesch, B. N. Chichkov, R. J. Crawford, J. Wang, E. P. Ivanova, *Langmuir* **2011**, *27*, 3012.
[90] M. Mateescu, S. Knopf, F. Mermet, P. Lavalle, L. Vonna, *Langmuir* **2020**, *36*, 1103.
[91] C. M. Bhadra, V. K. Truong, V. T. Pham, M. Al Kobaisi, G. Seniutinas, J. Y. Wang, S. Juodkazis, R. J. Crawford, E. P. Ivanova, *Sci. Rep.* **2015**, *5*, 16817.
[92] C. Chen, A. Enrico, T. Pettersson, M. Ek, A. Herland, F. Niklaus, G. Stemme, L. Wågberg, *J. Colloid Interface Sci.* **2020**, *575*, 286.
[93] X. Ge, Y. Leng, X. Lu, F. Z. Ren, K. F. Wang, Y. H. Ding, M. Yang, *J. Biomed. Mater. Res., Part A* **2015**, *103*, 384.
[94] J. Sjollema, S. A. J. Zaat, V. Fontaine, M. Ramstedt, R. Luginbuehl, K. Thevissen, J. Y. Li, H. C. van der Mei, H. J. Busscher, *Acta Biomater.* **2018**, *70*, 12.
[95] ISO 22196: Measurement of antibacterial activity on plastics and other non-porous surfaces, International Organization for Standardization, Geneva, Switzerland, **2011**.
[96] A. J. Cunliffe, P. D. Askew, I. Stephan, G. Iredale, P. Cosemans, L. M. Simmons, J. Verran, J. Redfern, *Antibiotics* **2021**, *10*, 1069.
[97] P. Hou, T. Z. Wang, B. Zhou, P. Song, W. Z. Zeng, T. Muhammad, Y. K. Li, *Biofouling* **2020**, *36*, 44.
[98] M. H. Muhammad, A. L. Idris, X. Fan, Y. C. Guo, Y. Y. Yu, X. Jin, J. Z. Qiu, X. Guan, T. P. Huang, *Front. Microbiol.* **2020**, *11*, 928.
[99] C. Wiegand, A. Völpel, A. Ewald, M. Remesch, J. Kuever, J. Bauer, S. Griesheim, C. Hauser, J. Thielmann, S. Tonndorf-Martini, B. W. Sigusch, J. Weisser, R. Wyrwa, P. Elsner, U. C. Hipler, M. Roth, C. Dewald, C. Lüdecke-Beyer, J. Bossert, *PLoS One* **2018**, *13*, e0194339.
[100] S. L. Walker, J. E. Hill, J. A. Redman, M. Elimelech, *Appl. Environ. Microb.* **2005**, *71*, 3093.
[101] J. Azeredo, N. F. Azevedo, R. Briandet, N. Cerca, T. Coenye, A. R. Costa, M. Desvaux, G. Di Bonaventura, M. Hébraud, Z. Jaglic, M. Kačániová, S. Knøchel, A. Lourenço, F. Mergulhão, R. L. Meyer, G. Nychas, M. Simões, O. Tresse, C. Sternberg, *Crit. Rev. Microbiol.* **2017**, *43*, 313.
[102] T. R. Neu, J. R. Lawrence, in *Microbial Biofilms: Methods and Protocols*, (Ed: J. M. Walker), Humana New York, NY, **2014**, *1147*, pp. 43–64.
[103] P. Stiefel, S. Schmidt-Emrich, K. Maniura-Weber, Q. Ren, *BMC Microbiol.* **2015**, *15*, 36.
[104] J. Robertson, C. McGoverin, F. Vanholsbeeck, S. Swift, *Front. Microbiol.* **2019**, *10*, 801.
[105] F. Pantanella, P. Valenti, T. Natalizi, D. Passeri, F. Berlutti, *Ann. Ig.* **2013**, *25*, 31.
[106] ISO 18593:2004(E): Microbiology of food and animal feeding stuffs - Horizontal methods for sampling techniques from surfaces using contact plates and swabs. International Organization for Standardization: Geneva, Switzerland, **2004**.
[107] R. M. A. Sullan, A. Beaussart, P. Tripathi, S. Derclaye, S. El-Kirat-Chatel, J. K. Li, Y. J. Schneider, J. Vanderleyden, S. Lebeer, Y. F. Dufrêne, *Nanoscale* **2014**, *6*, 1134.
[108] S. Aguayo, N. Donos, D. Spratt, L. Bozec, *Nanotechnology* **2015**, *26*, 062001.
[109] N. Thewes, A. Thewes, P. Loskill, H. Peisker, M. Bischoff, M. Herrmann, L. Santen, K. Jacobs, *Soft Matter* **2015**, *11*, 8913.
[110] C. Spengler, F. Nolle, J. Mischo, T. Faidt, S. Grandthyll, N. Thewes, M. Koch, F. Müller, M. Bischoff, M. A. Klatt, K. Jacobs, *Nanoscale* **2019**, *11*, 19713.
[111] E. Maikranz, C. Spengler, N. Thewes, A. Thewes, F. Nolle, P. Jung, M. Bischoff, L. Santen, K. Jacobs, *Nanoscale* **2020**, *12*, 19267.
[112] A. Beaussart, S. El-Kirat-Chatel, R. M. A. Sullan, D. Alsteens, P. Herman, S. Derclaye, Y. F. Dufrêne, *Nat. Protoc.* **2014**, *9*, 1049.
[113] J. Zubia Aranburu, B. Cappella, A. Zabala Eguren, L. Buruaga Lamarain, A. Aginagalde Lopez, K. Schwibbert, in *XL Congreso Anual de la Sociedad Espanola de Ingeniería Biomédica CASEIB*, **2022**, pp. 217–220.

[114] M. Michalska, R. Divan, P. Noirot, P. D. Laible, *Nanoscale* **2021**, *13*, 17603.
[115] R. Y. Siddiquie, A. Gaddam, A. Agrawal, S. S. Dimov, S. S. Joshi, *Langmuir* **2020**, *36*, 5349.
[116] K. Schwibbert, F. Menzel, N. Epperlein, J. Bonse, J. Krüger, *Materials* **2019**, *12*, 3107.
[117] A. Cunha, A.-M. Elie, L. Plawinski, A. P. Serro, A. M. B. do Rego, A. Almeida, M. C. Urdaci, M.-C. Durrieu, R. Vilar, *Appl. Surf. Sci.* **2016**, *360*, 485.
[118] X. Luo, S. L. Yao, H. J. Zhang, M. Y. Cai, W. J. Liu, R. Pan, C. H. Chen, X. M. Wang, L. N. Wang, M. L. Zhong, *Opt. Laser Technol.* **2020**, *124*, 105973.
[119] S. Papa, A. Abou Khalil, H. Hamzeh-Cognasse, M. Thomas, M. Maalouf, Y. Di Maio, X. Sedao, A. Guignandon, V. Dumas, *Appl. Surf. Sci.* **2022**, *606*, 154784.
[120] F. H. Rajab, C. M. Liauw, P. S. Benson, L. Li, K. A. Whitehead, *Food Bioprod. Process.* **2018**, *109*, 29.
[121] L. Lu, J. Zhang, K. Guan, J. Zhou, F. Yuan, Y. Guan, *J. Nanobiotechnology* **2022**, *20*, 365.
[122] A. K. Meinshausen, M. Herbster, C. Zwahr, M. Soldera, A. Müller, T. Halle, A. F. Lasagni, J. Bertrand, *J. Appl. Microbiol.* **2021**, *131*, 1498.
[123] C. Q. Lai, *IEEE Trans. Nanobioscience* **2020**, *19*, 203.
[124] L. Caro-Lara, I. T. Vargas, E. Ramos-Moore, C. Galarce, D. Diaz-Droguett, G. E. Pizarro, *J. Environ. Chem. Eng.* **2022**, *10*, 108497.
[125] D. W. Müller, S. Lößlein, E. Terriac, K. Brix, K. Siems, R. Moeller, R. Kautenburger, F. Mücklich, *Adv. Mater. Interfaces* **2021**, *8*, 2001656.
[126] V. Selvamani, A. Zareei, A. Elkashif, M. K. Maruthamuthu, S. Chittiboyina, D. Delisi, Z. Li, L. Cai, V. G. Pol, M. N. Seleem, R. Rahimi, *Adv. Mater. Interfaces* **2020**, *7*, 1901890.
[127] A. M. Emelyanenko, V. V. Kaminskii, I. S. Pytskii, A. G. Domantovsky, K. A. Emelyanenko, A. V. Aleshkin, L. B. Boinovich, *Bull. Exp. Biol. Med.* **2020**, *168*, 488.
[128] L. A. Gallarato, L. E. Mulko, M. S. Dardanelli, C. A. Barbero, D. F. Acevedo, E. I. Yslas, *Colloids Surf B Biointerfaces* **2017**, *150*, 1.
[129] D. Fajstavr, K. Neznalová, N. Slepičková Kasálková, S. Rimpelová, K. Kubičíková, V. Švorčík, P. Slepička, *Materials* **2020**, *13*, 3609.
[130] A. S. Ahmed, D. W. Müller, S. Bruyere, A. Holtsch, F. Müller, J. Barrirero, K. Brix, S. Migot, R. Kautenburger, K. Jacobs, J. F. Pierson, F. Mücklich, *ACS Appl. Mater. Interfaces* **2023**, *15*, 36908.
[131] L. Romoli, G. Lazzini, A. H. A. Lutey, F. Fuso, *CIRP Ann. - Manuf. Techn.* **2020**, *69*, 529.
[132] A. A. Nastulyavichus, S. I. Kudryashov, I. N. Saraeva, N. A. Smirnov, A. A. Rudenko, E. R. Tolordava, D. A. Zayarny, S. A. Gonchukov, A. A. Ionin, *Laser Phys. Lett.* **2019**, *17*, 016003.
[133] L. Grase, P. Onufrijevs, D. Rezevska, K. Racenis, I. Skadins, J. Karosas, P. Gecys, M. Iesalnieks, A. Pludons, J. Kroica, G. Raciukaitis, *Nanomaterials* **2023**, *13*, 2032.
[134] Y. Y. Chang, J. H. Zhang, H. L. Huang, *Materials* **2018**, *11*, 2495.
[135] P. Gregoričič, M. Conradi, L. Hribar, M. Hočevar, *Materials* **2018**, *11*, 2240.
[136] T. Primus, P. Zeman, J. Brajer, P. Kožmin, S. Syrovátka, *Materials* **2021**, *14*, 2228.
[137] F. H. Rajab, A. S. T. Tariq, A. K. Al-Jumaily, A. W. AlShaer, L. Li, K. A. Whitehead, *Appl. Surf. Sci.* **2021**, *540*, 148292.
[138] D. Patil, S. Aravindan, M. Kaushal Wasson, P. V. Rao, *J. Micro Nano-Manuf.* **2018**, *6*, 011002.
[139] I. Singh, S. M. George, A. Tiwari, J. Ramkumar, K. Balani, *J. Mater. Res.* **2021**, *36*, 3985.
[140] Y. L. Ma, L. Jiang, J. Hu, H. L. Liu, S. C. Wang, P. Zuo, P. F. Ji, L. T. Qu, T. H. Cui, *ACS Appl. Mater. Interfaces* **2020**, *12*, 17155.
[141] Q. F. Pan, Y. Cao, W. Xue, D. H. Zhu, W. W. Liu, *Langmuir* **2019**, *35*, 11414.
[142] C. Kunz, S. Engel, F. A. Müller, S. Gräf, *Nanomaterials* **2020**, *10*, 1187.
[143] A. M. Kietzig, S. G. Hatzikiriakos, P. Englezos, *Langmuir* **2009**, *25*, 4821.
[144] J. Bonse, S. Gräf, *Nanomaterials* **2021**, *11*, 3326.
[145] E. Dauvergne, C. Mullié, *Antibiotics* **2021**, *10*, 286.
[146] E. P. Ivanova, J. Hasan, H. K. Webb, V. K. Truong, G. S. Watson, J. A. Watson, V. A. Baulin, S. Pogodin, J. Y. Wang, M. J. Tobin, C. Löbbe, R. J. Crawford, *Small* **2012**, *8*, 2489.
[147] H. J. Ensikat, P. Ditsche-Kuru, C. Neinhuis, W. Barthlott, *Beilstein J. Nanotechnol.* **2011**, *2*, 152.
[148] X. X. Sheng, Y. P. Ting, S. O. Pehkonen, *J. Colloid Interface Sci.* **2008**, *321*, 256.
[149] U. Römling, M. Rohde, A. Olsén, S. Normark, J. Reinköster, *Mol. Microbiol.* **2000**, *36*, 10.
[150] P. G. Grützmacher, F. J. Profito, A. Rosenkranz, *Lubricants* **2019**, *7*, 95.
[151] D. Salatto, Z. Huang, P. T. Benziger, J. Y. Carrillo, Y. Bajaj, A. Gauer, L. Tsapatsaris, B. G. Sumpter, R. L. M. Takenaka, W. Yin, D. G. Thanassi, M. Endoh, T. Koga, *ACS Appl. Mater. Interfaces* **2023**, *15*, 3420.
[152] J. Krüger, J. Bonse, *Materials* **2023**, *16*, 819.
[153] C.-W. Chan, L. Carson, G. C. Smith, A. Morelli, S. Lee, *Appl. Surf. Sci.* **2017**, *404*, 67.
[154] S. A. Jalil, M. Akram, J. A. Bhat, J. J. Hayes, S. C. Singh, M. ElKabbash, C. Guo, *Appl. Surf. Sci.* **2020**, *506*, 144952.
[155] V. V. Kaminsky, A. M. Emelyanenko, A. V. Aleshkin, K. A. Emelyanenko, L. B. Boinovich, *Microbiology* **2021**, *90*, 643.
[156] K. Whitehead, L. I. Pilkington, A. J. Slate, F. Saubade, M. Amin, A. Lutey, L. Gemini, R. Kling, L. Romoli, *Food Bioprod. Process.* **2022**, *137*, 145.
[157] V. M. Villapun, A. P. Gomez, W. Wei, L. G. Dover, J. R. Thompson, T. Barthels, J. Rodriguez, S. Cox, S. González, *APL Mater.* **2020**, *8*, 091108.
[158] C. Z. Du, C. Y. Wang, T. Zhang, L. J. Zheng, *ACS Appl. Bio Mater.* **2022**, *5*, 272.
[159] C. Du, C. Wang, J. Sui, L. Zheng, *Colloids Surf., B* **2021**, *197*, 111393.
[160] B. Dashtbozorg, P. Penchev, J. M. Romano, X. Y. Li, R. L. Sammons, S. Dimov, H. S. Dong, *Appl. Surf. Sci.* **2021**, *565*, 150594.
[161] I. N. Saraeva, E. R. Tolordava, I. V. Sozaev, A. A. Nastulyavichus, S. I. Kudryashov, A. A. Rudenko, A. A. Ionin, S. A. Gonchukov, *Laser Phys. Lett.* **2021**, *18*, 035603.
[162] B. Grössner-Schreiber, M. Griepentrog, I. Haustein, W. D. Müller, K. P. Lange, H. Briedigkeit, U. B. Göbel, *Clin. Oral. Implants Res.* **2001**, *12*, 543.
[163] G. John, F. Schwarz, A. Kravchenko, M. A. Ommerborn, J. Becker, *Int. J. Implant. Dent.* **2021**, *7*, 51.
[164] K. Doll, E. Fadeeva, J. Schaeske, T. Ehmke, A. Winkel, A. Heisterkamp, B. N. Chichkov, M. Stiesch, N. S. Stumpp, *ACS Appl. Mater. Interfaces* **2017**, *9*, 9359.
[165] P. Komorowski, P. Sokolowska, M. Siatkowska, M. Elgalal, M. Rosowski, K. Makowski, L. Lipinska, M. Leszczewicz, A. Styczynski, K. Fogel, B. Walkowiak, *J. Biomed. Mater. Res., Part B* **2020**, *108*, 1790.
[166] V. Parmar, A. Kumar, M. Mani Sankar, S. Datta, G. Vijaya Prakash, S. Mohanty, D. Kalyanasundaram, *J. Laser Appl.* **2018**, *30*, 032001.
[167] M. L. Schröder, N. Angrisani, E. Fadeeva, J. Hegermann, J. Reifenrath, *Mater. Sci. Eng. C* **2020**, *109*, 110573.
[168] L. Sotelo, T. Fontanot, S. Vig, P. Herre, P. Yousefi, M. H. Fernandes, G. Sarau, G. Leuchs, S. Christiansen, *Adv. Mater. Technol.* **2023**, *8*, 2201802.
[169] F. H. Rajab, C. M. Liauw, P. S. Benson, L. Li, K. A. Whitehead, *Colloids Surf. B Biointerfaces* **2017**, *160*, 688.
[170] K. Doll, V. Veiko, Y. Karlagina, G. Odintsova, N. Heine, E. Egorova, M. Radaev, B. Chichkov, M. Stiesch, *Curr. Dir. Biomed. Eng.* **2021**, *7*, 875.
[171] X. H. Wu, H. Y. Ao, Z. R. He, Q. Wang, Z. X. Peng, *Coatings* **2022**, *12*, 414.

[172] M. Krzywicka, J. Szymańska, S. Tofil, A. Malm, A. Grzegorczyk, *J. Funct. Biomater.* **2022**, *13*, 26.
[173] C. Du, C. Wang, T. Zhang, X. Yi, J. Liang, H. Wang, *Proc. Inst. Mech. Eng., Part H* **2020**, *234*, 387.
[174] C. Du, Y. Yang, L. Zheng, T. Zhang, X. Zhao, C. Wang, *ACS Appl. Mater. Interfaces* **2022**, *14*, 8793.
[175] S. I. Kudryashov, A. A. Nastulyavichus, E. R. Tolordava, A. N. Kirichenko, I. N. Saraeva, A. A. Rudenko, Y. M. Romanova, A. Y. Panarin, A. A. Ionin, T. E. Itina, *Molecules* **2019**, *24*, 4488.
[176] R. Estevam-Alves, P. H. Ferreira, A. C. Coatrini, O. N. Oliveira, C. R. Fontana, C. R. Mendonca, *Int. J. Mol. Sci.* **2016**, *17*, 1243.
[177] E. Filipov, L. Angelova, S. Vig, M. H. Fernandes, G. Moreau, M. Lasgorceix, I. Buchvarov, A. Daskalova, *Polymers* **2022**, *14*, 2382.
[178] J. Siegel, B. Vyhnálkova, T. Savenkova, J. Pryjmaková, P. Slepička, M. Šlouf, T. Hubáček, *Int. J. Mol. Sci.* **2023**, *24*, 1432.
[179] A. Gillett, D. Waugh, J. Lawrence, M. Swainson, R. Dixon, *J. Laser Appl.* **2016**, *28*, 022503.
[180] B. Kryszak, K. Szustakiewicz, P. Dzienny, A. Junka, J. Paleczny, P. Szymczyk-Ziółkowska, V. Hoppe, M. Grzymajlo, A. Antończak, *Biomater Adv.* **2022**, *133*, 112648.
[181] B. Kryszak, K. Szustakiewicz, P. Dzienny, A. Junka, J. Paleczny, P. Szymczyk-Ziółkowska, V. Hoppe, A. Antończak, *Polym. Test.* **2022**, *116*, 107815.
[182] E. A. Cuello, L. E. Mulko, C. A. Barbero, D. F. Acevedo, E. I. Yslas, *Colloids Surf. B* **2020**, *188*, 110801.
[183] J.-M. Romano, R. Ahmed, A. Garcia-Giron, P. Penchev, H. Butt, O. Delléa, M. Sikosana, R. Helbig, C. Werner, S. Dimov, *J. Micro Nano-Manuf.* **2019**, *7*, 010901.
[184] J. Valle, S. Burgui, D. Langheinrich, C. Gil, C. Solano, A. Toledo-Arana, R. Helbig, A. Lasagni, I. Lasa, *Macromol. Biosci.* **2015**, *15*, 1060.
[185] O. Neděla, P. Slepička, N. S. Kasalkova, P. Sajdl, Z. Kolská, S. Rimpelová, V. Švorčík, *React. Funct. Polym.* **2019**, *136*, 173.
[186] S. Perni, P. Prokopovich, *Soft Matter* **2013**, *9*, 1844.

Karin Schwibbert obtained her diploma in biology and Ph.D. in microbiology from the University of Bonn, Germany, followed by a postdoctoral researcher position at the University of Münster in the Department of Biochemistry where she conducted research on osmoadaptation of halophilic bacteria. She is currently a Senior Scientist running a molecular microbiology laboratory at the German Federal Institute for Materials Research and Testing (BAM), Berlin, and leading manager of industry-related projects. Her research interests concentrate on biofilm formation on structured surfaces with a particular emphasis on laser-processed surfaces and how surfaces can be modified to attract or repel bacteria.

Anja M. Richter holds a Master's in Molecular- and Cell Biology and a Ph.D. in Microbiology from the Freie University Berlin and the Humboldt University of Berlin, respectively, followed by a postdoctoral researcher position at the Costerton Biofilm Center at the Copenhagen University, Denmark. During her Ph.D. and postdoc time, she investigated the intracellular regulation of biofilm formation in *Escherichia coli* and *Burkholderia cenocepacia*. Back in Germany, she joined Karin Schwibbert´s Laboratory at the Federal Institute for Materials Research and Testing (BAM) as a postdoc. Being part of an interdisciplinary research consortium, she analyzed bacterial adhesion and biofilm formation on laser-textured surfaces. In spring 2022, she joined the Unit for Hospital Hygiene, Infection Prevention, and Control at the Robert Koch Institute in Berlin, where she focuses on disinfection of biofilm-associated pathogens and the implementation of standardized protocols for disinfectant efficacy testing against biofilms.

Jörg Krüger received a diploma degree in physics from the Friedrich Schiller University Jena (Germany) and a doctoral degree with distinction from the Brandenburg University of Technology Cottbus (Germany). In 1991, he joined the Bundesanstalt für Materialforschung und -prüfung (BAM) in Berlin (Germany). Currently, he is Deputy Head of BAM's division "Interfacial Processes and Corrosion". His research interests include short and ultrashort pulse laser materials processing, laser applications for the preservation of the cultural heritage, and laser safety issues including secondary hazards.

Jörn Bonse received a diploma degree in physics from the University of Hannover and a doctoral degree from the Technical University of Berlin. He occupied research positions at the Laser Zentrum Hannover, the Max-Born-Institute in Berlin, and the Spanish National Research Council in Madrid and was appointed as a Senior Laser Application Specialist at Newport Spectra-Physics. Currently, he is a Senior Scientist at the German Federal Institute for Materials Research and Testing (BAM). His research interests include fundamentals and applications of laser-matter interaction, laser-induced periodic surface structures, surface functionalization, time-resolved optical techniques, and laser processes in photovoltaics.